JOURNAL OF GEOPHYSICAL RESEARCH, VOL. 112, E08009, doi:10.1029/2006JE002830, 2007

Click Here for Full Article

Geomorphic and stratigraphic analysis of Crater Terby and layered deposits north of Hellas basin, Mars

Sharon A. Wilson,[1] Alan D. Howard,[2] Jeffrey M. Moore,[3] and John A. Grant[1]

Received 20 September 2006; revised 12 February 2007; accepted 17 May 2007; published 24 August 2007.

[1] The geologic history of Crater Terby is developed through geomorphic and stratigraphic analyses within the regional context of the Hellas basin. Terby exhibits ~2-km-thick sequences of layers that consist of repetitive, subhorizontal and laterally continuous beds. The layers are predominantly fine-grained as indicated by their ease of aeolian erosion, although a few consolidated layers weather to form rubbly talus. The grain size or composition of the deposited materials fluctuated, producing layering, but the overall properties of the deposits are similar throughout the sequence and are comparable to layered deposits in other crater basins around Hellas. The original depositional geometry, physical and geological characteristics of the layers in Terby and the other basins lead us to favor a lacustrine origin, but a loess-like origin cannot be ruled out. The formation of the layers corresponds to a period when the circum-Hellas region may have been occupied by a lake(s) up to 3.6 km deep. Once the lake in Hellas decreased, the layers in Terby were incised by troughs and a moat-like depression. We attribute this erosion to scour beneath an ice cover due to a lack of integrated fluvial drainage or large aeolian deflation features. The presence of viscous flow features in a crater on Terby's northwestern rim and lobate features on Terby's crater floor are also indicative of ice. The lack of depositional features associated with the postulated glacial activity suggests there was a contemporaneous shallow (ice-covered?) lake covering the floor of Terby that transported material into the greater Hellas basin.

Citation: Wilson, S. A., A. D. Howard, J. M. Moore, and J. A. Grant (2007), Geomorphic and stratigraphic analysis of Crater Terby and layered deposits north of Hellas basin, Mars, *J. Geophys. Res.*, *112*, E08009, doi:10.1029/2006JE002830.

1. Introduction

[2] Characteristic morphologies of ubiquitous landforms in the ancient Martian highlands indicate a climate that was once capable of sustaining an active hydrologic cycle that consisted of precipitation and runoff in the Noachian [*Grant*, 2000; *Hynek and Phillips*, 2001, 2003; *Craddock and Howard*, 2002; *Irwin and Howard*, 2002; *Forsberg-Taylor et al.*, 2004]. High-resolution images and data from the Mars Exploration Rovers and several orbiting instruments including the Mars Orbiter Camera (MOC), the Thermal Emission Imaging System (THEMIS), the High Resolution Imaging Science Experiment (HiRISE) and the Mars Express Observatoire pour la Minéralogie, l'Eau, les Glaces et l'Activité (OMEGA) visible-near-infrared hyperspectral imager permit detailed observation and interpretation of layered deposits on Mars that may have been deposited in water-rich environments [e.g., *Malin et al.*, 1998; *Christensen et al.*, 2003; *Squyres et al.*, 2004; *Gendrin et al.*, 2005; *Bibring et al.*, 2006]. Several craters surrounding the Hellas impact basin (Figure 1), including Crater Terby, have been filled with layered deposits [*Moore and Howard*, 2005b; *Korteniemi et al.*, 2005a, 2005b].

[3] High-resolution images from MOC and THEMIS reveal a suite of intricately layered landforms banked along the northern edge of Terby (~28°S, 74°E, elevation range −5000 to 0 m; Figure 2). These include 2-km-deep, north trending troughs that are carved into layered deposits, mantled ramps that extend across layered sequences, fans, channels, avalanche deposits, bowl-shaped depressions, scoured caprock, grooved surfaces, viscous flow features, sinuous ridges, and arcuate scarps. The diversity of landforms within Terby and its surroundings suggest that spatially and temporally varying geomorphic processes were involved, perhaps as a response to changes in climate throughout a portion of Martian history.

[4] This study of Terby and other craters north of Hellas utilizes images from the global coverage by Viking Orbiters (MDIM 2.1), THEMIS visible wavelength (VIS) and day and nighttime thermal infrared (IR) systems, the narrow angle (NA) MOC, the HiRISE imager [*McEwen et al.*, 2006] as well as data from the Mars Orbiter Laser Altimeter (MOLA). Through geologic and geomorphic mapping and analysis of the available topographic, infrared remote sensing and image data, this study (1) describes the major

[1]Center for Earth and Planetary Studies, National Air and Space Museum, Smithsonian Institution, Washington, D. C., USA.
[2]Department of Environmental Sciences, University of Virginia, Charlottesville, Virginia, USA.
[3]Space Sciences Division, NASA Ames Research Center, Moffett Field, California, USA.

Copyright 2007 by the American Geophysical Union.
0148-0227/07/2006JE002830$09.00

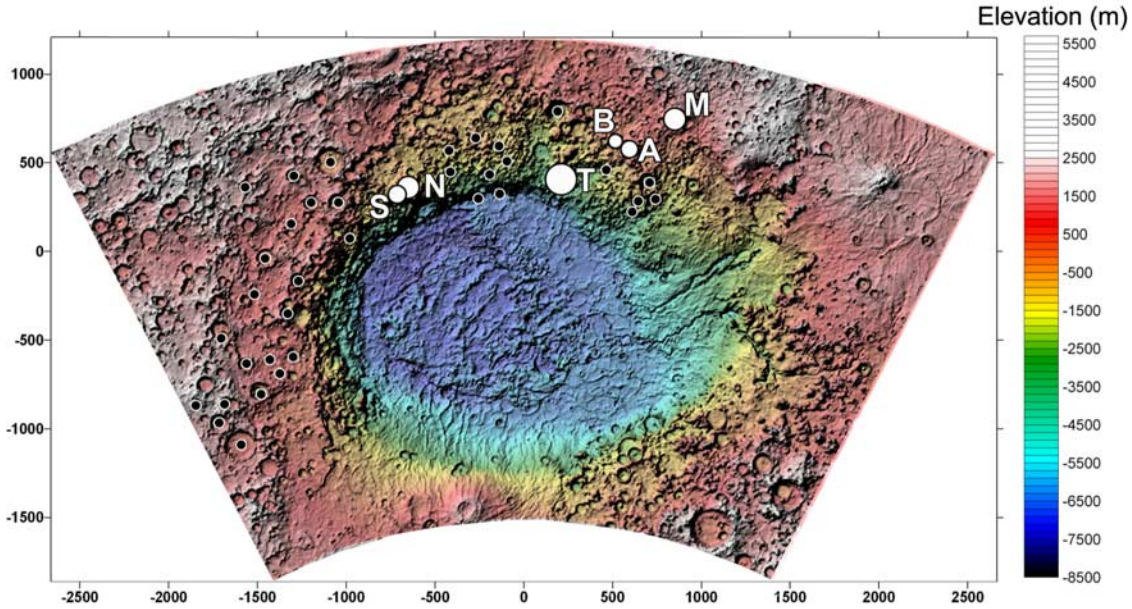

Figure 1. Numerous craters around the Hellas basin, marked with black and white circles, contain interior layered deposits [after *Moore and Howard*, 2005b]. Layered deposits discussed in the text are located in Craters Terby ("T"), Millochau ("M") [*Mest and Crown*, 2005], "A" and "B" from *Korteniemi et al.* [2005a], Niesten ("N") and the informally named SW crater ("S"). This MOLA shaded relief map of the Hellas region is in Lambert Conformal projection and covers the region from 25°E to 115°E between 15°S and 60°S. Scale along axes is in kilometers relative to projection center at 75°E and 35°S; top of image is north.

geomorphic units within Terby, (2) characterizes the nature and geometry of the layered deposits in relation to other interior deposits to ascertain their origin and processes responsible for their formation and (3) provides a possible geologic evolution of Terby that details the relative timing of major depositional and erosional events couched in the regional context of Hellas and the Southern Highlands. We complement our analysis of Terby through a comparison with other craters on the northern flank of the Hellas basin that contain a similar sequence of layered deposits (Figure 1).

1.1. Layered Deposits on Mars

[5] Most of the layered outcrops on Mars are exposed in a belt between 30°N and 30°S and their distribution is clustered in the Valles Marineris, Mawrth Vallis and western Arabia Terra, Terra Meridiani and northern Hellas regions [*Malin and Edgett*, 2000]. Layered deposits occur in a variety of geomorphic settings including intercrater terrain, chaotic terrain, the interiors of structural basins, but are most commonly associated with crater interiors where the material is typically exposed in the floors and walls of pits within the interior deposits or in mounds and mesas on the crater floor [*Malin and Edgett*, 2000]. Layered deposits in the northern Hellas region are the focus of the present study, with particular emphasis on the >2-km-thick sequence in Terby.

[6] In considering the origin of the layered deposits in Terby and other craters in the Hellas region, several general observations serve as touchstones. The first of these is that thick sections of layered deposits, and especially light-toned deposits, occur within craters and other basins in several locations in the highlands of Mars, one of which is the Hellas region [*Malin and Edgett*, 2000]. These intricately layered deposits attest to a complex history of deposition and erosion [e.g., *Tanaka*, 1997; *Malin and Edgett*, 2000, 2001; *Edgett and Malin*, 2002]. *Malin and Edgett* [2000, 2001] interpret the layers to be sedimentary rocks on the basis of their repetitive, fine-grained and indurated nature. We likewise classify layered sequences in Terby and other craters on the Hellas rim as sedimentary deposits, using this term to describe materials deposited or precipitated from a fluid or moving medium. This broad definition can include fluvial and lacustrine deposits, aeolian loess and sand dunes, glacial till, as well as pyroclastic deposits [e.g., *Reading*, 1996; *Branney and Kokelaar*, 2002].

[7] Secondly, *Malin and Edgett* [2000] observe a fairly consistent vertical sequence of deposits, with light-toned layered deposits overlain by light-toned thick-bedded units, with dark- to intermediate-toned mesa sediment unconformably overlying the earlier deposits. The bulk of the layered deposits must be fine-grained and only moderately cemented, because wind erosion appears capable of removing almost all of the deposits without leaving a significant protective lag of centimeter-size or larger material [*Malin and Edgett*, 2000].

[8] Three issues must be considered when resolving the origin of a sedimentary deposit: (1) the source of the granular material, (2) the mode of transport into the region, and (3) the final depositional mechanism, which we term, respectively, as the origin, transport mechanism, and deposition mechanism. These three requisite steps may or may not be causally and temporally interrelated. Fine granular material can be produced by a variety of processes, includ-

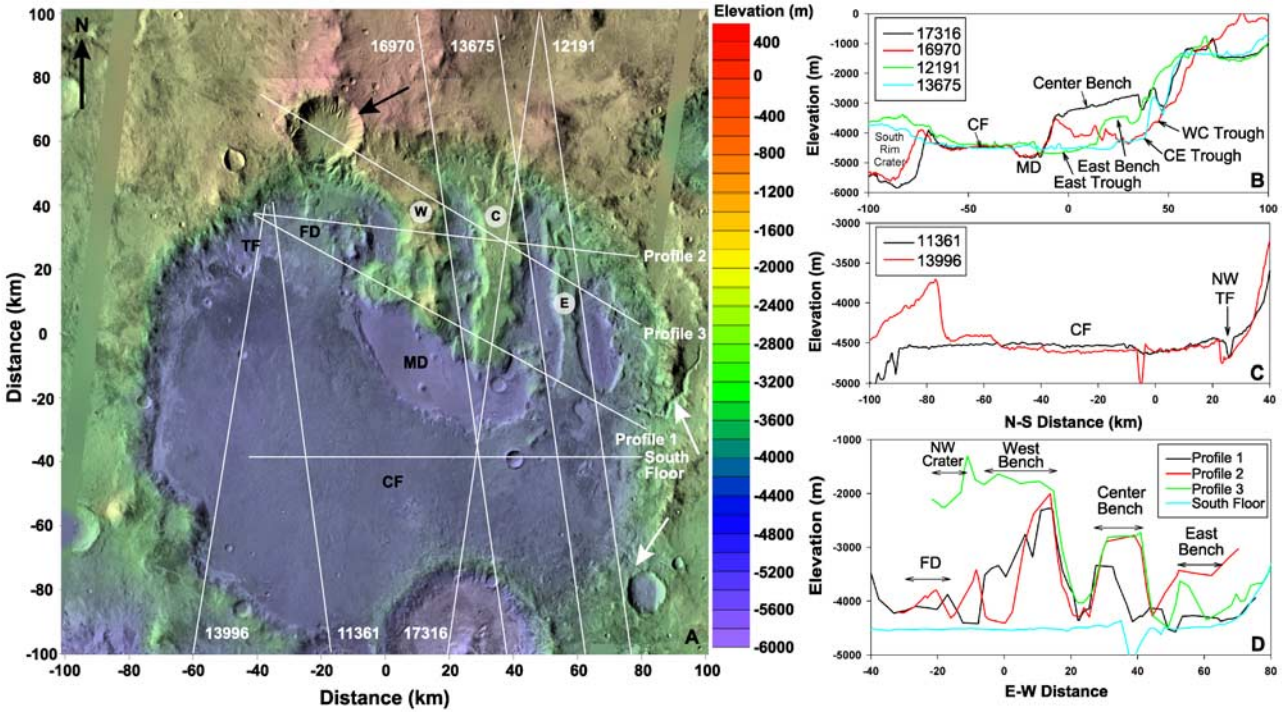

Figure 2. (a) MOLA topography over THEMIS Day IR mosaic (P. R. Christensen et al., THEMIS Public Data Releases, Planetary Data System node, Arizona State University, http://themis-data.asu.edu) (hereinafter referred to as Christensen et al. data set) of Terby (D = 165 km), a Noachian crater located on the northern rim of Hellas. The western (W), central (C) and eastern (E) layered benches extend from the northern rim and terminate abruptly at the moat-like depression (MD) in the center of the crater, adjacent to the flat crater floor (CF). Black arrow denotes the location of "NW crater," whose breached southern rim is the apex of the fan deposit (FD). White arrows mark unbranched valleys that breach Terby's eastern rim. Numbers on axes (kilometers) are relative to image center at 74°E and 27.5°S and are keyed to elevation profiles in Figures 2b, 2c, and 2d. Image is sinusoidal projection. (b) Elevation profiles corresponding to MOLA orbits 17316, 16970, 12191, and 13675 in Figure 2a, projected laterally onto a north-south orientation. "East Trough" refers to the enclosed depression east of the eastern bench, "WC Trough" refers to the trough between the western and central benches, and "CE Trough" refers to the trough between the central and eastern benches. (c) Elevation profiles corresponding to MOLA orbits 11361 and 13996 in Figure 2a, projected in a north-south orientation. The ~280-m-high, north-facing scarp at the base of the northwest trough floor ("NW TF"; see Figure 3 for context) exposes light-toned layered deposits beneath the CF. The CF is relatively smooth and flat, at an elevation of −4.5 km. Terby's southern crater rim at its lowest point is also at an elevation of −4.5 km. (d) The western, central and eastern bench surfaces are nearly planar, dip primarily toward the south and are nearly horizontal in the east-west direction (Profiles 1 − 3). The elevation of the western, central and eastern benches decreases from west to east in a step-like fashion, with a roughly 1000 m drop from the western to the central bench, and an additional 800- to 1000-m drop to the eastern bench. The flat topography of the CF is shown in the "South Floor" profile. All profiles in Figure 2d are from gridded MOLA data and are projected in an east-west orientation.

ing physical and chemical weathering, pyroclastic eruptions, impact cratering, comminution during transport, and chemical precipitation. Long-distance transport into a region can occur by pyroclastic surges, airfall deposition from a variety of sources (wind erosion, volcanic ash, globally distributed ejecta from basin-scale impacts), fluvial and lacustrine processes. The terminal depositional process can be the same as the long-distance transport mechanism, or it may involve reworking by wind, fluvial, lacustrine, mass-wasting, or glacial processes. The origin, transport and deposition may be related to a single environment, such as the bedrock scour, comminution, transport and deposition of till by a glacier, or a sequence of environments may be involved, such as production of a fine regolith by impact cratering, its erosion, transport and sedimentation onto a lake by wind, and its final deposition by lacustrine processes.

[9] Finally, the top surface of a sedimentary deposit may represent the final surface of deposition or it may be erosional. The presence of an erosional surface is obvious on layered exposures with steep slopes, but may not be as evident on gentle slopes where later impact cratering and aeolian reworking can mask the underlying layers.

1.2. Geologic Setting: Hellas Planitia

[10] Hellas Planitia is a 2300-km-wide impact basin with 9 km of relief (Figure 1), making it the deepest and broadest

enclosed depression on Mars [*Smith et al.*, 1999; *Leonard and Tanaka*, 2001]. Recent interpretations of the deposits within Hellas suggest the basin may have hosted glaciers and proglacial lakes [*Kargel and Strom*, 1992], was the site of ice-covered lakes [*Moore and Wilhelms*, 2001], or was a basin-wide sea [*Malin and Edgett*, 2000] in the Noachian. Using topographic, morphologic and stratigraphic evidence, *Moore and Wilhelms* [2001] suggest that contours of constant elevation extending for thousands of kilometers (most prominently at elevations of −5.8 and −3.1 km) are putative stands of water or ice. Terby is located on the northern flank of Hellas Planitia (Figure 1) and is mapped within part of the oldest and outermost of the basin-filling unit [*Moore and Wilhelms*, 2001]. The dominant thermal signature of Hellas Planitia based on the Viking thermal infrared mapper [*Kieffer et al.*, 1977] and the Thermal Emission Spectrometer (TES) [*Christensen et al.*, 2001] indicates that the material on the floor is no larger than sand or crust-bonded dust [*Moore and Edgett*, 1993], an interpretation that is consistent with (but, in itself, does not prove) the hypothesis that water-laid and later ice-rich sedimentation dominated the Hellas interior [*Moore and Wilhelms*, 2001]. The origin of the material in the lower portions of the Hellas basin is most consistent with a lacustrine environment as opposed to deposition by aeolian processes given the nature of the grains and the strong correlation between elevation, suites of landforms and unit contacts [*Moore and Wilhelms*, 2001].

[11] The thick sequence of exposed layers in Terby remains relatively unstudied. *Leonard and Tanaka* [2001] mapped the deposits within Terby as late Noachian-aged etched material (HNe), a unit described as a partly degraded plains deposit of varying thickness that occurs on local high plains and larger craters in the circum-Hellas region including Terby, Schaeberle and Millochau. *Leonard and Tanaka* [2001] describe the unit as a fine-grained and friable material, indicative of dust, loess or tephra that may include interstitial ice. *Moore and Wilhelms* [2001], *Ansan and Mangold* [2004] and *Ansan et al.* [2005, 2006] proposed a fluvio-lacustrine origin (alluvial fan or prograding delta) for the layers and forwarded a dissolution process to explain the presence of the troughs. The spectral signature of a few pixels that correlate to the light-toned layers detected by OMEGA is indicative of hydrated (phyllosilicate) minerals [*Ansan et al.*, 2005; *Bibring et al.*, 2006], which is consistent with, but not limited to, a lacustrine depositional environment.

[12] In section 2 we discuss the landforms and stratigraphy of Terby. The features of Terby are then compared in section 3 to layered deposits in other large craters on the northern rim of the Hellas. Section 4 presents crater-frequency relative age dating for layered deposits in Terby and the other craters discussed in section 3, and section 5 presents our interpretations and conclusions concerning the geologic evolution of the layered deposits.

2. Geology of Crater Terby

2.1. Rim of Crater Terby

[13] The elevation of the Terby rim relative to the MOLA datum ranges from roughly −40 m along the northern rim to −3500 m along the southern rim (Figure 2). The crest of Terby's rim defines a plane sloping approximately 1° toward the south, reflecting the regional gradient established by the formation of the Hellas impact basin on which it is superimposed. Mapped as undifferentiated, rough terrain (RT) (Figure 3), the rim of Terby has been heavily modified subsequent to its formation and exhibits spatially variable morphology (Figure 2a). Several channels incise the northern, northwestern and northeastern rim of Terby (Figure 4). The northern rim of Terby directly adjacent to the interior deposits has the steepest interior slopes of roughly 8−10° (Figure 2b) and exhibits highly degraded, mottled, hummocky and so-called "softened" [*Squyres and Carr*, 1986; *Squyres et al.*, 1992] morphology that contrasts with strongly fluvially dissected rims on craters that are located higher on the Hellas basin ejecta sheet a few hundred kilometers to the north and east (e.g., Crater Millochau [*Mest and Crown*, 2005, 2006]). The few MOC NA images that detail the boundary between the crater rim and the interior layered deposits indicate that the layers postdate the "softening" of the crater rim although subsequent erosion has produced a rough, multimeter-scale surface texture.

[14] The western and eastern rims of Terby are comparable in elevation (roughly −2500 to −3000 m) and are typically ∼250 m higher than the topography exterior to the crater. Two large fluvial valleys cut through presumably resistant material on the eastern rim of Terby, but there is no apparent deposit on the crater floor at the terminus of either valley (Figure 2a). The most prominent of these unbranched valleys is 38 km long, originating −2815 m above the rim and terminating inside the crater at an elevation of −4100 m. Roughly 45 km south, a smaller valley originates at −3310 m and terminates on the floor of Terby at approximately −4360 m.

[15] In addition to the crater rim, the RT unit also includes an isolated mound of rough, hummocky terrain with intermediate-toned mantled or dust-covered slopes on the moat floor between the central and eastern benches (Figure 3). This mound of material, which does not exhibit any layering and is presumably more resistant than the layered deposits, may be a partial exposure of a ring structure or a massive slump related to the formation of Terby. The scarp of a flat-topped, smooth plateau near the center of this mound exhibits light-toned layers that appear to be deposited on top of, and are therefore younger, than this mound of RT.

2.2. Crater Terby Interior Deposits

[16] The interior deposits within Terby are banked along the north-northeastern edge of the crater and extend roughly to the center of the crater, occupying an area of approximately 6500 km^2 (Figures 2a and 3). Terby has a diameter (D) of ∼165 km and a depth (d) of 2.25 km, yielding a d/D ratio of 0.014. The minimum elevation in Terby, approximately −5000 m, is located near the center of the crater, and the maximum is roughly −40 m on the northern rim (the average rim elevation is about −2750 m). On the basis of calculations for "B/C" craters, characterized as flat-floored craters lacking central peaks with eroded ejecta blankets and low-relief, sharp to rounded rim crests [*Craddock et al.*, 1997], Terby should be ∼4.43 km deep (d/D ≈ 0.027). Another approximation of fresh crater depth by *Garvin et*

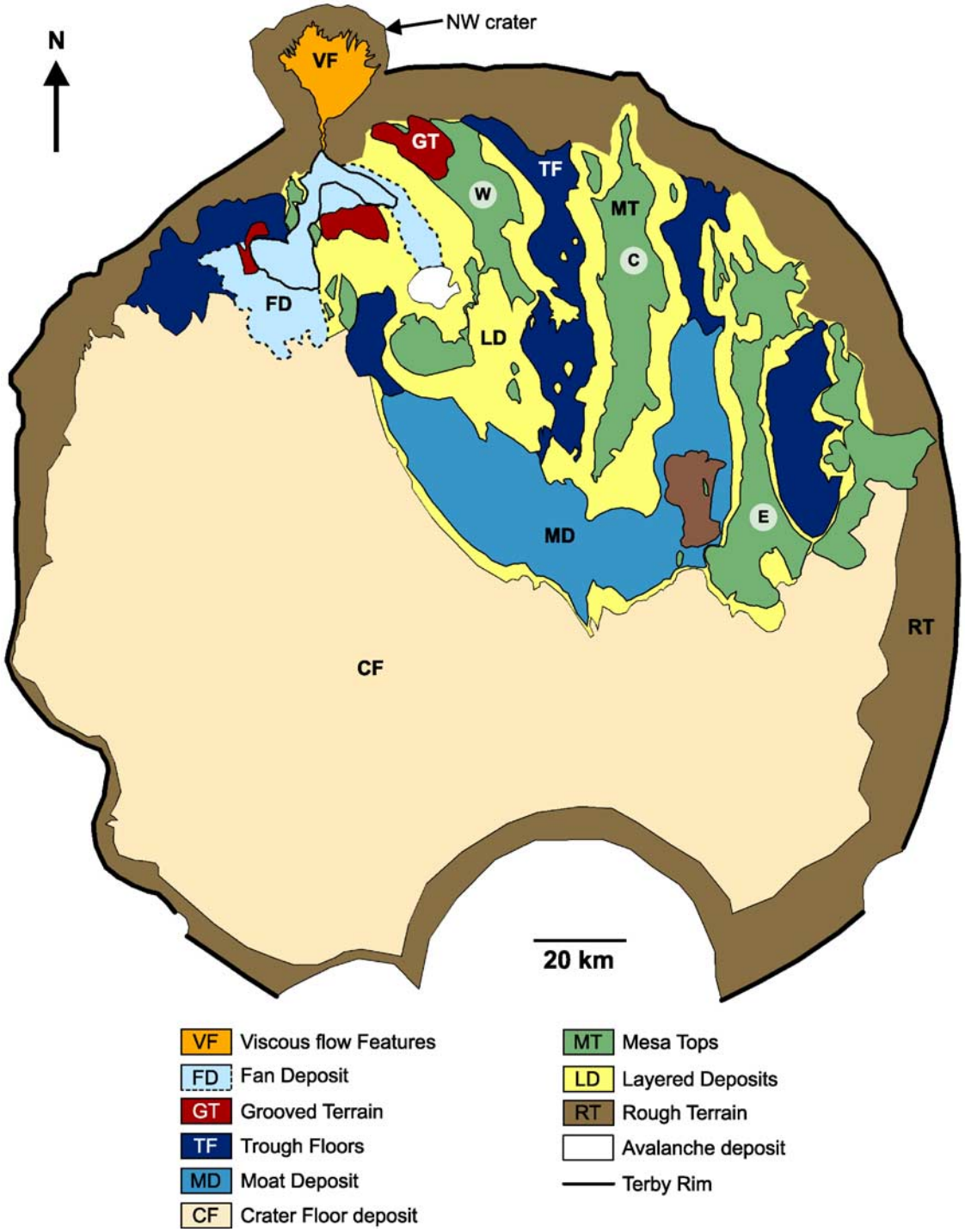

Figure 3. Geomorphic map of Terby showing location of terrains discussed in section 2. The western (W), central (C), and eastern (E) benches are labeled. Two subunits of the alluvial FD are shown: An extensive fan surface (dashed line) is defined by its smooth surface and relatively uniform gradient radiating from NW crater, and a smaller, younger fan surface (solid line) with a slightly steeper gradient is overlain on the northern portion of the earlier fan and is characterized by apparent radial distributary deposits etched into relief by aeolian deflation.

al. [2003] using calculations for complex crater relationships yields an estimate of ~4.38 km ($d = 0.36D^{0.49}$; d/D for Terby ≈ 0.027). Given these crater depth calculations and the present depth of Terby relative to its average rim height, there may be approximately 2.1–2.2 km of unexposed fill below the level of the exposed layered deposits. The absence of a central peak or well-exposed peak ring within Terby, which would be expected in a fresh crater of this size, gives further evidence of a thick crater floor deposit.

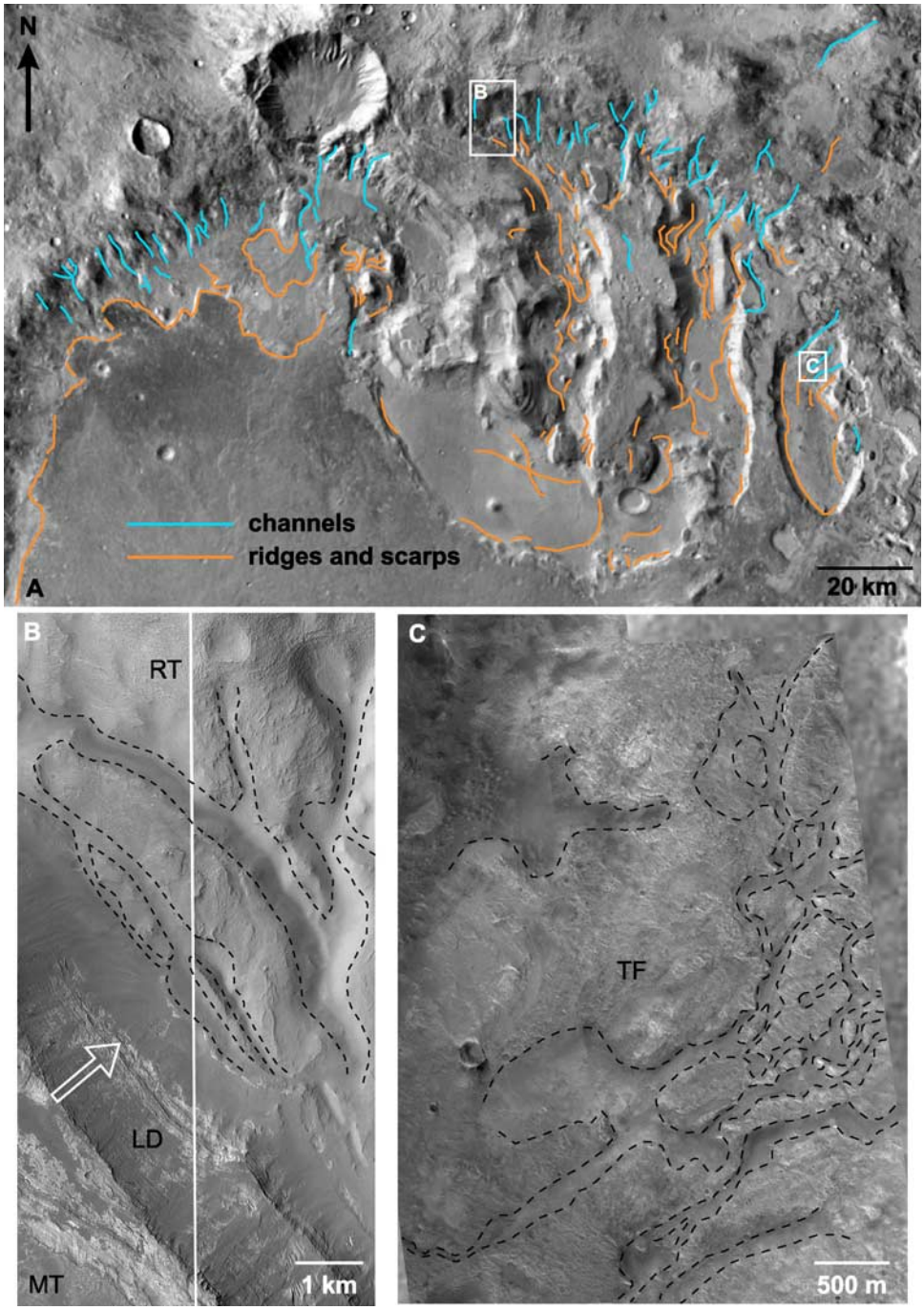

Figure 4. (a) Subframe of THEMIS Day IR mosaic (Christensen et al. data set) detailing channels and ridges and/or scarps that modify the Terby rim (RT), trough floors (TF), interior layered deposits (LD) and moat floor. (b) Channels (outlined with dashed lines) along the northern rim of Terby (RT) converge into the deep TF between the layered benches (hollow arrow points downslope). Image is subframe of MOC NA images R08-00957 and R05-02016. (c) Plateau of sediment incised by a complex channel system (outlined with dashed lines) at the base of an inflow channel at the northern edge of the eastern TF. Image is subframe of MOC NA images E13-02159 and E12-01972.

[17] The remarkable morphology of Terby (Figure 2a) was noted by *Ansan and Mangold* [2004] and *Ansan et al.* [2005, 2006], who identified three geologic units within Terby: (1) layered mesas, (2) a thick, medium-toned layer that occurs on the top of the plateau, and (3) mesas and the floor of the "W-shaped" depression. We further classify the major geomorphic terrains in Terby and its immediate surroundings on the basis of morphology, layering characteristics and tone (i.e., visible albedo) of the material as seen in THEMIS, MOC NA and HiRISE images, and variations in thermal properties based on THEMIS data. The eight terrains (Figure 3) include Layered Deposits (LD) (section 2.2.1),

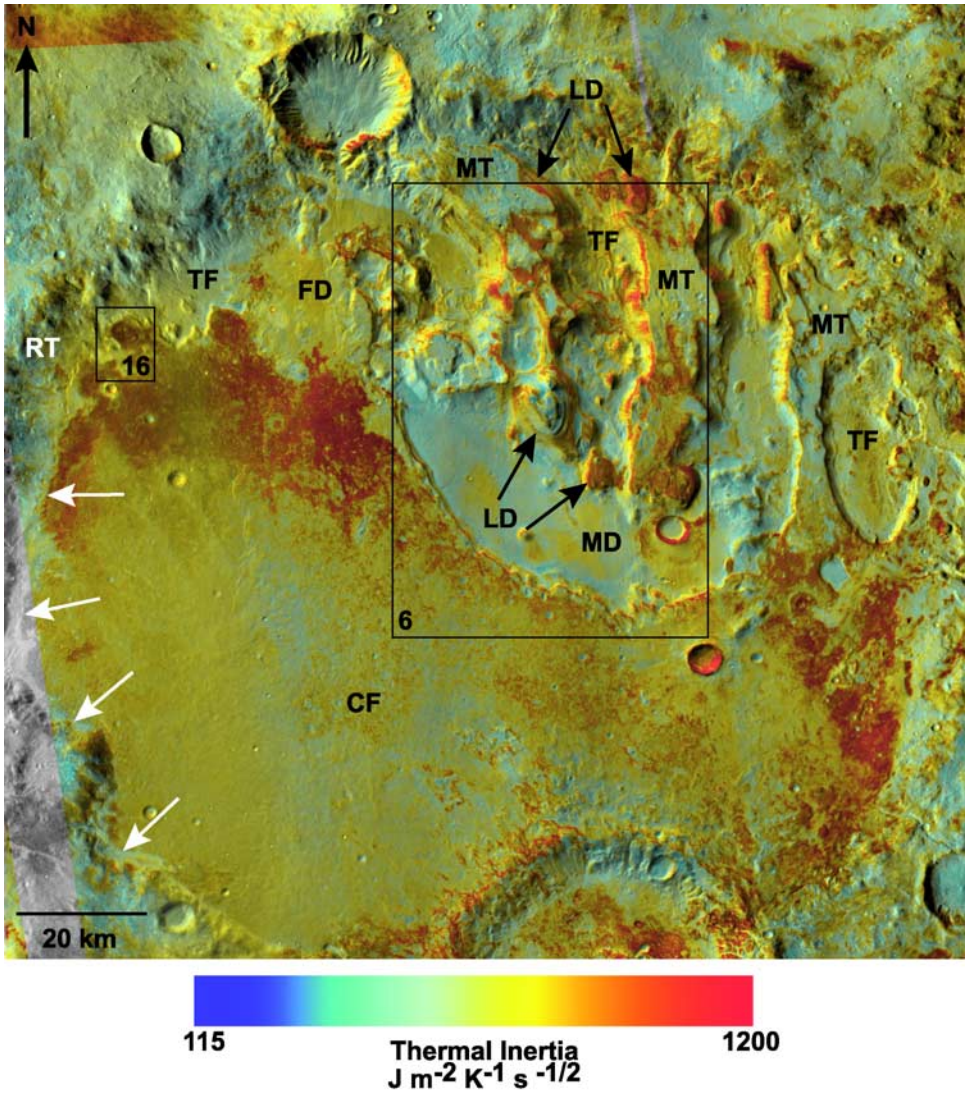

Figure 5. Thermal inertia (TI) on day infrared (IR) mosaic (THEMIS colorized TI mosaic overlaid onto day IR mosaic in online version from Christensen et al. data set). The TI in Terby ranges from 115 to 1200 J m^{-2} K^{-1} $s^{-1/2}$ (see section 2.2 for complete interpretation of the nature of the surface materials in and around Terby and reference Figure 3 for a complete illustration of units). Arrows along western edge of crater floor (CF) illustrate sharp boundary between the smooth (at 100 m/pixel resolution) and nearly level CF deposits and rougher crater rim materials (RT). In the southern part of the image, the CF deposits embay the rim and ejecta from the crater modifying the southern rim of Terby. Boxes show location of Figures 6 and 16a.

flat, dark-toned Mesa Tops (MT) (section 2.2.2), the smooth Crater Floor (CF) (section 2.2.3), the "Moat" Deposit (MD) (section 2.2.4), Viscous flow Features (VF) (section 2.2.5), a Fan Deposit (FD) (section 2.2.6), the Grooved Terrain (GT) and associated landforms (section 2.2.7) and the rough Trough Floors (TF) (section 2.2.8) [*Wilson and Howard*, 2005]. Although these terrains are defined by their broad-scale visual and thermal properties, all except the RT (section 2.1) and possibly the MD are expressions of specific sedimentary deposits. Portions of the LD and the TF are covered by mass-wasted debris derived from backwasting of the LD and MT, in addition to a dark-toned mantling unit (MU) (section 2.2.9) that is a partly eroded, <1 m thick deposit that covered the entire region after most of the other units were deposited and eroded to essentially their present extent.

[18] The thermal inertia (TI) within Terby and the surrounding area, as derived from THEMIS IR data [*Fergason et al.*, 2006], ranges from 115 to 1200 J m^{-2} K^{-1} $s^{-1/2}$ (Figure 5). Blue and red (light and dark in grayscale) correspond to low and high TI values, respectively (Figure 5), and these values represent the uppermost surface-particle sizes [e.g., *Mellon et al.*, 2000; *Christensen et al.*, 2003]. The TI is generally lowest (~300–600 J m^{-2} K^{-1} $s^{-1/2}$) on the floor of the crater (VF) perched on the northwestern rim of Terby (hereafter referred to as "NW crater," Figures 2a and 3), sections of the MT on the western and eastern benches, and the majority of the

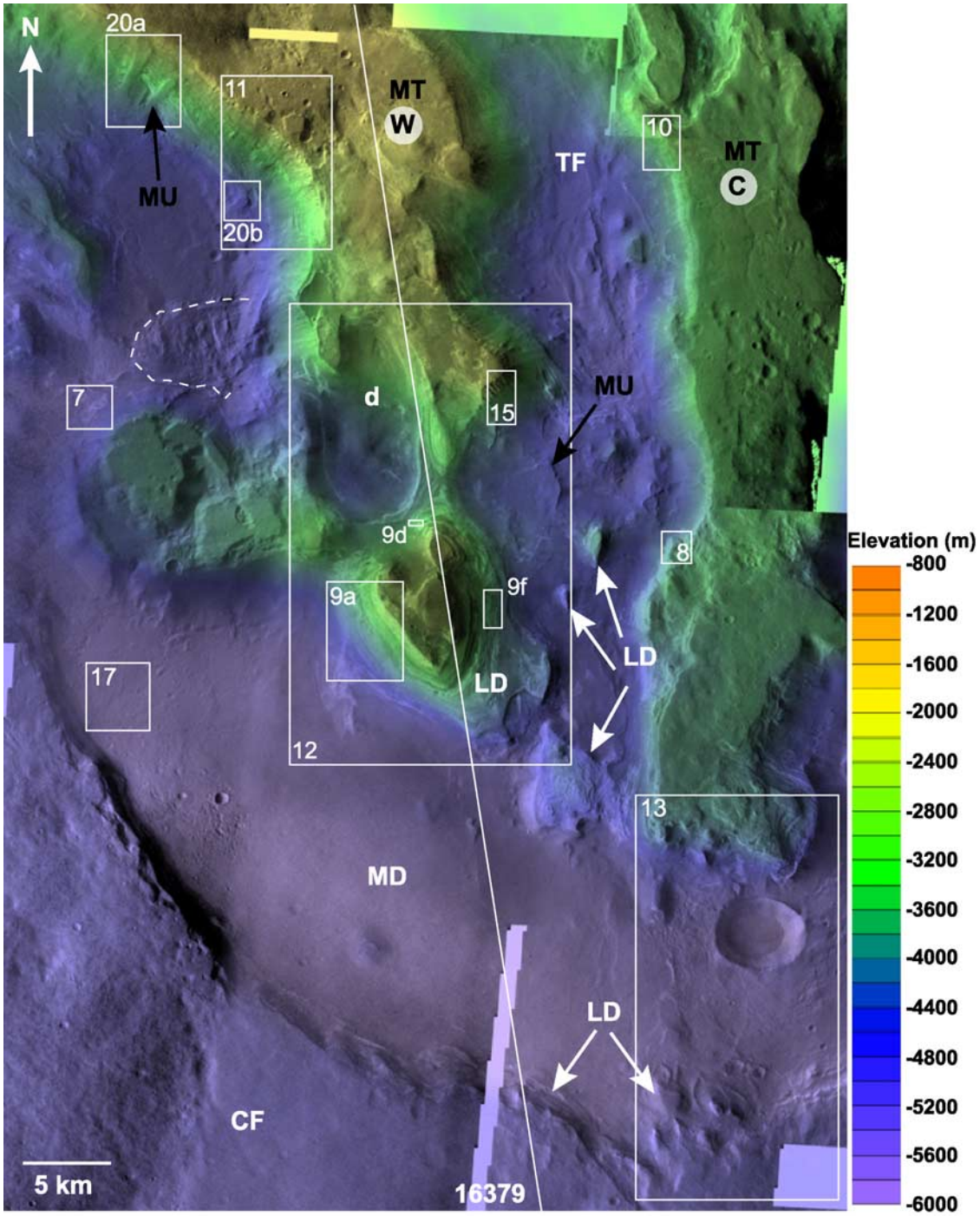

Figure 6. THEMIS VIS mosaic (Christensen et al. data set) (overlaid with MOLA topography in color version online) detailing the western (W) and central (C) layered benches capped by the flat mesa tops (MT) in Terby. Layered deposits (LD) are exposed along the scarps of the benches, along the north-facing scarp of the moat deposit (MD), and as isolated, layered mounds and ridges on the trough floors (TF) between the layered benches. A bowl-like depression ("d") in center of western bench contains light-toned, concentric layers beneath a dark, pervasive mantling unit (MU). Other examples of the MU occur on the TF and as remnant, finger-like ramps in positive relief on the western slope of western ridge (Figure 20). Dashed line indicates massive avalanche deposit; solid line represents MOLA orbit 16379 that corresponds to elevation profile in Figure 12b. Boxes detail location of Figures 7, 8, 9a, 9d, 9f, 10–13, 15, 17 and 20.

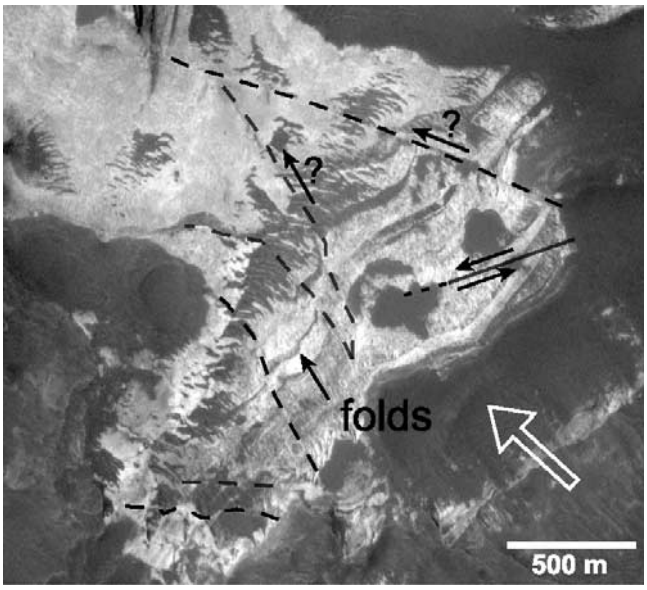

Figure 7. Indurated, light-toned layers in the western bench, often mantled by dark-toned material, preserve evidence of faulting (observed offset indicated by solid line, and possible offsets shown by dashed lines) and possible folds (hollow arrow points downslope; see Figure 6 for context). Note sparse cover of dark-toned dunes in center of image. Image is subframe of MOC NA image M10-03145; top of image is north.

MD floor including the isolated mound of RT (Figure 3), likely corresponding to a fine-grained dust cover [*Mellon et al.*, 2000; *Christensen et al.*, 2003]. The majority of the landforms within Terby have an intermediate TI ($\sim$600–800 J m^{-2} K^{-1} s$^{-1/2}$), including the TF, the majority of the CF and FD, the MT on the central bench, patches on the floor of the MD, and LD obscured by mantling material. The physical properties of material that exhibit intermediate values of TI could represent a surface covered with well-sorted submillimeter-scale particles (i.e., sand sized), finer-grained material that is indurated into a crust (i.e., well-cemented), or a surface with a few percentage block cover within a matrix of fines [e.g., *Christensen*, 1986; *Jakosky and Christensen*, 1986; *Mellon et al.*, 2000]. The northwestern and southeastern CF, "fresh" exposures of LD and the GT on the surface of the FD have the highest TI values, approximately 900–1200 J m^2 K^{-1} s$^{-1/2}$, possibly representing a combination of coarse sand, strongly crusted fines, abundant rocks, and/or scattered bedrock exposures [*Mellon et al.*, 2000].

2.2.1. Layered Deposits (LD)

[19] The northern portion of Terby exposes thick sequences (up to $\sim$2.5 km) of primarily light-toned layers (LD) (Figure 3) that extend as benches (we use "bench" in the sense of a long, nearly planar surface dropping off steeply on one or both sides) from the northern rim of Terby to the center of the crater (Figure 2a). The western and central benches strike north/northwest and are $\sim$60 km and 55 km long, respectively, with relatively constant widths of $\sim$10 km (Figure 6). The mean north-south surface gradient of the western and central benches is 20 m/km (1.1°) and 15 m/km (0.9°) to the south, respectively, reflecting the overall gradient of Terby (17 m/km). Although the western and central benches terminate abruptly at elevations several hundred meters above the moat to the south (Figures 2a and 2b), the easternmost bench descends as a $\sim$5-km-wide ramp toward the main CF that is isolated by a large, bowl-like depression on its eastern side. The eastern ramp may provide an "unbroken" connection between the LD in the benches and the layers in the CF, but the dearth of MOLA tracks and high-resolution images in this area leave the topography and stratigraphic relationships difficult to characterize. Layers are primarily exposed along the scarps of the benches and are also present on the TF between the benches, in the walls of depressions, in craters on the CF and MD, and exposed by scarps in the CF (section 2.2.3.) (Figure 6).

[20] The LD are inferred to be partially indurated and predominantly fine-grained on the basis of their appearance, preservation of fractures, possible folds and fault contacts (Figure 7), their ability to form steep scarps (e.g., Figures 6–9), ease of erosion (Figure 8) and thermal signature (Figure 5). Despite the fine-grained nature of the sediment, the layered slopes are partially covered with talus that contains numerous boulders, typically 0.5 m to over 2 m in diameter (smaller boulders at or below the resolution of HiRISE images likely exist). The boulders are eroding from fine-grained, indurated layers lower in the sequence that weather along multimeter-spaced joints (Figure 9b) as well as apparently boulder-rich layers near the top of the sequence (Figure 9c). The layers are generally exposed by differential weathering of subhorizontal (inclined less than 10°) bedding units [*Ansan and Mangold*, 2004; *Ansan et al.*, 2005, 2006] and are laterally continuous on a kilometer scale.

[21] Several layered scarps in Terby exhibit a scalloped texture that we interpret to be the result of aeolian deflation (Figure 8). The aligned ridges are similar to terrestrial and Martian yardangs [e.g., *Ward*, 1979; *Malin and Edgett*, 2001], but yardangs typically feature aligned, nearly flat-floored troughs that serve as corridors for saltating sand whose abrasion is largely responsible for eroding the yardangs. Flat-floored troughs are not apparent on the scallops that have eroded into the LD. Rather, the broadly concave depressions with sharp, aligned ridges appear to be more analogous to fluting eroded by currents in soft sediment and to similar solutional features in limestone [e.g., *Allen*, 1984, pp. v2-253–v2-291]. The occurrence of fluting rather than yardangs in Terby may be related to the size of the material in the layers, that is, the grains plucked by wind are not coarse or durable enough to cause subsequent abrasion and sand sized particles are not present in sufficient quantity to accumulate in the troughs or as dune fields. Dunes occur at scattered locations within Terby (e.g., Figure 7), but they are not as prevalent as might be expected if the observed wind erosion were deflating LD composed primarily of sand-sized sediment. The observed dunes are also dark-toned, suggesting that if they are derived from erosion of the LD, they represent a minor component of the LD. The dunes are similar in tone to the dark mantling materials that may be derived in part from the LD.

[22] Typically, most exposures of layered sequences in Terby are at least partially obscured by material mantling the slopes (Figures 6–11). Although physical correlation of layered sequences over long distances could not be

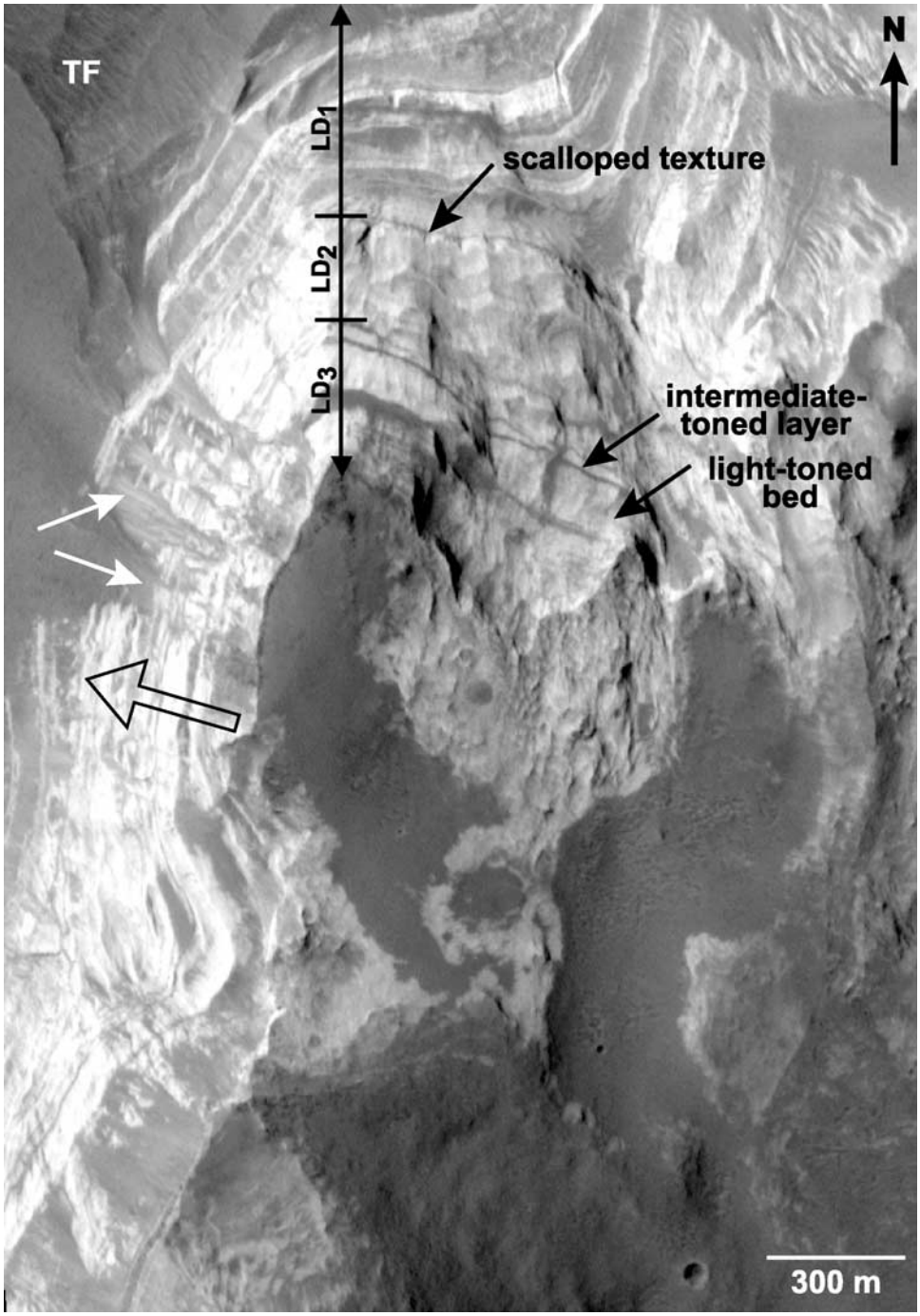

Figure 8. The massive, cliff-forming nature of the light-toned and intermediate-toned layered deposits (LD) is detailed along the western scarp of the central bench (hollow arrow points downslope; see Figure 6 for context). Presumably loose, granular material (white arrows) commonly cascades down slopes and obscures the LD. The shallow scalloping along the northern edge is suggestive of aeolian deflation. A tentative correlation of stratigraphic subunits with those in the western bench (Figure 9) is indicated: Subunits 1 (LD_1) and 3 (LD_3) are characterized by alternating light- and intermediate-toned layers separated by subunit 2 (LD_2), a light-toned bed lacking obvious layering at MOC NA scale. Subunit 4 (LD_4) is not present at this location. Image is subframe of MOC image R03-01404.

conducted owing to mantling covering critical places along the slopes, detailed analysis of the layers in the central (Figures 8 and 10) and western (Figures 9, 11, and 12) benches using THEMIS VIS, MOC NA and HiRISE images revealed the presence of four distinct subdivisions within the stratigraphic sequence. Subunits 1 (LD_1) and 3 (LD_3) are characterized by regularly interbedded light- and intermediate-toned layers, subunit 2 (LD_2) is a predominantly

light-toned, deformed or poorly bedded unit, and subunit 4 (LD_4) contains light-toned layers that are "sandwiched" between distinctive dark-toned layers composed of boulder-sized clasts at the top of the sequence. The "tone" of the material refers to the relative brightness (i.e., visible albedo) as seen in MOC NA and HiRISE images [*Malin and Edgett*, 2000]. "Light-toned" describes a feature that is relatively bright, "dark-toned" implies a qualitatively low albedo and "intermediate-toned" describes material that is in between "light-toned" and "dark-toned" [*Malin and Edgett*, 2000].

[23] The stratigraphy is best exposed in a ~2-km-thick layered mesa at the southern end of the western bench (Figure 9a; see Figure 6 for context). Stratigraphically lowest, LD_1 is at least 1000 m thick (a lower boundary is not visible) and is characterized by laterally continuous, thin (~1–25 m thick) intermediate-toned layers interbedded with thicker (typically ~80 m thick, ranges from ~10 to over 150 m thick) light-toned beds (Figure 9b).

[24] The regularity in which these layers are interbedded with the light-toned beds may be indicative of climatic modulation of deposition rates, perhaps in response to quasicyclical orbital variation [*Laskar et al.*, 2004]. The intermediate-toned, indurated, meter-scale layers do not appear to be finely interbedded (although layering may exist below the resolution limit of HiRISE images) and weather along multimeter spaced joints to produce meter-scale boulders (Figure 9b). The downslope movement of the boulders in some cases is evident from boulder tracks on the slopes (Figure 9b). The light-toned beds are highly fractured and appear nearly homogenous on the western face of this

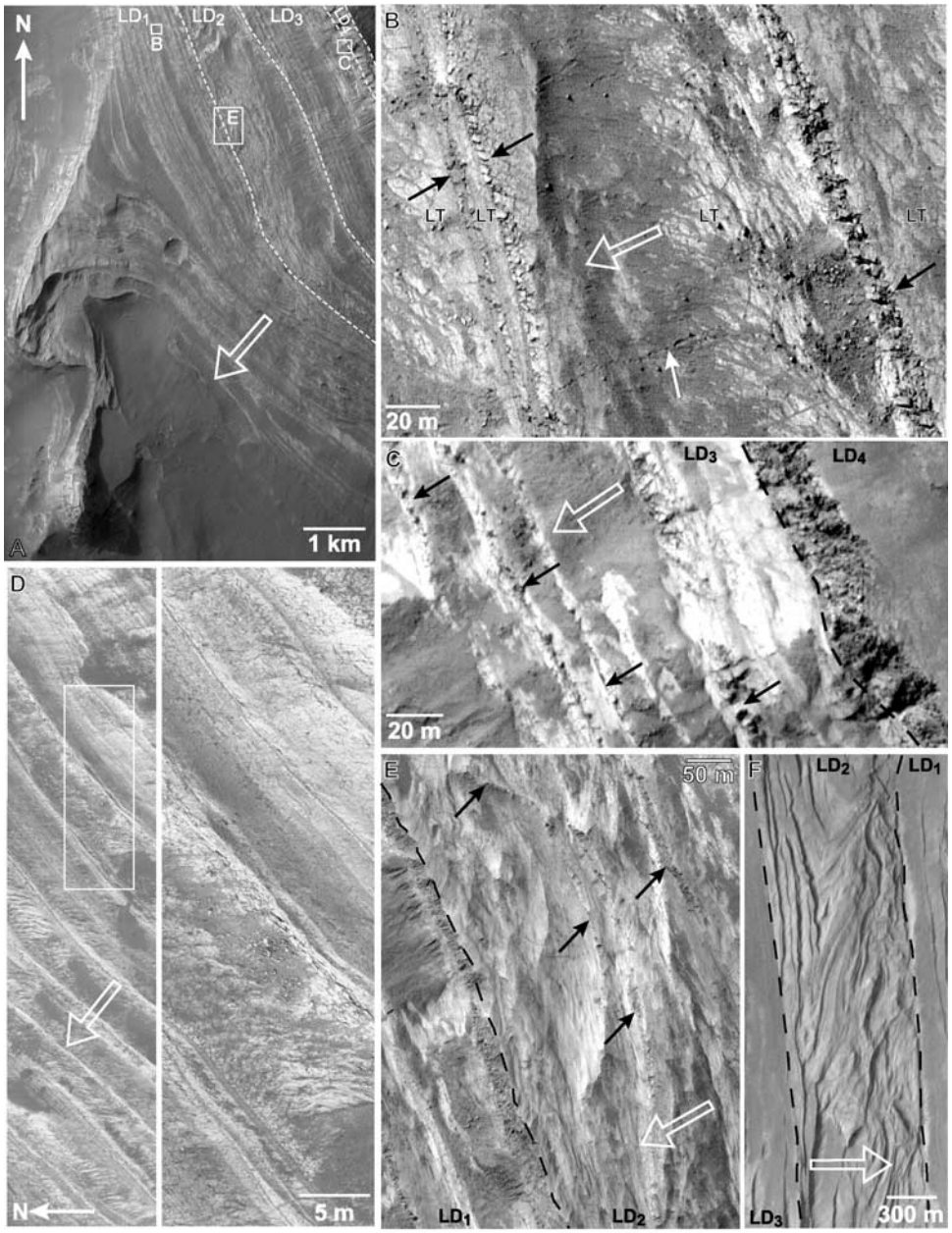

Figure 9

mesa although there are hints of submeter-scale layers or laminations. The nature of these light-toned beds is obscured in this location both by remnant granular material that has cascaded downslope from erosion higher on the layered scarp as well as mantling from darker, residual dust or fine-grained material deposited as part of a mantling unit (MU) (Figure 9b). A HiRISE image of layers in LD_1 along the northern face of this mesa, however, reveals fine-scale (submeter), continuous layers that are indicative of deposition from suspension (Figure 9d). The difference in surficial mantling (probably reflecting variations in slope steepness) and contrast in tone of layers within this unit suggests differences in composition such as grain size or degree of cementation or induration.

[25] The contact between LD_1 and LD_2 is well-defined, likely representing an unconformity and/or change in depositional environment (Figure 9a). LD_2 is light-toned, roughly 400 m thick at this location, and is characterized by irregular, nonhorizontal, discontinuous and folded (?) beds of varying thicknesses as well as horizontal bedding (Figure 9e). Hints of submeter-scale layers or laminations exist within the thicker, light-toned sections on the western face of the mesa. The curved, discontinuous beds are intermediate-toned and appear similar to the fine-grained, indurated, intermediate-toned layers in LD_1 and LD_3 (Figures 9b and 9c). Assuming that a discontinuous mantle and loose, granular talus emplaced on LD_2 is not responsible for the appearance of varying layer thickness and possible folds, there are several distinct processes and related environments that could have created these curved, discontinuous beds and apparent folds, including large-scale aeolian dunes, dune-like structures related to pyroclastic surge deposits [*Fisher and Schmincke*, 1984], deformation of solid rock, diapiric intrusions related to ductile evaporate beds within the sequence, or soft sediment deformation (SSD) [*Allen*, 1984]. Although aeolian cross-bedding and structures related to pyroclastic surge deposits can vary in morphology and size on the basis of the depositional regime, the observation of curved, discontinuous beds, possible folds and evidence of horizontal bedding in the same subunit does not favor these processes. Deformation related to tectonic activity is also possible, although it is not likely that the layer was solid at the time deformation occurred because the underlying unit does not appear to be highly deformed with the exception of some preserved faulting (Figure 7), suggesting that the structures are likely inherent to the subunit itself.

[26] Discerning between primary sedimentary features of the bed, such as cross-bedding or turbidity current deposits, and secondary features related to postdepositional, SSD, such as folding, slumping and intrusions, is difficult at MOC NA, and even HiRISE resolution. However, on the basis of the presentation of the layers in Terby, the scale of the deformation structures, and the regional context of the Hellas impact basin, SSD is a likely process.

[27] Structures related to SSD typically occur on a centimeter-to-meter scale when liquidized, hydroplastic sediment (commonly loosely packed cohesionless sand or coarse silt rather than gravel or cohesive mud) is stressed during deposition or shortly after burial [*Allen*, 1984]. Deformation structures related to SSD, such as folds, hummocky topography, domes, wavy ridges, pipes, dish structures and ball and pillow structures [*Owen*, 1995], are prevalent in water-laid environments, such as deep-water

Figure 9. Layered deposits in the western bench (hollow arrows point downslope). (a) Detail of ~2.5-km-thick layered sequence exposed on the western bench in HiRISE image 1662–1520 (see Figure 6 for context). Dashed lines show contacts between subunits that may correlate to the central bench (Figure 8). Subunits 1 (LD_1) and 3 (LD_3) are characterized by alternating light- and intermediate-toned layers separated by subunit 2 (LD_2), a light-toned bed that lacks regular, horizontal layers. Subunit 4 (LD_4) is an intermediate-toned, massive layer "sandwiched" between distinctive thin, dark-toned layers. The layered sequence is capped by a flat mesa top (MT), as seen in the upper right-hand corner of image. Boxes show details of LD_1 (Figure 9b), the contact between LD_3 and LD_4 (Figure 9c), and the contact between LD_1 and LD_2 (Figure 9e). NASA/JPL/University of Arizona. (b) LD_1 in the western bench is characterized by thicker, light-toned (LT) beds interbedded with thin, intermediate-toned layers (black arrows) that are weathering along meter-spaced joints to produce boulders. The boulders accumulate on the slopes and their downslope movement is often recorded by boulder tracks that can be over 1 km long (e.g., white arrow). Although the LT beds are typically heavily mantled, there are hints of finer layers or laminations at HiRISE resolution (28 cm/pixel). Subframe of HiRISE image 1662–1520; top of image is north. (c) Distinct contact between LD_3 and LD_4 (dashed line) is marked by a dark-toned, boulder-rich layer that is weathering to produce meter-scale boulders that accumulate on slopes. LD_3 is characterized by thicker light-toned beds interbedded with thin, indurated, intermediate-toned layers (black arrows). The slopes are generally obscured with talus derived from backwasting of the layers and the MT themselves, as well as the residual, dark-toned mantling unit (MU). Subframe of HiRISE image 1662–1520; top of image is north. (d) Subframe of HiRISE image 1596–1525 (left) showing submeter-scale layering within LD_1 in the western bench that is indicative of deposition by suspension (see Figure 6 for context). Inset (right) highlights differences in the tone (visible albedo) of the layers, perhaps indicative of varying mineralogy. At least one light-toned bed is weathering to produce boulder-sized clasts that accumulate downslope. North to left of image. NASA/JPL/University of Arizona. (e) The contact between LD_1 (lower left) and LD_2 (upper right) is very distinct (dashed line) in the western bench. LD_2 is predominantly light-toned and is characterized by irregular, nonhorizontal, discontinuous (folded?) beds of varying thicknesses (arrows) as well as horizontal bedding. Hints of submeter-scale layers or laminations exist within the thicker, light-toned sections on the western face of this mesa. Image is subframe of HiRISE image 1596–1525; top of image is north. (f) Distorted, nonhorizontal nature of the bedding in LD_2 is also observed on the eastern face of the layered mesa (see Figure 6 for context). The well-defined contacts between LD_1, LD_2 and LD_3 (dashed lines) likely represent an unconformity and/or change in depositional environment. Image is subframe of MOC image R05-01482; top of image is north.

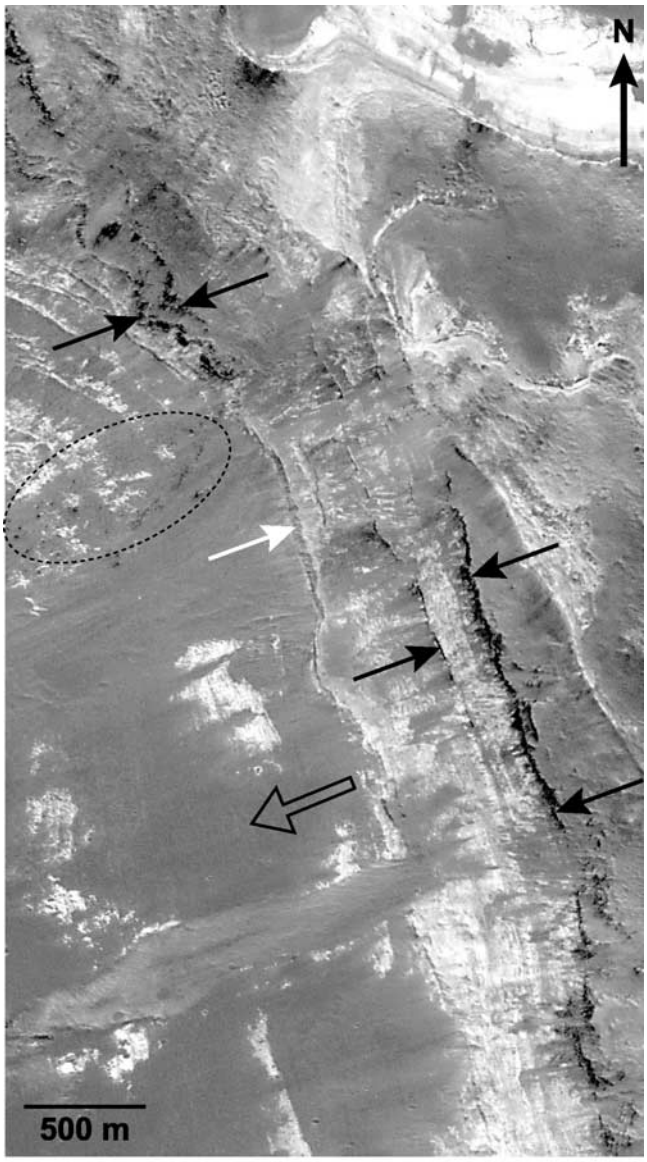

Figure 10. Detail of subunit 4 (LD_4) at the top of the stratigraphic sequence in the northwestern scarp of the central bench (hollow arrow points downslope; see Figure 6 for context). A massive (or finely bedded) light-toned layer is sandwiched between two thin, dark, knobby layers (black arrows). The dark layers in some cases appear to be weathering nonuniformly into a small-scale knobby surface, perhaps representing a more resistant material. Dark, boulder-sized clasts on the slopes (e.g., dashed line) are presumably derived from the dark layers, suggesting that these layers are more indurated and are either coherent beds that break down along widely (multimeter) spaced fractures or they occur as beds of multimeter-scale clasts. The latter is the case if this subunit correlates to LD_4 in the western bench (Figure 9c), which cannot be unequivocally determined owing to the lack of high-resolution imaging. The correlation between the dark layers at the top and bottom of the image is uncertain owing to partial mantling. A resistant, intermediate-toned layer of variable thickness (white arrow) correlates to unit LD_3. Image is subframe of MOC image R12-00672.

basins subject to turbidity currents, shallow-water marine environments, deltas and river floodplains [*Allen*, 1984]. Triggers forming these structures include mass movements [*Reading*, 1996], impact cratering [*Alvarez et al.*, 1998], instabilities related to slope or sediment burial or load [e.g., *Sarkar et al.*, 1982], tectonic activity [e.g., *Silva et al.*, 1997; *Alfaro et al.*, 1997; *Heifetz et al.*, 2005], glacial activity [e.g., *Van der Wateren*, 1995; *Iverson*, 1999] or wave action and tsunamis [e.g., *Dalrymple*, 1979; *Rossetti et al.*, 2000]. Many of the postulated triggers are plausible given the regional context of the Hellas impact basin.

[28] LD_3 is ~500 m thick and occurs near the top of the stratigraphic sequence (Figure 9a). Like LD_1, LD_3 is characterized by regular, laterally continuous beds with relatively constant thicknesses. There are two, ~10-m-thick, intermediate-toned beds at the base of this unit and approximately six, ~1- to 10-m-thick, intermediate-toned beds at the top of the sequence interbedded with thicker, light-toned beds (Figure 9c). The layering in the lower section of this unit, however, is expressed by subtle changes in slope that causes differential mantling of the layers, not as layers with contrasting tone (Figure 9a), possibly representing differences in cementation rather than mineralogy. Despite the fractured nature of these beds and the pervasive mantling, hints of small-scale layering or laminations within the light-toned beds are visible at HiRISE resolution.

[29] The layered sequences in the western (Figures 9 and 11) and central (Figure 10) benches are capped by LD_4, a ~100-m-thick unit that is characterized by light-toned layers "sandwiched" between distinctive dark-toned, rubbly layers. These dark-toned layers appear to consist of large, resistant, meter-scale clasts as opposed to indurated beds that break down along widely (multimeter) spaced fractures as seen in LD_1 (Figure 9b) and LD_3 (Figure 9c). These rubbly layers are weathering nonuniformly into a small-scale knobby surface to produce several meter-scale boulders that accumulate on the slopes. The boulder-rich layers in the western bench are approximately 5–15 m thick although the thickness varies along strike (Figure 9c).

[30] Owing to difficulties associated with tracing layers obscured by mantling, varying resolutions between images and differing slope angles, a unique "marker bed" or specific sequence of layers could not be traced (correlated) between the layered mesa discussed above and the western-facing slope on the same bench, located approximately 40 km to the north (Figure 11; see Figure 6 for context). The steep (~20°), ~2.5-km-thick, western-facing slope at the northern end of the western bench, however, exposes a similar sequence of regular, subhorizontal and interbedded light- and intermediate-toned layers at the base and stratigraphically near the top of the bench (interpreted to correspond to LD_1 and LD_3, respectively) separated by a poorly bedded section (LD_2) that is capped by distinctive dark-toned layers (LD_4) (Figure 11a). A few "windows" through the mantling material obscuring LD_2 at this location shows layers with irregular strike that may be broadly distorted, and do not appear as regularly bedded as LD_1 and LD_3 (Figure 11b). It is uncertain whether the layers between 'x' and 'y' correlate to LD_1 or LD_2; the layers in this sequence appear more similar to the regularly bedded nature of LD_1, despite their unconformable dip (Figure 11b). It is possible, however, that the sequence between 'x' and 'y' is part of LD_2.

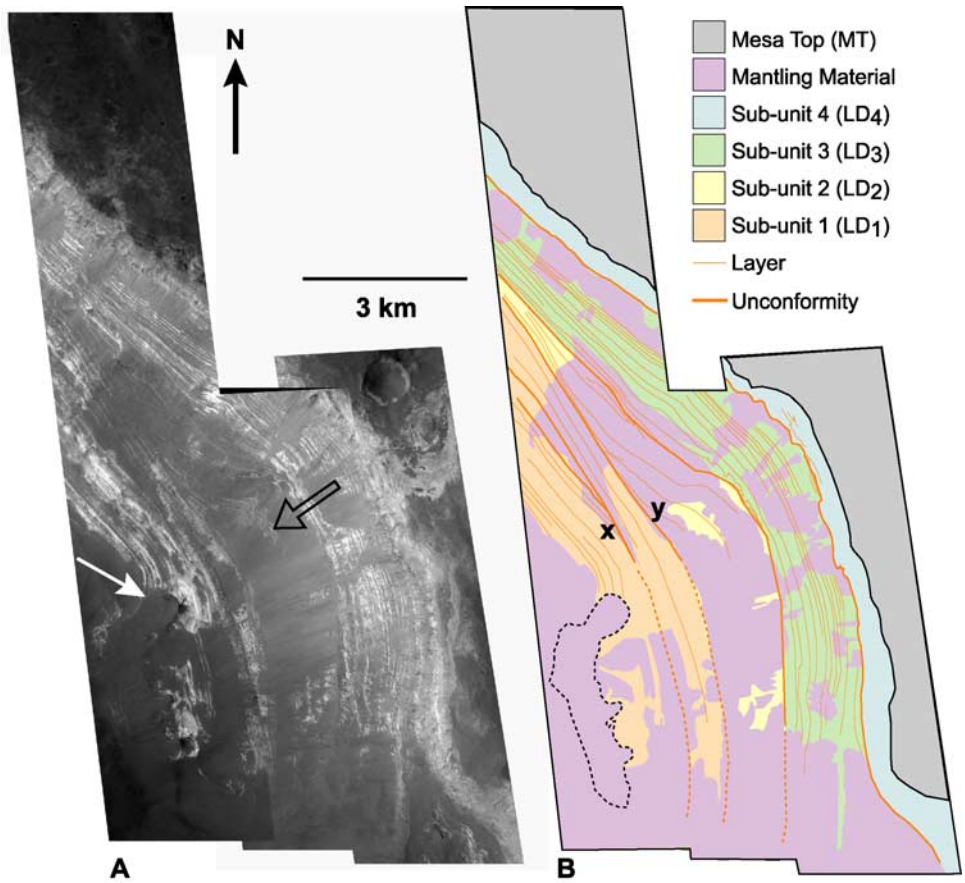

Figure 11. (a) Detail of layered sequence on northwestern slope of western bench (hollow arrow points downslope; see Figure 6 for context). The base of the bench is mantled by a dark and presumably indurated material (MU) as evidenced by the rounded, positive-relief lobe with prominent scarp edges that exposes underlying layers (white arrow; see Figure 20b). Mantling materials of two ages are present; the older is the darker-toned mantling unit at the slope base etched into positive relief, and the younger is the slightly lighter-toned, granular material obscuring the layered slope that has presumably eroded from the layers and/or mesa tops (MT). Image is from MOC images R09-00856, R08-00448 and R08-01718. (b) Geomorphic map detailing subunits that may correlate to the subunits in the mesa at the southern end of the western bench (Figure 9) and the central bench (Figure 8). Light lines indicate lateral continuity of layers in each unit that could be identified beneath the pervasive mantling covering the slopes. Thick solid and dashed lines represent unconformities and/or proposed divisions between subunits (enclosed black dashed line in lower left represents boundary of the older, indurated MU that is raised into relief). The layers in LD_1 and LD_3 appear more regularly bedded than LD_2, whose layers may be broadly distorted and exhibit an irregular strike. The layers between 'x' and 'y' are dipping more steeply than the underlying layers, and although their fairly regular bedding is more consistent with the nature of LD_1, this sequence may be part of LD_2.

Unlike the sequence in the mesa to the south, LD_2 and LD_3 are separated by an angular unconformity [*Ansan et al.*, 2005] (Figure 11b). The upper units in this exposure, correlating to LD_3 and LD_4, appear to be conformable with the surface of the bench, which slopes southward at about 1.1°.

2.2.1.1. Correlation of Layers Across Troughs

[31] An unambiguous correlation of individual layers across the trough between the western and central benches is inhibited by image resolution and mantling material on the slopes, but we suggest a correlation between subunits exposed on the sides of the central bench (Figure 8) with those of the western bench (Figures 9 and 11). If correct, this correlation indicates that the layers once extended across the troughs as a continuous deposit, as further evidenced by the isolated, horizontally layered mounds on the TF between the benches (Figure 6). This correlation remains tentative, however, because of the large difference in elevation between the western and central bench tops.

[32] The elevation of the western, central and eastern benches decreases from west to east, but this decrease does not define a smooth, southeastward dipping surface (Figures 2a and 2d). MOLA data indicates that the bench surfaces are nearly planar, they dip primarily towards the south (Figures 2a and 2b), and are nearly horizontal in the east-west direction (Figure 2d, profiles 1–3). Thus there are step, rather than smooth, decreases in elevation in bench-top

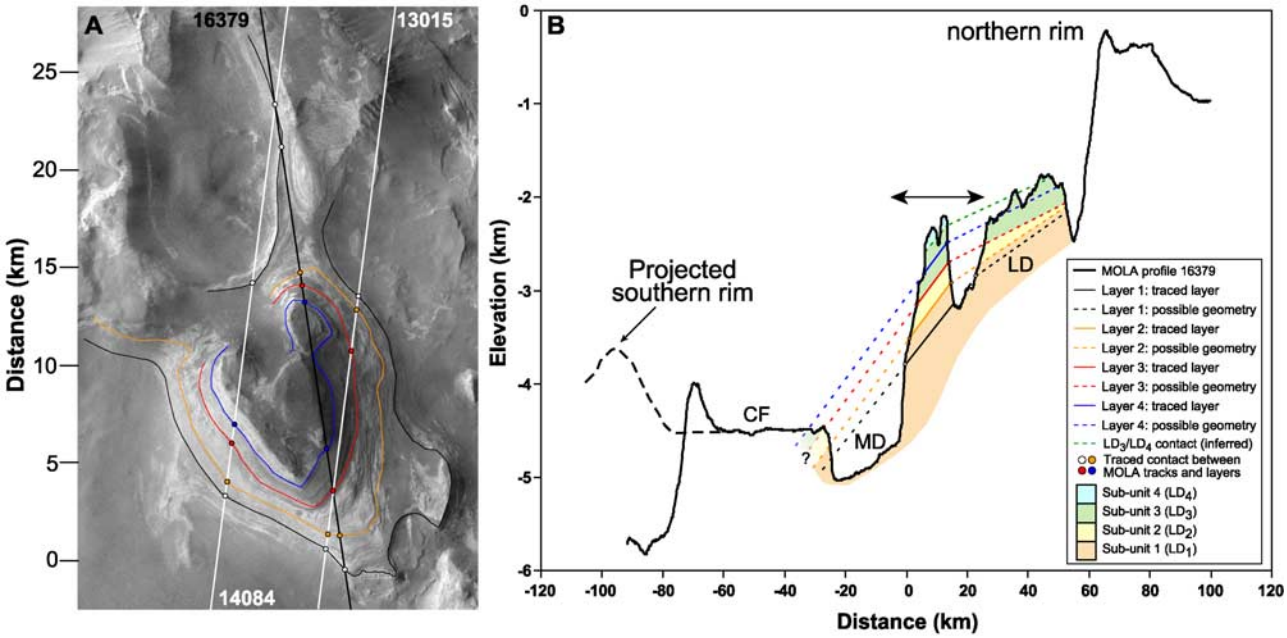

Figure 12. (a) THEMIS VIS mosaic map (Christensen et al. data set) showing location of the four marker beds and MOLA orbits used to estimate the dip of the layered deposits at the southern end of the western bench (see Figure 6 for context). The marker beds occur within unit LD_1 (layer 1), at the contact between LD_1 and LD_2 (layer 2), at the top of LD_2 (layer 3) and within LD_3 (layer 4). The elevation of the marker beds on the southern and northern end of the mesa (derived from MOLA orbits 13015, 14084, and 16379) resulted in nearly parallel bedding sloping about 3° southward along-track, as illustrated by solid lines in Figure 12b. Distance in kilometers corresponds to Figure 12b and is referenced to Figure 2a. Top of image is north. (b) Profile illustrates the geometry of the layers traced in Figure 12a using MOLA orbit 16379 (see Figure 6 for context; double-headed arrow shows approximate area represented in Figure 12a). Solid lines represent dip of layers in mesa as determined from contacts between traced layers and MOLA data in Figure 12a. The possible geometry of the layers to the north and south of the mesa is shown by dashed lines. Vertical exaggeration is 30X; distance in kilometers corresponds to distances in Figures 12a and 2a.

elevation progressing from the western to the eastern benches, with a roughly 1000 m drop from the western to the central bench, and an additional 800–1000 m drop to the eastern bench.

[33] The step decrease in bench height from west to east (Figure 2d) could indicate at least three scenarios about the layer relationships between the three benches. The first is that layer sequences in the three benches are uncorrelated, possibly reflecting a temporal lateral migration in deposition site. In this scenario, the trough locations would presumably be related to processes associated with the lateral shifts, and layers might never have extended across the present troughs. A second possibility is that the lower subunits correlate across the three benches (also suggested by the lateral continuity of layering exposed in the southern wall of the MD), but the eastern limit of deposition episodically shifted westward. A third scenario is that the layers initially formed a coherent deposit across the northern half of Terby (although possibly thickening to the west), but the upper surface of the LD is a result of erosional planation, with erosion occurring at sequentially lower levels and the site of erosion shifting to the east. We favor the latter two scenarios because we find no evidence suggesting that the original extent of layers was limited by location of the present troughs and isolated mounds exhibiting horizontal layers exist on the TF between the western and central benches (Figure 6), suggesting lateral continuity of the original layers. Under the first scenario we would expect, but do not see, evidence of change in facies, thickness, or dip associated with the lateral edges of the benches, or associated structural features such as slumps or trough-paralleling faults with large displacements.

2.2.1.2. Depositional Geometry and Original Lateral Extent of the Layers

[34] The abrupt southward termination of the layered benches at the northern end of the moat deposit (MD) is difficult to interpret in terms of the original depositional geometry and extent of the LD as well as the origin of the troughs and moat (Figure 2). The three-dimensional structure of the layers, and in particular, whether they are level or sloping is potentially diagnostic of their composition and origin. Although extensive mantling prevents physical correlation of layers along the entire length of the benches, the mesa at southern end of the western bench (Figure 12a) lacks appreciable obscuration by thick mantling material. Four marker beds on the southeastern flank of the mesa were defined in MOC NA images and traced counterclockwise around the mesa and the lowest bed (layer 1) was traced across the domical exposure north of the mesa. These marker beds occur within unit LD_1 (layer 1), at the contact

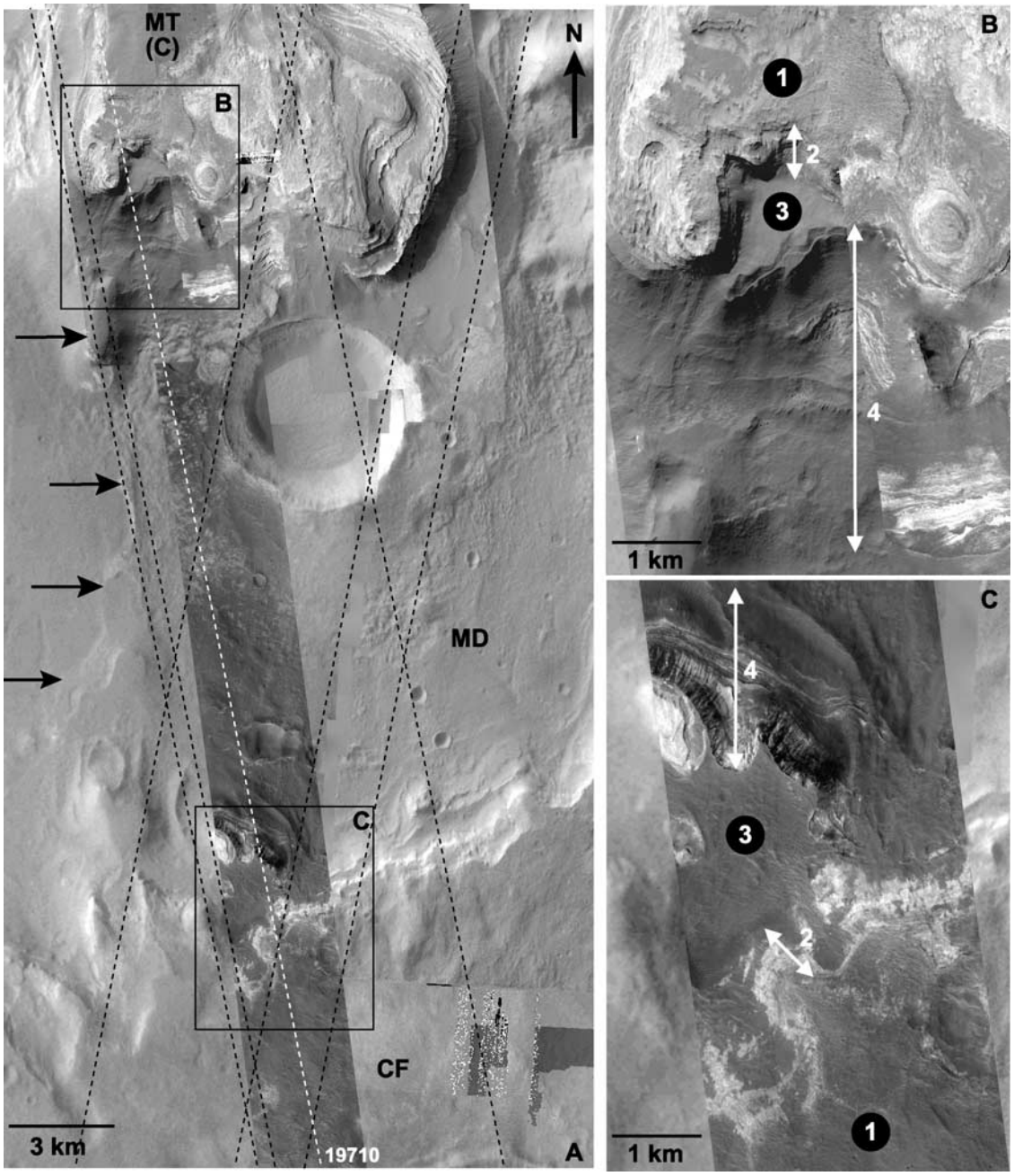

Figure 13. (a) Detail of the layers at the southern end of the central bench and the ~400 m of layering exposed along the southern scarp of the moat deposit (MD) wall (see Figure 6 for context). Available MOLA orbits in this area (dashed lines) were used to assess possible correlations between the layers across the MD, and a portion of MOLA orbit 19710 (white dashed line) is shown in Figure 14. Arrows point to a possible sedimentary ridge of layers extending across the floor of the MD. Boxes show location of Figures 13b and 13c. Image is from THEMIS VIS images V10446001 and V03356003 and MOC NA images R03-01404, R03-00753, R03-01060, R12-00951 and M19-01933. (b) Detail of layers at southern end of central bench. Units 1 (topographic high) through 4 (topographic low) may correlate to the same units in the CF detailed in Figure 13c. Image is from subframes of MOC images R12-00951 and M19-01933. (c) Detail of layered sequence in the CF exposed along the southern wall of the MD, roughly 20 km south of the layers in Figures 13b; units 1 (topographic high) through 4 (topographic low) potentially correlate to the same units in Figure 13b. Image is subframe of MOC image R12-00951.

between LD_1 and LD_2 (layer 2), at the top of LD_2 (layer 3) and within LD_3 (layer 4) (Figure 12). Because of heavy mantling of the northwestern flank of the mesa, layers could not be completely followed around the mesa. Owing to relief distortion inherent in high-relief terrain from non-vertical MOC NA images, layer traces identified in MOC NA images were transferred to a THEMIS VIS mosaic base map (Figure 12a). The VIS mosaic with the traced layers

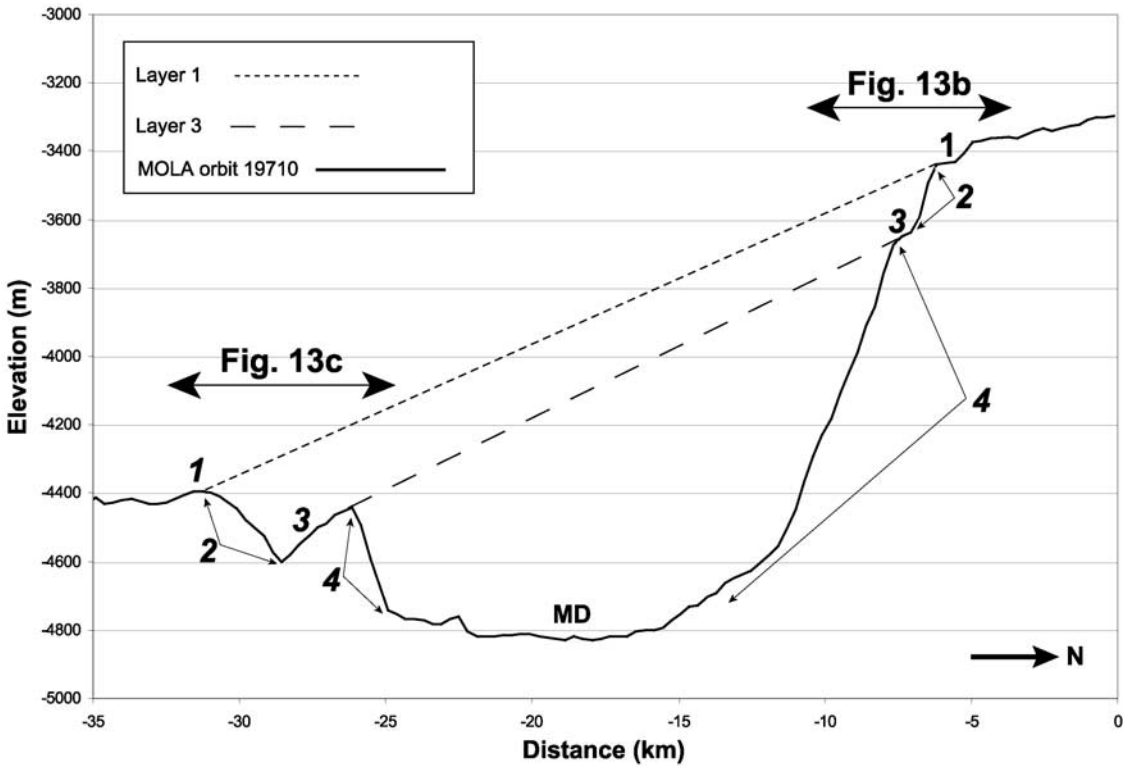

Figure 14. Topographic profile of moat deposit (MD) from MOLA orbit 19710 (see Figure 13a for context) and possible correlation of units 1–4 from observations in Figure 13b and 13c (double headed arrows represent approximate extent of each figure). The slope of layers 1 and 3 across the MD are approximately 2.2° and 2.4° to the south, respectively.

was overlaid onto a topographic contour map of Terby produced from MOLA data in the commercial program SURFER® (Figure 12a). Twelve MOLA orbits cross the mapped mesa, and the coordinates of the crossings of the four traced layers was noted for three MOLA profiles crossing the top of the bench (orbits 13015, 14084 and 16379). The bed crossings were marked on profiles of the MOLA orbits, giving an approximate elevation of the exposed beds on the southern and northern end of the mesa. All profiles provided a consistent picture of nearly parallel bedding sloping about 3° southward along-track. Orbit 16379 was selected for stratigraphic interpretation (Figure 12b) because it extends northward across most of the western bench and southward across the moat and onto the flat crater floor (Figure 6).

[35] Although the thick layered benches abruptly terminate at the northern end of the MD, the southern scarp of the moat wall exposes roughly 400 m of layers (Figure 13a; see Figure 6 for context). Horizontal banding, assumed to be expressions of layering, also occurs in crater walls on the MD and CF. The smooth topography of the CF suggests there is flat-lying material beneath the surface but the presence of layering and correlation of layers with other outcrops cannot be readily determined because of lack of exposure, the mantled surface, and dearth of high-resolution images in the southern portion of Terby. If the layers at the southern end of the western bench, dipping at about 3° southward, are projected ~20 km across the MD, most of the layered sequence would intersect the moat scarp (Figure 12b). Although the exact geometry of the layers at the northern end of the western bench is unknown, we suggest the upper units (LD_3 and LD_4) decrease in dip to be conformable with the top surface of the bench (sloping ~1.1° to the south), LD_2 pinches out toward the north and LD_1 also decreases in dip but is still slightly steeper at the northern end than the top surface of the bench on the basis of the attitude of the layers exposed on the northern end of the bench (Figure 11b).

[36] Further support for a correlation of layers across the MD comes from relating layers or packages of layers at the southern end of the central bench with the sequence exposed in the north-facing moat scarp (Figure 13). The sequence in both localities consists of similar layers or packages of layers that are preferentially eroding to exhibit variations in texture, thickness and tone (Figures 13b and 13c). The upper level (1) is a highly eroded, mottled surface of intermediate tone that caps a sequence of alternating light- and dark-toned layers that appear fairly massive in nature (2). Layer 3 is a relatively thin, dark-toned bed that appears very smooth and resistant and is located stratigraphically above a thick sequence of layers at the base (4). Using part of MOLA orbit 19710, whose track passes through the high-resolution images in Figures 13b and 13c (Figure 13a), we present one possible interpretation of the geometry of the units across the MD in Figure 14 based on visual interpretation of the stratigraphy and topographic data. The slope of layers 1 and 3 across the MD are approximately 2.2° and 2.4° to the south, respectively, but

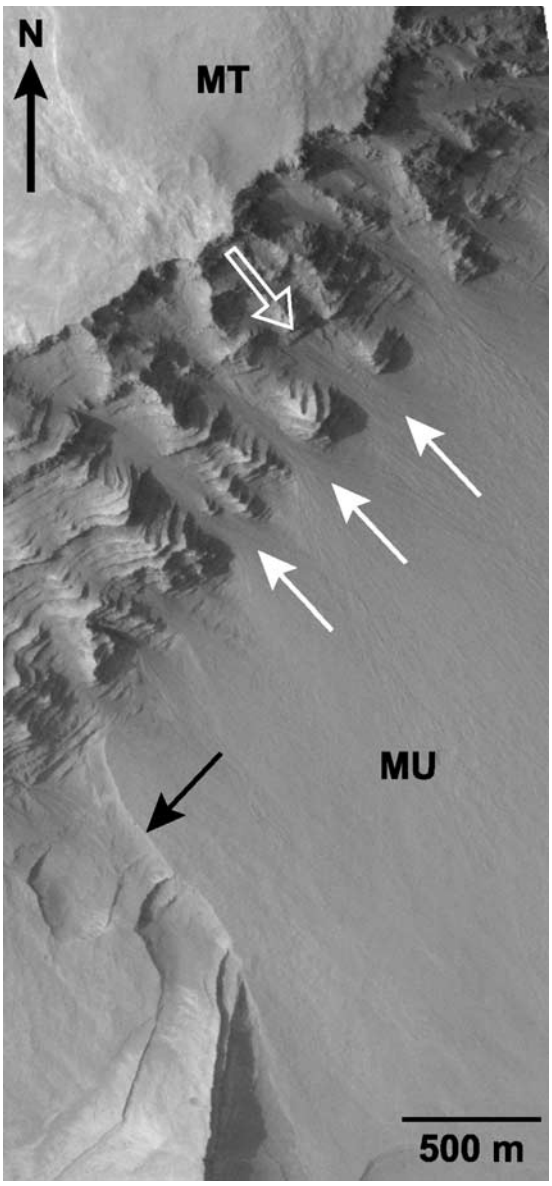

Figure 15. Detail of material mantling the slopes on the western bench (hollow arrow points downslope; see Figure 6 for context). This indurated mantle, which exhibits low scarps along its margin (black arrow), appears to be derived from the MT or the layers themselves, as suggested by the alcoves carved into the layered slope (e.g., white arrows). This mantling material, likely consisting of loose granular material and with some possible contribution from airfall deposits, may have become indurated over time as evidenced by the erosional marginal scarp. Image is subframe of MOC image R06-00037.

they may increase in slope toward the south. Despite the possible error associated with the uncertain correlation of layers, the paucity of MOC NA images and MOLA tracks in this area, and the distance between MOLA shots, these results are consistent with the scenario presented in Figure 12b. Additional evidence for the correlation between layers in the benches with layers in the CF exposed by the north-facing moat scarp is strengthened by (1) the fact that the eastern bench extends without an obvious break to the level of the CF (Figure 2a), (2) there is no obvious evidence for a past lateral obstruction that would have caused the deposition of layers to abruptly terminate in the center of the crater, and (3) a low ridge on the moat floor, displaying possible indistinct layering, appears to connect the layered benches with the southern moat wall (Figure 13a), suggesting a correlation with lower layers in the bench. As discussed in section 3.1, layered deposits in crater Niesten and an adjacent crater on the northwest interior rim of Hellas (Figure 1) appear to have accumulated with a gently sloping top surface and a steeper southern flank, a pattern that is similar to the possible layer correlation in Terby suggested above (Figures 12b and 14). It is possible, however, given the observation that the layers in the CF appear nearly horizontal, that the layers in the CF may have been deposited after extensive lateral erosion of the LD in the benches, yielding no stratigraphic relationship between the layers in the CF and the LD in the benches. Although this scenario cannot be ruled out, the visual similarity between the layering in the benches and the layers in the CF exposed along the north-facing scarp of the MD makes this scenario unlikely.

2.2.2. Mesa Tops (MT)

[37] The surface of the relatively planar, layered benches in Terby (Figure 2a) are mapped as flat mesa tops (MT) (Figure 3), and exhibit a relatively pitted and scoured surface that caps thick sequences of indurated layers (Figure 6). Continuous sections of the MT generally have a darker visual appearance than the underlying LD (e.g., Figures 6 and 11), and the TI values of the MT range from low to intermediate (Figure 5). Sections of the MT have eroded to reveal the underlying LD and in a number of locations, backwasting of the topmost layers has produced steep, fan-like mantles that cover the LD along the bench slopes (Figure 15). These mantles are presumably created by dry avalanching of eroded granular material. It is uncertain whether the dark-toned deposits on the MT occur as a conformable unit overlying the LD, or whether they are a later deposit that was emplaced after appreciable erosion of the LD.

2.2.3. Crater Floor (CF)

[38] The crater floor (CF) deposit is located in the southern half of Terby, occupying an area of roughly 10,100 km^2 (Figure 3). The CF is flat with a relatively constant elevation of −4500 m ("South Floor" profile in Figure 2d) with the exception of the 50–100 m gentle rise on the CF at the boundary of the MD (Figure 2b). Deposits on the CF seem to embay ejecta from the large crater superimposed on the south rim of Terby and form a concentric rim-facing ridge against the interior of the crater rim (Figures 4 and 6).

[39] A portion along the CF deposit near the western and northwestern rim of Terby exhibits a series of scalloped, lobe-like indentations along its edge (Figure 16a; context in Figure 5). The steep, Terby-rim-facing scarp, up to 280 m tall (Figure 2c), exposes light-toned, horizontal layers (Figures 16b and 16c) typical of layering exposed on the north-facing moat wall (Figures 6 and 13). The deposit north of the scalloped scarp exhibits a surface with a lineated, flow-like texture with lobes at its terminus

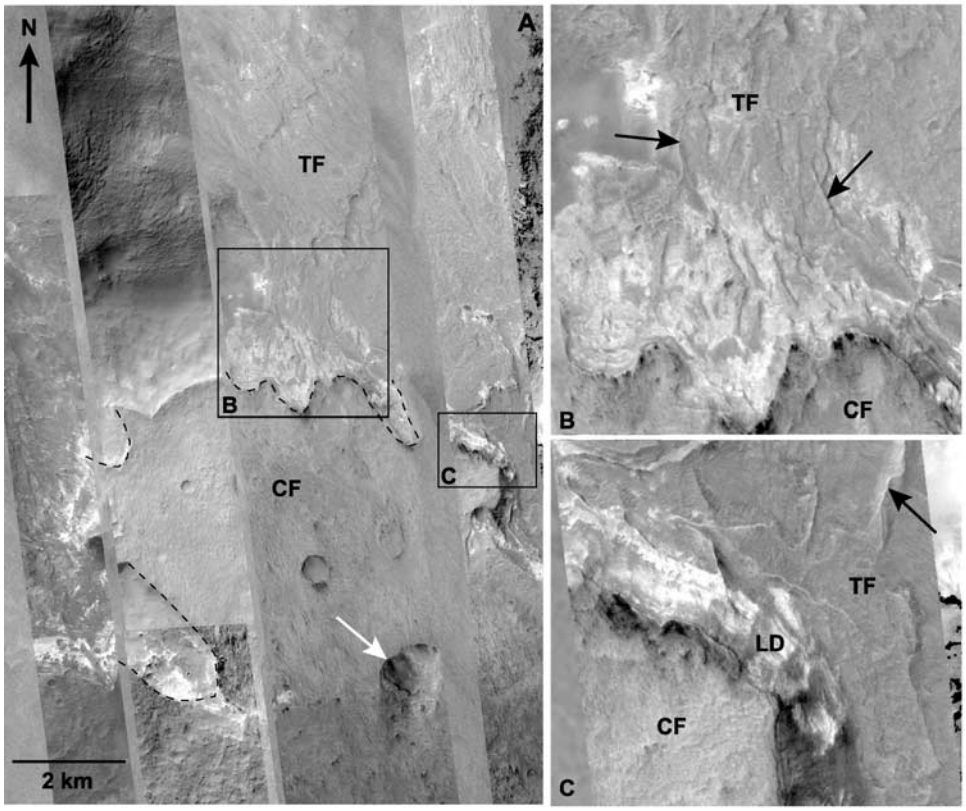

Figure 16. (a) Crater floor (CF) deposit at the boundary of the trough floor (TF) near the northwestern rim of Terby (see Figure 5 for context) has a scalloped appearance around its edge (indicated by the dashed lines; note that the indentations into the CF are eroded alcoves rather than positive-relief features). The generally northwest-facing scarp is approximately 280 m high (Figure 2c). The white arrow points to a pit that exposes layering, suggesting that layers are present beneath the CF. Linear features assumed to be yardangs are present on the surface of the CF near the white arrow. Boxes show location of Figure 16b and 16c. Image is mosaic of MOC images M21-01421, E21-01441, E14-01286, E12-00097, M10-02330 and THEMIS VIS V06789001. (b) Detail of bright-toned, horizontal layering exposed along the scarp that is capped with a resistant layer on the CF. Ridges along TF (e.g., black arrows) may be moraines or eskers related to glacial ice. Image is subframe of MOC image E14-01286. (c) Detail of lobate indentations into the CF, exposing layered deposits (LD). Locally, the scarp edge on the CF has a slightly raised rim. Raised lineations on the lower portion of the TF (e.g., arrow) and shallow grooving to the north suggest either erosion by slope winds or deposition by glacial flow. The curving and branching nature of the lineations and grooves, however, and their association with the eroded alcoves, may be most consistent with subglacial erosion and deposition. Image is subframe of MOC image E12-00097.

(Figure 16b), and the depression north of the CF unit at this location is mapped as part of the TF unit. The CF deposit is capped by an apparently well-cemented, very rough, mottled surface with narrow grooves aligned in a NNW–SSE orientation, indicative of yardangs resulting from aeolian deflation (Figure 16a). Crude layering is exposed on the deflated surface and on the walls of craters excavated into this unit (Figure 16a). The high TI in this region may be a result of preferential aeolian removal of fine-grained material that overlies, or was mixed with, coarse sedimentary deposits flooring the CF unit (Figure 5). This capping unit is darker than the LD exposed on the north-facing scarp of the MD, suggesting that the CF deposit is a distinct unit on top of the underlying LD. Available images of the CF deposit do not reveal diagnostic sedimentary features (e.g., channels, bedforms, etc.) indicative of the depositional mechanisms.

2.2.4. Moat Deposit (MD)

[40] The moat deposit (MD) occurs in the center of the crater at the southern end of the interior deposits, occupying an area of roughly 1300 km^2 (Figure 3). This large, flat-floored depression is the lowest topographic point in Terby with an elevation of roughly −5000 m (Figures 2a and 2b). The scarp at the southern end of the MD exposes a ~400-m layered sequence of the CF, described previously in section 2.2.1. (Figure 13). The surface morphology of the moat floor is generally smooth at THEMIS VIS scale although isolated layered mounds, small craters, and north-south trending ridges expose layering (Figure 13a). MOC NA images on the western edge of MD detail smooth and mottled textures as well as narrow, sinuous, symmetrical and parallel ridges that are roughly 2 km long (Figure 17; see Figure 6 for context).

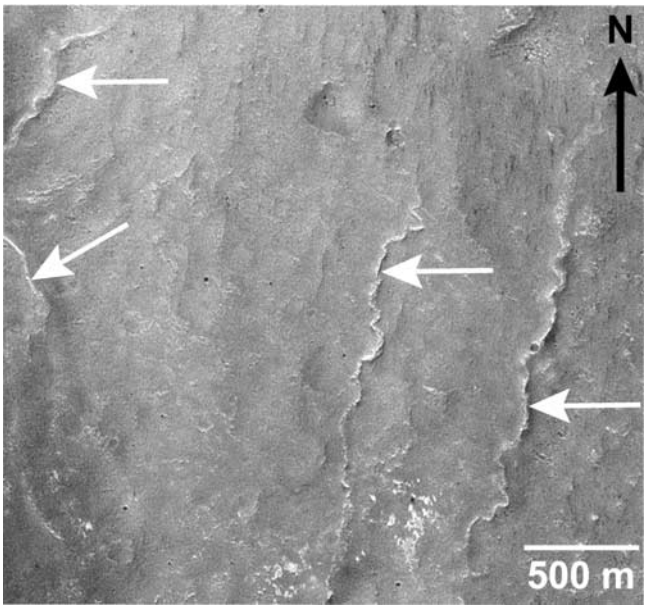

Figure 17. Detail of sinuous, ~2-km-long ridges on the moat floor that are possible eskers (see Figure 6 for context). Image is subframe of MOC image E11-03824.

2.2.5. Viscous Flow Features (VF)

[41] NW crater (D = 23 km), on the northwestern rim of Terby (Figure 3), exhibits viscous flow features (VF) [*Milliken et al.*, 2003] on the crater floor (Figure 18). The VF on the crater floor originate along the northern rim and the lobes converge downslope towards the breach in the southern rim (Figure 18a). The surfaces of the lobes are streamlined around the edges (Figures 18b and 18c) and exhibit cracks or lineations that are oriented perpendicular to the direction of flow (Figure 18b). *Aittola et al.* [2003] interpreted these features to be sedimentary flow features related to a period of fluvial activity, but the parallel, curved lineations are more indicative of plastic flow as is seen on viscous flow features elsewhere on Mars [e.g., *Milliken et al.*,2003; *Mangold*, 2003; *Head and Marchant*, 2003; *Head et al.*, 2005] and its low TI value is indicative of dust-covered ice (Figure 5).

2.2.6. Alluvial Fan Deposit (FD)

[42] A broad surface descends about 1000 m in elevation over 23 km from its origin on the flanks of NW crater to its terminus where it overlaps onto the CF unit (Figure 19a). This surface slopes about 2.3° in its upper portion declining to about 0.7° near its terminus. The western end of the surface radiates from the breached rim of NW crater, and the eastern end of the surface merges headward with valleys incised into the outer rim of NW crater. This surface features low ridges that follow the dip of the surface and, thus, also radiate from NW crater in addition to incised valleys on the outer NW crater rim. A few sinuous channels have incised the surface of this unit.

[43] On the basis of the uniform slope of the surface, a gradient averaging about 1.2°, its radiation from distinct sources at the southern rim of NW crater, and the low surficial ridges, we interpret this to be an alluvial fan, which we map as a fan deposit (FD) (Figure 3) because of its similarity in morphology and surface features to large alluvial fans in other craters on the northern rim of Hellas, previously described by *Moore and Howard* [2005a]. Although the FD appears to predate the viscous flow features (VF), the fan likely formed by episodic releases of melt water from NW crater and cut valleys into its southeastern rim. Unlike the VF, the surface of the FD features low-relief ridges radiating from the fan apex in a manner analogous to alluvial fans found elsewhere on Mars [*Moore and Howard*, 2005a], and these ridges are likely distributary channels raised into relief by aeolian deflation (Figure 19b). A possible inverted channel occurs on the distal end of the fan (Figure 19b), and several sinuous channels preserved on the upper fan surface (Figures 19a and 19b) are indicative of late-stage fluvial incision, reflecting a transition to a higher water-to-sediment ratio [*Howard et al.*, 2005]. Abrupt distal termination of the fan in some places results in outward facing scarps and pits that expose light-toned layers, indicating preferential erosion of the LD (relative to the fan surface) subsequent to fan deposition (Figure 19b). The FD appears to have eroded low benches exposing LD that descend southward from NW crater (shown in Figure 3 and by "b" in Figure 19a). These benches are well below the level of the western bench and may merge with, or be buried by the CF deposits at their southern terminus, analogous to the eastern bench.

[44] We distinguish two subunits of the alluvial FD (Figure 19a). An earlier, extensive fan surface is defined by its smooth surface and relatively uniform gradient radiating from NW crater to both the southwest and southeast. A smaller, younger fan surface with a slightly steeper gradient is overlain on the northern portion of the earlier fan, and is characterized by apparent radial distributary deposits etched into relief by aeolian deflation.

2.2.7. Grooved Terrain (GT) and the Age of NW Crater

[45] The western and southeastern margins of the fan complex terminate at an underlying, strongly grooved surface (unit GT, Figure 3) that exhibits a high TI indicative of coarse-grained or strongly indurated deposits (Figure 5). The grooves are subparallel but somewhat sinuous in pattern (outlined in Figure 19a with details in Figures 19b–19e). The fan units appear to overlie the western and central GT exposures such that the grooving has been reexposed by erosion of formerly more extensive fan deposits, although present imaging is not definitive. A broadly grooved surface with lobate ridges is also visible in a single MOC NA image (Figure 19e) covering a portion of the northwestern terminus of the western bench where it abuts NW crater. We interpret this to be an exposure of GT that is located at a considerably higher elevation (~−1750 m) than the central (~−3700 m) and western (~−4200 m) exposures of GT (Figure 19a). A lineated deposit appears to unconformably overlie the LD along the northwestward edge of the west-facing scarp of LD on the western bench (Figure 19f) and may also be GT.

2.2.7.1. Interpretation

[46] We interpret the GT to be exposures of fluidized ejecta emplaced by the impact of NW crater. The lineations in the GT exposures are roughly radial to NW crater, and lobes, where present, point away from NW crater (Figure 19a). The radial texture of the eastern GT deposit can also be seen in THEMIS IR images (Figure 5). Because

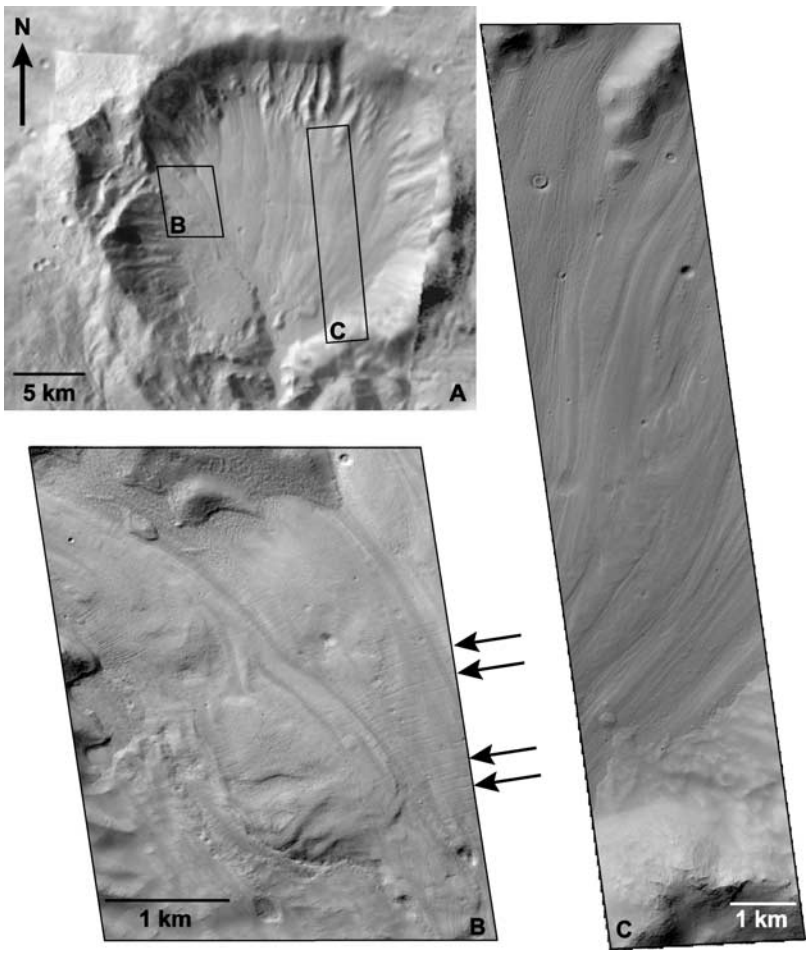

Figure 18. (a) Floor of a small (D = 23 km) crater on northwestern rim of Terby ("NW crater") exhibits streamlined, viscous or plastic flow features that converge toward the breach in the southern rim (see Figures 3 and 19 for context). Boxes show location of Figures 18b and 18c. Image is THEMIS VIS image V02295003. (b) Arrows point to cracks on lobes oriented perpendicular to presumed direction of flow (toward the bottom of image). Superimposed undeformed small craters suggest flow has not been active during the late Amazonian. Image is subframe of MOC image E20-01565. (c) The lobes exhibit a somewhat smooth, streamlined texture. Image is MOC image E20-01105.

the GT exposures occur both on the surface of the western bench and at considerably lower elevation below the scarp defining the west side of western bench, we infer that the impact occurred subsequent to deposition of the LD and formation of the deep erosional troughs within the LD. The floor of NW crater is well below the level of the western bench, and if NW crater had been present before LD deposition the crater would likely have been filled with sediment associated with the LD. Furthermore, light-toned materials along the southern rim of NW crater may be LD deformed by the impact (Figure 19g), and large protuberances on the surface of a layered bench just south of NW crater may be coarse ejecta (Figure 19h). The mantling material on the northern end of the western bench where it approaches closest to NW crater may be draping of ejecta sheet material falling over the edge from the north, perhaps including the finger-like ramps (Figure 20a). The avalanche deposit (Figures 3 and 6) sourced from the western bench might have been triggered by the impact of NW crater. A difficulty with the interpretation of GT as fluidized ejecta from NW crater is the apparent paucity of fluidized ejecta north and west of the crater (although high-resolution image coverage is sparse). Ejecta directed in these directions may have been primarily composed of Terby rim materials, and therefore less fluid than the LD that were impacted along the southern rim of NW crater. The incorporation of resistant, coarser rim materials into the fluidized ejecta could account for its relative resistance to erosion compared to the LD and possibly also for the presence of large blocks that have mass wasted into the pits (Figure 19d).

[47] The western and central exposures of GT terminate at their southern end in large, broadly concave depressions excavated into the underlying LD (Figures 19a, 19c, and 19d). The largest depressions occur at the end of the GT beyond the southeastern margin of the FD and often contain smaller interior depressions and narrow sinuous ridges (Figure 19c and 19d). Despite heavy mantling on the interior slopes of this depression, concentric, light-toned layers are exposed in its walls and dark multimeter-scale boulders have eroded down the slopes from a layer near the

top of the GT (Figure 19d). The limited exposures of light-toned layers within the depressions show no obvious evidence of collapse by folding or faulting, suggesting that the depressions formed by differential surface erosion of the LD. The relationship between the fan surface with prominent channels, the depressions and the GT is unresolved; the lineations predate the latest stages of the fan activity but the depressions that formed within the GT lack deposition from the fan. The earlier FD appears to extend southward along both the eastern and western margins of these major

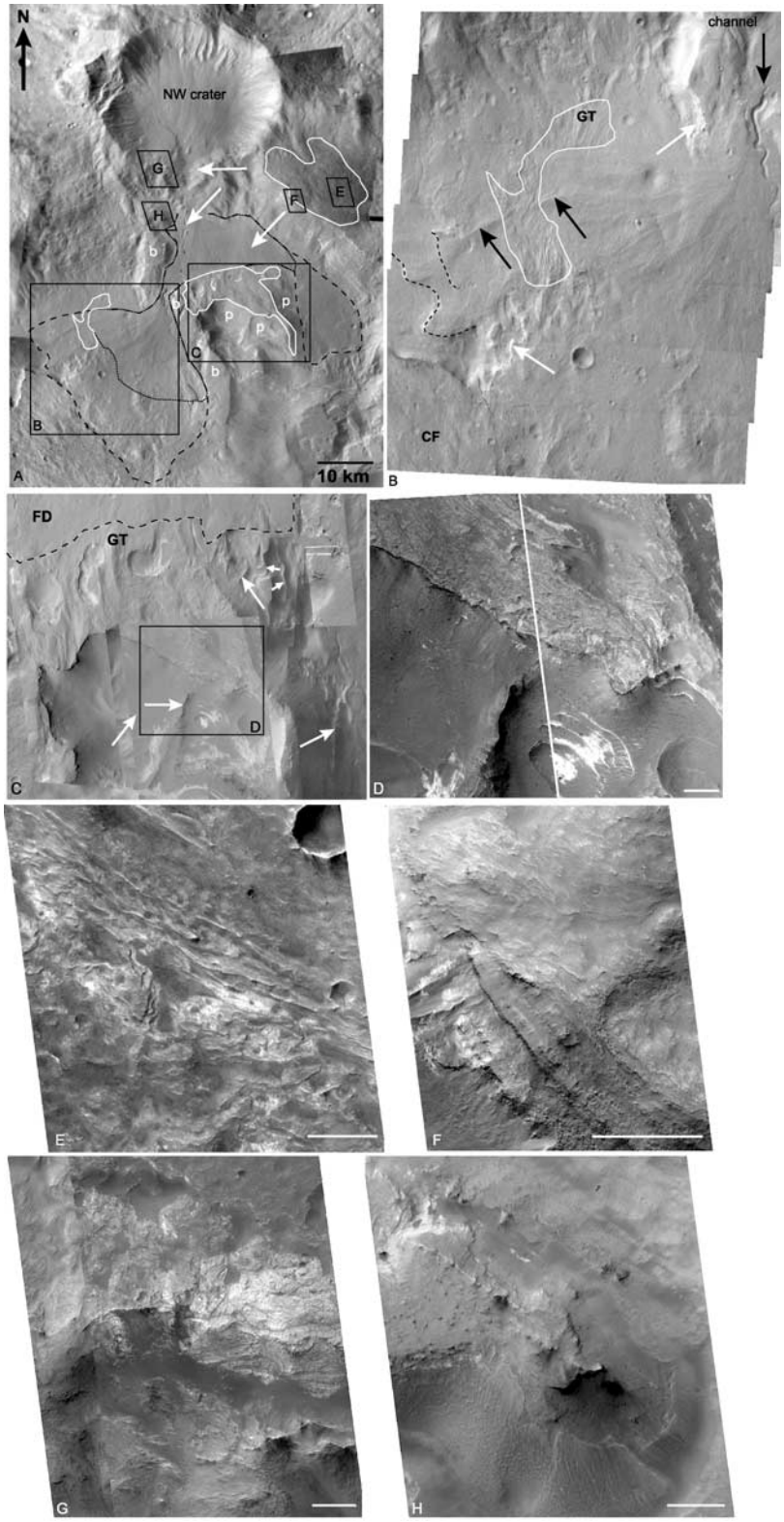

Figure 19

depressions, suggesting either that formation of the depressions postdate the fan deposition or that a topographic obstacle was present at the location of the depressions during fan deposition.

[48] Several deep depressions in the LD within and beyond the curvilinear GT discussed above (Figure 19c) may have formed at the same time or subsequent to the formation of the GT, and may also have been present prior to creation of the GT but enlarged by subsequent mass wasting. Because most of the erosion forming troughs in the LD appears to have preceded the impact of NW crater and emplacement of the GT ejecta sheet, the deep erosion of the LD in close proximity to the GT may have been causally related to the impact due to the atmospheric blast, thermal effects (e.g., melting of ice) or, if a deep lake were present within Hellas at the time of impact, seiches. Formation of the linear ridges within the main depressions (Figure 19c) may have occurred during erosion of the pits.

2.2.8. Rough-Textured Trough Floors (TF)

[49] The trough floors (TF) located on either side of the central bench are ~10 km wide and up to 2 km deep (Figure 3). The TF unit also includes the enclosed depression east of the eastern bench as well as terrain adjacent to the boundary between the CF and FD ("NW TF" in Figure 2c). The varied morphology of the TF include horizontally layered, streamlined mounds as well as ridges and scarps whose long axes is oriented parallel to the axis of the troughs (Figures 4 and 6). There are a number of ridges that are not obviously layer exposures that also strike parallel to the orientation of the troughs, but locally exhibit lobate terminations (Figures 4 and 6). Linear and anastomosing shallow channels are also present, primarily in the northern portions of the TF (Figure 4). The TF are mantled with remnant dark-toned, fine-grained material described in section 2.2.9.

2.2.9. Mantling Unit (MU)

[50] A smooth, indurated, dark-toned, presumably fine-grained, terrain-conforming mantling unit (MU), typically exhibiting low scarps along its margins, is prevalent on the trough floors (TF) as well as the scarps of the main benches (Figures 6 and 20). The low scarps at the edges of the MU indicate that subsequent modest erosion of this deposit (and the underlying LD) has occurred. Layers on the scarp of the western bench below the level of the top of the remnant

Figure 19. Fan deposit (FD), grooved terrain (GT), and related features associated with NW crater. (a) Index map of region south of NW crater (see Figure 3 for context). The FD in Terby likely formed by episodic releases of melt water from the remnant ice on the floor of NW crater (Figure 18). The dashed line delineates the inferred earlier surface of the FD, defined by its smooth surface and relatively uniform gradient radiating from NW crater to both the southwest and southeast that has subsequently eroded and developed bowl-like depressions on its surface. A smaller, younger fan surface (solid black line) with a slightly steeper gradient is overlain on the northern portion of the earlier fan. The younger fan surface is incised by sinuous channels (white arrows) and is characterized by apparent radial distributary deposits etched into relief by aeolian deflation. The GT is outlined in white (although the boundaries of the northeast patch are approximate owing to poor resolution of available images) and the location of major pits ("p") excavated below the level of the GT are marked (note smaller pits within the central exposure of the GT). Benches ("b") are underlain by light-toned layered deposits (LD). Image is subframe of THEMIS VIS mosaic (Christensen et al. data set). (b) The distal end of the FD near its terminus at the crater floor (CF) exhibits radial textures, distinct fan margins (likely enhanced by subsequent erosion), sinuous scarps (dashed lines), and linear, inverted topography that may be a feeder channel (black arrows on either side of GT). The surface of the FD has eroded to expose the underlying GT that predates the fan as well as underlying layered material (e.g., white arrows). Sinuous channel in upper right (black arrow) is incised into younger fan surface. Image is THEMIS VIS image V02295003; image is ~20 km wide. (c) Dashed line marks transition between smooth FD and GT. The GT exhibits prominent, parallel grooving and narrower ridges describing a broad curving pattern, which we interpret to be equivalent in age and process to the GT in Figure 19b. The GT is interrupted by pits exposing underlying LD and bordered on its downslope end by deep depressions into LD. The larger depressions have complex morphology with smaller interior depressions and several resistant ridges (white arrows). The concentric, continuous, light-toned layers exposed on the interior walls of the depressions disfavors a process related to structural collapse (i.e., karst origin). The formation of the depressions could be related to (1) failure of the material that caused their removal in large blocks, (2) a weaker layer beneath a more coherent upper layer may have encouraged localized scour, or (3) chemical dissolution of minerals in the layers during interactions with surface melt water or ground water. Image is subframe of THEMIS VIS mosaic (Christensen et al. data set); image width is ~18 km. (d) Detail of GT, illustrating morphology characterized by narrow, sometimes lobate, ridges and broad troughs in broadly curvilinear patterns. Images are subframes of MOC NA images E1400578 and E1103824; scale bar is 500 m. (e) GT exposed on the northwest terminus of the western bench ("W" in Figure 2a). Image is subframe of MOC NA image R1400141; scale bar is 500 m. (f) Possible exposure of GT that appears to unconformably overlap layered deposits of the western bench. Image is subframe of MOC NA image M1901485; scale bar is 500 m. (g) Light-toned deposits exposed along the southern rim of NW crater. Note that the surface expression and tone are similar to exposures of LD but the exposure lacks horizontal bedding. Lineation and linear tone patterns may indicate origin as folded and faulted LD. Image is from subframes of MOC NA images M1103243 and E1501402; scale bar is 500 m. (h) Bench underlain by light-toned LD and capped with 20- to 30-m isolated protuberances that may be coarse boulders. Image is subframe of MOC NA image E1501402; scale bar is 500 m. We interpret the GT to be fluidized ejecta from NW crater; light-toned deposits in Figure 19g to be LD deformed by the impact; and the protuberances in Figure 19h to be coarse ejecta from the impact. Impact of NW crater is inferred to have occurred after deposition of the LD and after erosion of the LD to form the major troughs.

mantle have undergone approximately 50–70 m less vertical erosion than the layers on the unmantled slopes (based on estimations of horizontal offset of individual layers shown in Figure 20b), indicating that the thickness of the remnant mantle at this location is likely less than a meter. Although thickness of the MU may vary depending on preexisting terrain, the ability of such a thin, indurated layer to persist as tens of meters of adjacent LD are eroded suggests strong induration relative to softer layered sediments.

[51] The original extent of the MU is uncertain. Its presence is most obvious where deflation of more erodible underlying sediment leaves it in relief and although we speculate that some mantling material may have been derived from the MT or the layers themselves (Figure 15), the presence of extensive mantling on the TF suggests a regional blanket (Figure 6). The blanket of mantling material was presumably emplaced over the entire crater after the deposition of the LD and the formation of the TF and MD. It is possible that there was more than one mantling event separated by interval(s) of erosion inasmuch as at some locations on the TF, smooth platforms of dark material, bordered by short scarps, occur at multiple levels. The MU identified in Terby might be equivalent to the "thin mesa" unit described by *Malin and Edgett* [2000], who noted that this dark-toned, thin, mesa-forming unit almost always lies unconformably over previously eroded massive and/or layered units.

[52] In addition to the indurated MU, apparently loose, dark-toned mantles occur as sheets or fan-like accumulations on the mesa sideslopes, most of which are inset below the MU. Most loose-sediment mantling in Terby appears to have been derived from material that originated from backwasting of the upper layers on the mesas scarps or possibly from aeolian material blowing over the mesa tops (i.e., Figures 8, 10 and 15). Loose and indurated mantling

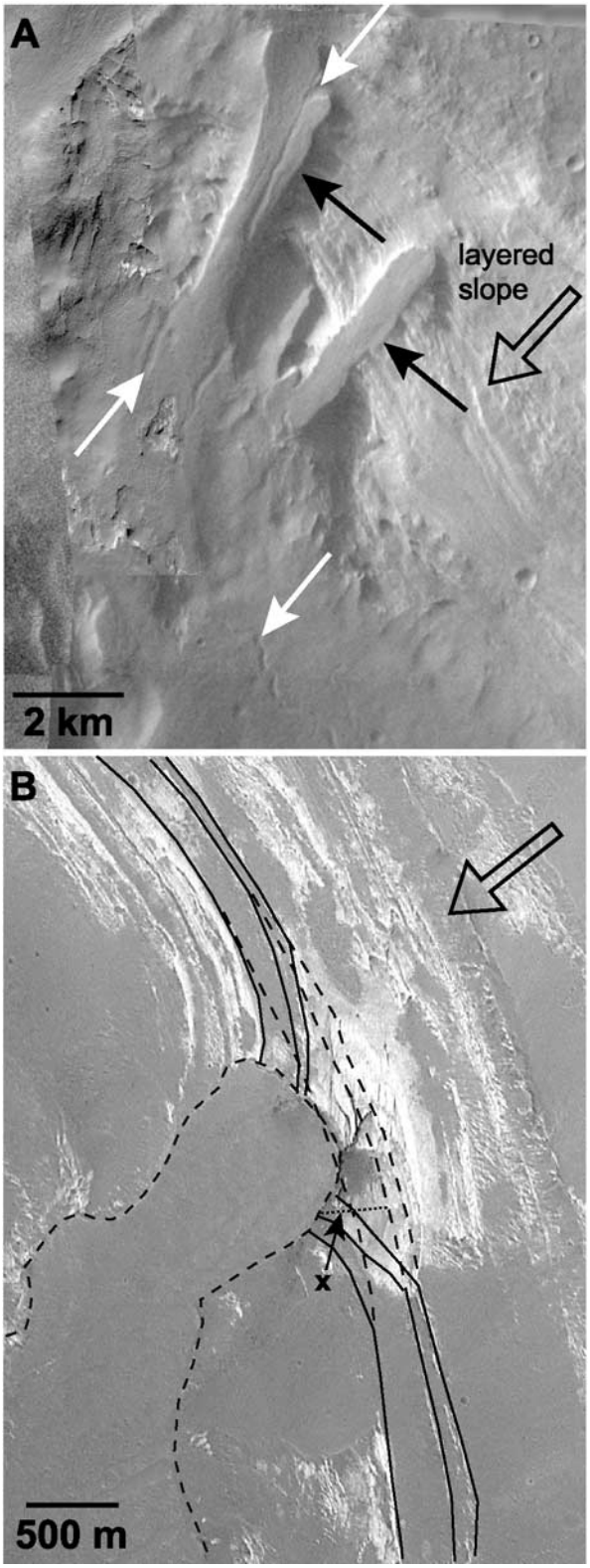

Figure 20. Mantling unit (MU). (a) The MU is a smooth, dark-toned, presumably fine-grained, terrain-conforming unit that typically has low scarps along its margins and is most prevalent on the trough floors and the scarps of the main benches. Channels (white arrows) on the surface of the remnant mantled ramps deposited on slopes of the western bench (black arrows) indicate some amount of (fluvial?) erosion after the deposition of the MU. Image is from subframes of VIS image V03381003 and MOC image M1901485. (b) Layered sequence at base of the western bench that is partially covered by a lobe of remnant MU. Layers on the scarp of the western bench just below the level of the top of the remnant mantle have undergone approximately 50–70 m (Δh) less vertical erosion than the layers on the adjacent unmantled slopes based on estimations of horizontal offset of individual layers (x = 125–250 m, dashed line) and a slope of 20° ($\Delta h = x (\sin 20°)$). The layers near the remnant mantle tip (solid lines) in this location visibly curve to meet the bottom of the mantle, indicating that the thickness of the remnant mantle at this location is likely much less than a meter, but mantle thickness may vary elsewhere depending on differences in preexisting terrain. The ability of such a thin layer to persist as ~60 m of adjacent layered deposits are eroded suggests strong induration relative to softer layered sediments. Image is subframe of MOC image R09-00856. Hollow arrows in Figures 20a and 20b point downslope; see Figure 6 for context. Top of images is north.

material may form a temporal continuum, such that loose deposits may gradually acquire induration (Figure 15), possibly resulting from moisture cycling associated with quasiperiodic climate changes [e.g., *Laskar et al.*, 2004; *Mustard et al.*, 2001; *Head et al.*, 2003].

3. Comparison With Other Crater Interior Deposits in the Hellas Region

3.1. Crater Niesten and Its Contiguous Companion

[53] Crater Niesten (D = 115 km) and a contiguous, slightly younger, unnamed crater (D = 94 km, herein called "SW crater") to its southwest lie on the northwest interior wall of Hellas (Figure 1) and contain layered sediment with several parallels to those of Terby. The deposits occupy a similar elevation range (∼−3000 m to −1200 m) and are also banked against the northern wall of the host craters (Figure 21a). The deposits in these craters are less eroded than those of Terby, and potentially offer clues as to the original extent and attitude of Terby's deposits.

[54] The deposits within Niesten are at least 1200 m thick although the shallowness of the crater suggests a thick unexposed sequence underlying the exposed deposits. The main deposit extends about a third of the way across the crater interior and appears to be only modestly eroded since its emplacement. The gross morphology of the interior deposit resembles a terrestrial alluvial delta in that it extends farthest into the crater interior at its center, has a nearly planar upper surface sloping gently (∼0.4°) southward toward the center of the basin, and has a steeper marginal gradient of about 1.7 to 3.4° (although, as discussed below, origin of the deposit as an alluvial delta is unlikely). The upper surface appears to be terraced, with extensive surfaces at about −1300 m and −1400 m and a smaller terrace at about −1100 m. The uppermost exposed sediment is about 200 m thick, moderately dark-toned, erodes to a relatively smooth, undulating surface, and has an intermediate thermal inertia based upon nighttime THEMIS IR. Where this upper unit has been stripped (likely by aeolian erosion), a light-toned underlying unit is exposed which is coarsely layered, has a higher thermal inertia, and erodes to a knobby or scabby texture. Most of the southern crater floor is nearly level, lying between about −2000 to −2200 m. Lobate ejecta sheets from two superimposed craters on the south (C2) and southeastern rim (C1) of Niesten blanket the southern interior of Niesten (Figure 21a). Ridges extending northwest from crater C1 appear to be capped by ejecta deposits from the crater with a maximum positive relief of about 250 m (Figure 21a). Layers are exposed on the sides of the scarps (Figure 21b), indicating postimpact erosion of the center of the Niesten floor, reaching a maximum in the center of the crater. Total erosion diminishes towards the east and south on the crater floor, where the ejecta does not stand in appreciable relief.

[55] Like Terby, the rim of Niesten has a smooth (at 100-m scale), undulating morphology that suggests either extensive modification by slow, shallow mass-wasting or deposition of a thick mantling layer over the crater rim. In places the contact of the crater rim with the dark-toned layered deposits seems gradational, but in other places there are short scarps or textural gradations. If the crater rim has been modified by deposition, it is likely that the mantling preceded or was correlative to the deposition of the dark-toned layered deposits because subsequent deposition on the crater rim would have mantled the crater interior as well. The superimposed crater on the southeastern rim of Niesten (C1) also exhibits a smooth, undulating texture. The ejecta from this deposit overlie most of the deposits within the interior of Niesten, likewise suggesting a mantling age correlative with the dark-toned deposits. If, however, the smooth undulating texture of the rims of Niesten, Terby, SW crater, and most superimposed craters is due to intensive mass wasting, the dark- and light-toned layered deposits of the interior must not have been susceptible to diffusive mass wasting. As will be discussed below, the rounded rims of Niesten, Terby and SW craters differs considerably from those of higher, and lower latitude craters containing layered deposits that were extensively dissected by fluvial processes subsequent to deposition of the light- and dark-toned layered deposits.

[56] The deposits in SW crater have a similar location, morphology, extent, and exposed stratigraphy as those in Niesten (Figure 21a). The top surface of the depositional stack is likewise nearly planar, at an elevation of about −1500 m and dipping less than 0.5° towards the interior of the crater. The steeper marginal slopes also incline at about 1.7 to 3.4°. The major differences with Niesten are a greater degree of postdepositional erosion, a lower, but still nearly flat southern crater floor at about −2750 m, exposed central peak materials, and large depressions in the interior deposits. The stratigraphic sequence appears to be similar to that of Niesten, with a smooth-surfaced dark-toned upper unit overlying a coarsely layered, lighter-toned unit eroding into a scabby and knobby surface. Deeper erosional pits expose underlying light-toned materials that appear to be more massive than the upper, light-toned layers.

[57] MOC NA images of SW crater interior reveal numerous aligned ridges and grooves with a NNW-SSE orientation, suggesting that wind erosion has been the dominant erosional process exposing the layering. Sparse shallow valleys similar to those on the fan and mantling deposits in Terby (Figures 4, 19a, and 19b) eroded into the layered sequences of Niesten and SW crater.

[58] The stratigraphic sequence in SW crater is provisionally interpreted in Figure 21c from two MOLA topographic profiles (transects A and B in Figure 21a). The interpretation is based upon the MOLA topography, THEMIS VIS and IR images, a HRSC image (Figure 21a), and MOC NA images. Although the exposures are not definitive, the similarity of surface texture and tone of the nearly planar surface at the north end of the transect and of the more steeply dipping surface in the middle of the transect suggests that the surface layers are conformable with the highest portions of the overlying surface ("Dark-toned Layered Deposit" in Figure 21c). By this interpretation, the highest elevations along the profile are essentially the final depositional surface of the main sequence of layers. Where the underlying light-toned layered deposits are exposed, they appear to be conformable with the overlying deposits (Figure 21c). The knob at relative distance 22 km in Figure 21c, lying along MOLA profile 17549, displays no obvious layering and is interpreted as an exposure of the central peak complex ("Central Peak Materials" in Figure 21c). The nearly level, smooth crater floor at the south end of the transects has a relatively high brightness

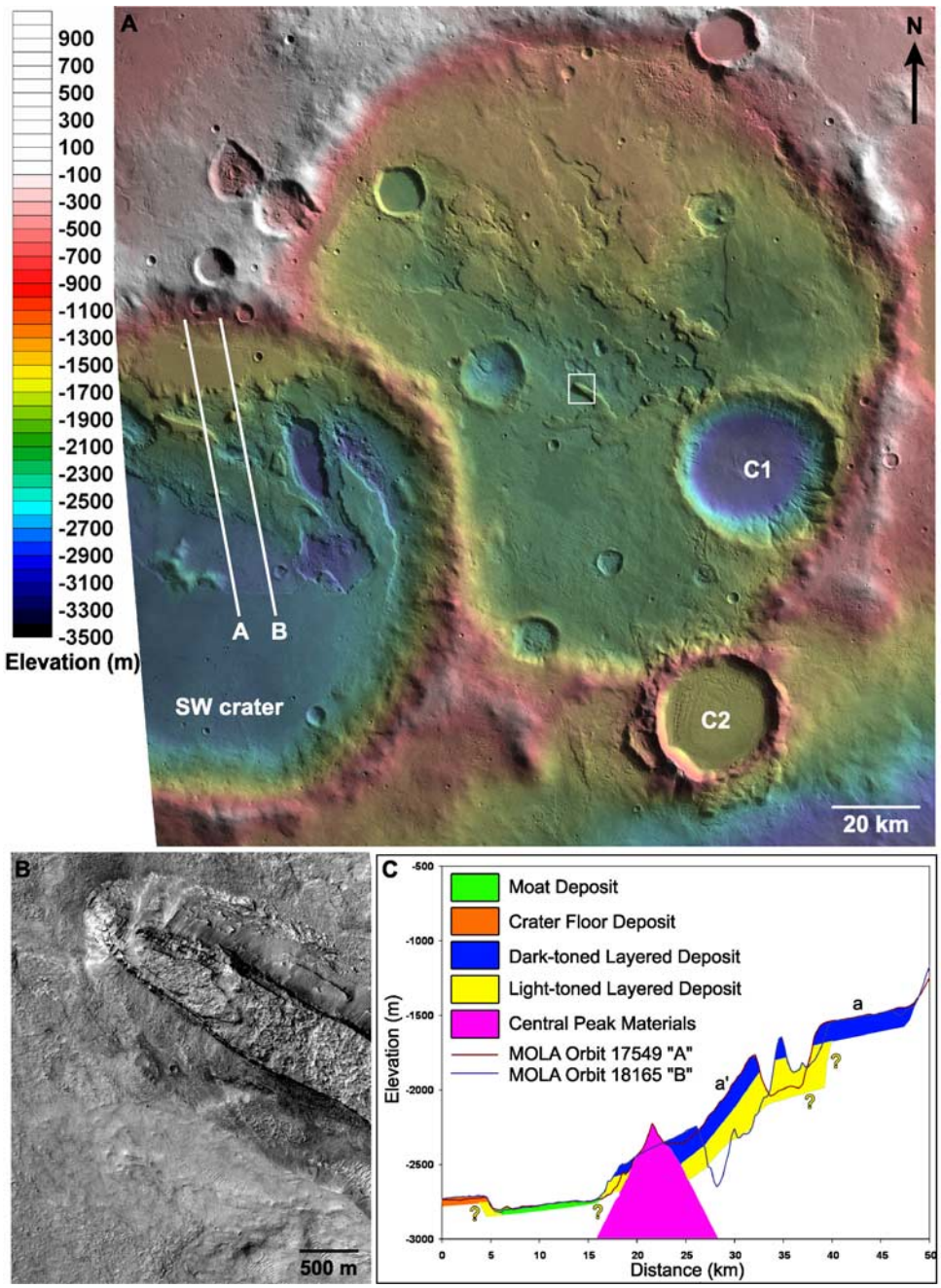

Figure 21. (a) Crater Niesten and part of a younger crater to its southwest ("SW crater") from a portion of HRSC rectified nadir image H0554-0000 centered at about 57.6°E and 28.2°S (elevation-cued in color version online). Hellas basin extends to the southeast of the image (see Figure 1 for context). Layered deposits in these craters, like those in Terby, are banked against the north walls of the craters. The northern portion of the layered deposits slope gently southward from the crater rim, but the layers steepen in dip near the center of the crater. Deposits in these craters are less eroded than those in Terby. Transects A and B are MOLA profiles shown in Figure 21c, and craters C1 and C2, emplaced after deposition of the layered deposits in Niesten, are discussed in the text. Box shows location of Figure 21b. (b) Detail of remnant bench capped by ejecta from crater C1. Bench stands about 250 m above surrounding plains, where erosion has revealed layered deposits beneath the ejecta. Image is subframe of MOC NA image R16-01100. (c) Interpretive geologic cross section of SW crater from MOLA orbits 17549 (transect 'A') and 18165 (transect 'B') shown in Figure 21a. Legend shows deposits in age sequence from bottom to top. Deeper holes (e.g., near 28 km) expose underlying massive, light-toned deposits. Note that layered deposits are interpreted to steepen in dip from a to a', similar to one interpretation of layer stratigraphy in Terby (Figure 12b). The flat crater floor deposit and the moat deposit appear analogous to those in Terby (Figure 2).

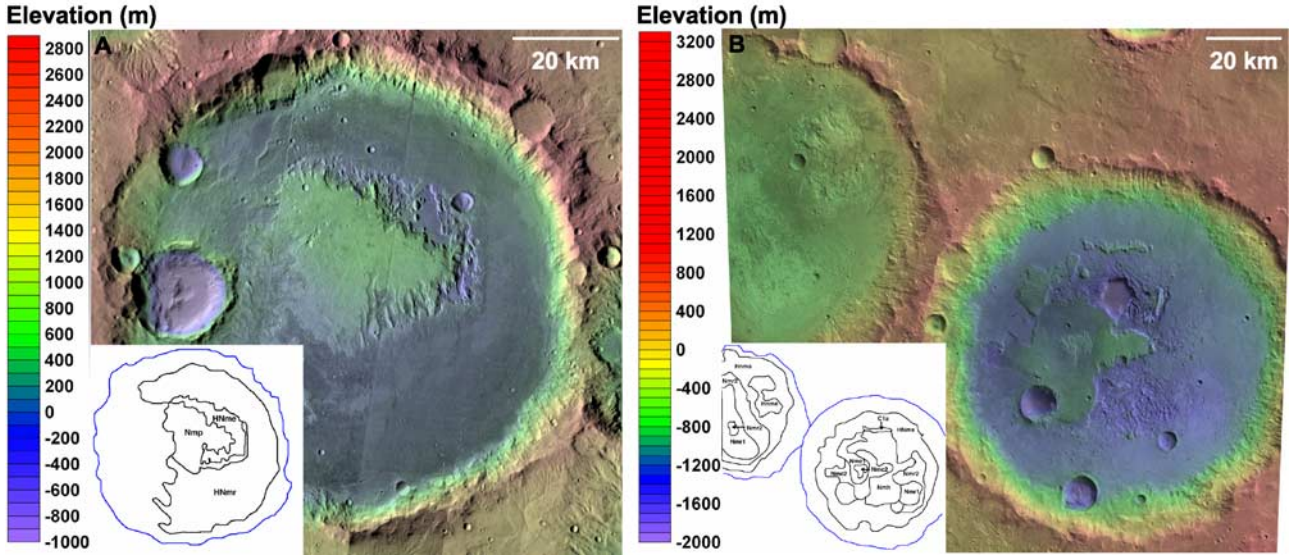

Figure 22. (a) THEMIS day IR mosaic of Crater Millochau (elevation-cued in color version online), located at about 81.1°E and 21.1°S, roughly 725 km northeast of Terby (see Figure 1 for context; top of image is north). Inset shows geologic map of exposed layered deposits generalized from *Mest and Crown* [2005] using their unit classification terminology. Unit HNmr is a fluvial bajada-like surface of sediment presumably derived from crater rim erosion that is younger than the layered deposits Nmp and HNme. Like Niesten and SW crater (Figure 21), the layered deposits feature a gently southward sloping top surface that steepens near the center of the crater. The pits surrounding three sides of the layered deposits have presumably been incised into the layered deposits subsequent to deposition of the HNmr unit. The original northward extent of the layered deposits is uncertain because deposition of the HNmr unit may have been accompanied by layer erosion. Top of image is north. (b) The informally designated craters A (D = 95 km, lower right) and B (D = 83 km, upper left) of *Korteniemi et al.* [2005a] from subframe of HSRC rectified nadir image H0389 (elevation-cued in color version online; see Figure 1 for context). Inset shows simplified version of the geologic map from *Korteniemi et al.* [2005a] using their unit classification terminology. Layered deposits in crater B have experienced little postdeposition erosion and extend to a higher elevation near the northeast crater wall. As with Millochau in Figure 22a, deposition of a fluvial bajada unit (HNms) has occurred subsequent to deposition of the layered deposits, possibly also burying and eroding layered deposit exposures. Units Nmr1 and Nmh in crater A are probably eroded remnants of layers still preserved under units Nmc1 and Nmc2. In contrast to *Korteniemi et al.* [2005a], we interpret unit C1a to be underlain by layered deposits rather than being exposures of crater wall/floor materials. Top of image is north.

temperature in nighttime THEMIS IR and we interpret this to be a distinct, later mantling unit based both on the horizontality of the surface and the higher thermal inertia ("Crater Floor Deposit" in Figure 21c). Dark, smooth, low-thermal inertia deposits mantle the ~100-m-deep trough from 6 to 16 km ("Moat Deposit" in Figure 21c) and embay exposures of the light-toned, layered unit. The trough deposit appears to be the youngest significant sedimentary accumulation along the transect, although similar accumulations floor the deeper eroded basins in SW crater.

[59] Although the sequence of a darker, smooth-textured deposit overlying a light-toned layered deposit that weathers to a knobby and scabby appearance occurs in many of the pitted craters on the northwest and western rims of Hellas basin [*Moore and Howard*, 2005b], correlation with the sequence within Terby is less certain. The top unit is similar to the materials exposed on the plateau surfaces and LD_4 in Terby, whereas the underlying layered, light-toned deposits may correspond to LD_3 within Terby.

[60] The layered deposits exposed in Niesten and SW crater suggest that the original surface of layer accumulation involved both a gently sloping upper surface and a steeper southern margin (i.e., that layers are continuous beneath both a and a' in Figure 21c). This would be consonant with the interpretation of original layer deposition within Terby depicted in Figure 12b. It is uncertain whether the crater floor deposit formed contemporaneously with or subsequently to the light-toned layered deposits (Figure 21c). Limited exposures of the light-toned unit leaves uncertain its extent and attitude at both the north and south ends of the transect.

3.2. Craters Northeast of Terby

[61] *Korteniemi et al.* [2005a] and *Mest and Crown* [2005] described the morphology and stratigraphy of crater basins to the northeast of Terby which are higher in elevation than Terby, Niesten, and SW crater but contain a similar stratigraphic sequence of basin floor sediment. Crater Millochau (D = 118 km) lies about 725 km northeast of Terby (Figure 1) and contains basin floor deposits in the elevation range from about 0 to +500 m [*Mest and Crown*, 2005] (Figure 22a). Crudely layered, light-toned deposits are exposed in scarps and pits primarily around the northern

and eastern edges of a plateau in the northern portion of the basin floor (units HNme and Hk of *Mest and Crown* [2005]). As in Niesten and SW crater, the top units of the light-toned deposits are relatively resistant to erosion and are eroded into a scabby and knobby surface. The plateau is capped by about 160 m of dark-toned sediments which have a resistant cap overlying more erodible layers that have been stripped back from the underlying light-toned deposits (unit Nmp of *Mest and Crown* [2005]). The dark-toned surface layers cap the nearly flat summit of the layered plateau and they appear to conformably overlie the southern portion of the plateau which slopes southwestward at a dip of about 0.6°.

[62] The morphology of a nearly level plateau surface and a south-dipping southern flank is similar to that of Niesten and SW crater, except that the northern edge of the plateau is separated from Millochau's wall by about 20 km. The northern edge of the plateau is an erosional scarp, so that the original extent of the layered plateau in this direction is uncertain. Unlike Terby, Niesten and SW crater, the rim of Millochau displays extensive fluvial dissection of the inner crater rim and a bajada-like landform interior of the rim sloping at about 0.5° towards the basin center and impinging upon the interior layered deposits (unit HNmr of *Mest and Crown* [2005]). The sediment underlying this surface is presumably fluvial sediment derived from rim erosion. Shallow, wide valleys on the south-sloping flank of the Nmp dark-toned layers, and a narrow fan-like form at the base of this slope apparently intergrading with the HNmr deposits, suggest modest fluvial erosion of the southern flank of the Nmp unit contemporaneous with deposition of the HNmr unit. The intricately dissected crater rim and the ring of bajada deposition are lacking at Terby, Niesten and SW crater. The plateau of layered deposits in Millochau may have originally extended to the north crater wall (as in Terby, Niesten, and SW crater), being eroded back during the episode of fluvial incision of the crater rim and formation of the bajada surface. The steep northern flank of the layered plateau and the accompanying exposure of the layered deposits are consistent with appreciable erosion of this side of the plateau.

[63] The informally named craters A (D = 95 km) and B (D = 83 km) of *Korteniemi et al.* [2005a] lie about 400 km northeast of Terby (Figure 1) and contain layered sedimentary deposits on their floors in the elevation range of about −1500 m to about −200 m (Figure 22b). Layered deposits in crater B have not been deeply eroded to provide definitive cross sections. Broad areas of light-toned deposits are exposed on the central floor (unit Nmr1 of *Korteniemi et al.* [2005a]). Light-toned deposits are also exposed in the center of a bench on the northeastern crater wall about 200 m above the crater floor (unit HNme of *Korteniemi et al.* [2005a]) that may be correlative with the Nmr1 unit. Dark-toned layered deposits (unit Nmr2) are present only in scattered, thin exposures, mostly as an annulus surrounding the Nmr1 deposits, suggesting that they either were thin and restricted in area of deposition or they became extensively eroded. As in Millochau, crater rim erosion resulted in deposition of a bajada deposit around the inner crater wall (unit HNms).

[64] The deposits in crater A record a complex erosional and depositional history that generally follows the stratigraphic sequence described in the other craters in the region. In general terms, light-toned deposits (Nmh and Nmr1) are overlain by dark-toned deposits (Nmc1, Nmc2, Nmr2), but the dark-toned deposits occur on at least two distinct, undulating geomorphic surfaces separated by scarps. It is uncertain whether these distinct surfaces reflect intervening erosional episodes, tectonic deformation, or possible subsurface subsidence. Another distinctive feature is the presence of resistant ridges in the light-toned deposits that occur as reticulate, dike-like masses that produce a honeycomb series of depressions in the more erodible light-toned deposits (unit Nmh of *Korteniemi et al.* [2005a]). These ridges do not appear to continue into the overlying dark-toned layered deposits, and thus they probably predate deposition of units Nmc1, Nmc2, and Nmr2.

[65] Our interpretation of the stratigraphy of crater A differs somewhat from that of *Korteniemi et al.* [2005a]. MOC NA image M11-02708 suggests that the unit C1a (Figure 22b), previously interpreted as crater ring material, is capped by layered deposits and is a small erosional remnant of more extensive deposits, probably correlative with Nmc1 or Nmc2. We interpret the light-toned layered deposits Nmr1 to be correlative with the more eroded Nmh deposits and the Nmr2 unit to be correlative with the Nmc1 and Nmc2 units. The isolated light-toned deposit mapped as Nmc2, and pointed at by the arrow in Figure 22b, is probably younger than both the other mapped Nmc2 unit and the Nmc1 unit. Finally, the bulk of the units mapped as Nmc1 and Nmc2 appear to be mostly a single, broadly warped geomorphic surface with the exception of the higher plateau forming the northwestern portion of their mapped Nmc1 unit.

4. Relative Age Dating from Crater Counts

[66] Relative ages of planetary surfaces have traditionally been determined by crater size-frequency statistics, and a crater-age chronology has been established for Mars [*Tanaka*, 1986; *Hartmann*, 2005]. The determination of well-constrained relative ages requires large sample areas, but the geomorphic units within Terby are generally smaller than 10^4 km^2, therefore limiting the precision of crater counts. To minimize the uncertainty associated with small sample areas, two of the larger units, the crater-floor unit (CF, 10,135 km^2) and the moat floor (MD, 1270 km^2) were selected for counting of all craters greater than 125 m diameter using THEMIS VIS and daytime IR images. The results from the crater counts were grouped into $\sqrt{2}$ $\log_{10}$ diameter bins [*Hartmann*, 2005]. Only 15 of the 121 craters on the CF unit exceed 1 km in diameter, and only 1 of the 37 craters in the MD deposit exceeded 1 km. The apparent age of these surfaces varies with crater size (Figure 23). Craters >1 km diameter suggest an effective age near the Hesperian-Amazonian boundary for the CF unit, but for smaller craters the CF and MD units suggest a younger age of about 0.1 Gy. The use of craters <1 km diameter to date Martian surfaces is a topic of current debate [*Neukum et al.*, 2004; *Quantin et al.*, 2005; *McEwen and Bierhaus*, 2006; *Quantin et al.*, 2007] because of the large relative proportion of secondary craters whose temporal and spatial stochasticity complicate interpretation and may create large

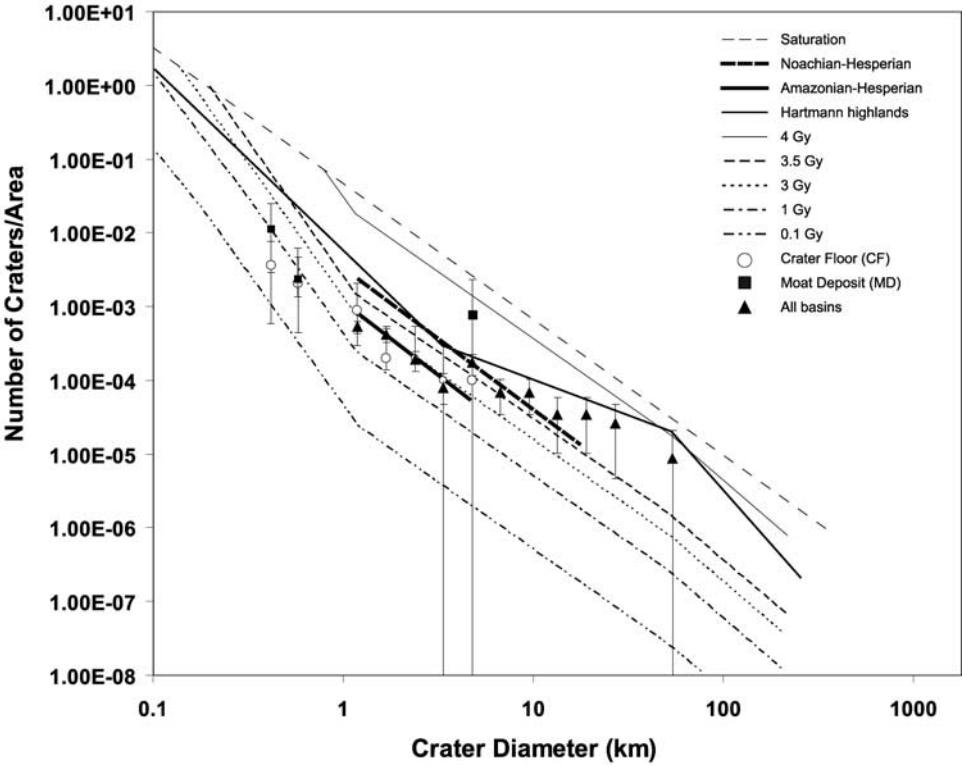

Figure 23. Crater counts for basins containing layered deposits, plotted using the density of craters in $\sqrt{2}$ $\log_{10}$ diameter bins. Unit boundaries, age contours, and the Martian highland reference curve are from *Hartmann* [2005]. Open circles are crater counts from the crater floor (CF) unit in Terby and filled squares are for the moat deposit (MD) in Terby. The solid triangles are a pooled count of all craters greater than 1 km in diameter interpreted to be younger than the layered deposits occurring within Terby, Niesten, Millochau, A, B, and SW craters (Figure 1).

statistical uncertainties. In addition, most exposed LD on Mars have very young crater ages because of geologically recent modification of the surfaces by aeolian erosion and mantling [e.g., *Malin and Edgett*, 2000, 2001; *Arvidson et al.*, 2003].

[67] Determining the age of emplacement of the LD is handicapped by the small number of craters of a size range (greater than about 1 km in diameter) that are unaffected by secondary impacts or destruction by subsequent aeolian modification. We have adopted the approach of pooling counts of >1 km diameter craters for all of the crater basins containing layered deposits in this study (Terby, Millochau, Niesten, SW crater, and A and B craters, for a total area of 1.92×10^5 km^2) under the working hypothesis that all the layered deposits in this region accumulated within a narrow time interval. We have excluded from our count all craters that appear to predate the layered deposits, and craters that straddle the rim of the basins are counted as one half. The count of craters >5 km diameter suggest a Noachian age of emplacement of the LD (Figure 23), which is consistent with previous studies that suggest that the layered deposits in Terby and the other crater basins were emplaced before the end of the Hesperian [*Ansan and Mangold*, 2004; *Ansan et al.*, 2005, 2006; *Mest and Crown*, 2005; *Korteniemi et al.*, 2005a]. Crater frequency in the 1 to 5 km diameter range suggests that appreciable modification of the layered deposit surfaces may have occurred up to the Hesperian-Amazonian boundary.

5. Discussion

5.1. Layered Deposits in the Hellas Region

[68] Analysis of the characteristics and stratigraphy of the layered deposits (LD) in Terby and other large craters in the Hellas region reveals several critical observations, which we summarize below.

[69] 1. As much as 2.5 km of light-toned, LD accumulated in Terby, Niesten, Millochau, SW crater, and A and B craters. The layers range from beds 10 or more meters thick to less than 1 m. At the resolution of HiRISE imaging (about 1 m on low-gradient erosional slopes), many of the thick beds display no obvious fine layering.

[70] 2. The ease of aeolian erosion of the layers suggests that the layers are primarily composed of partially indurated sediment finer than sand. Some beds are more strongly indurated and weather to blocky fragments that partially mantle the layer exposures and a few beds at the top of the sequence may be composed of directly emplaced, rubbly, meter-scale debris.

[71] 3. Many of the thicker beds and sequences of layers can be traced laterally over tens of kilometers in MOC NA images without appreciable change in apparent thickness, and meter-scale beds can be traced hundreds of meters.

Channel deposits and cross-bedding are not apparent in available high-resolution images.

[72] 4. The LD are generally of greatest thickness on the northern, anti-Hellas side of their respective basins. This is particularly evident in Terby, Niesten, B, and SW craters, but less marked in Millochau and crater A. The surface of the LD in Terby, Niesten, Millochau, and SW crater slope gently towards the south (less than 1° slope) from their northern termination at the inner crater rim to near the center of the crater. In Terby, the LD are bound by abrupt erosional scarps at their southern end, but in Niesten, Millochau, and SW crater, the surfaces of the LD steepen near their southern terminus to slopes of about 2°–3°. Erosional exposures in Terby, Niesten, and SW crater indicate that the uppermost several hundred meters of layers conform to the overlying surfaces, and thus steepen at their southern end.

[73] 5. Unconformities occur at both a regional and local scale within the LD. These do not appear to involve tectonic deformation or steeply dipping bedding. One layer sequence about 400 m thick at the southern end of the western bench in Terby appears to have distorted bedding.

[74] 6. At least portions of the LD have a chemical signature (detected by OMEGA) indicative of hydrated minerals interpreted to be phyllosilicates [*Ansan et al.*, 2005; *Bibring et al.*, 2006] that could be related to primary (i.e., lacustrine environment or evaporate sequence) or secondary (i.e., geothermal or surficial alteration) processes.

[75] From observations 1–3, above, we conclude that majority of the LD have been deposited by suspension from a fluid (air or water) rather than from shear flows (e.g., fluvial bedload, mass flows, or glacial till).

[76] The LD in Terby and other craters on the northern rim of Hellas (Figure 1) probably share a common age and mechanism of emplacement. As discussed above, the LD exposed in these craters exhibit similar tone, layering properties, and stratigraphy. Most of the LD in the larger craters share a similar asymmetrical distribution, with greater depth of accumulation on the northern, anti-Hellas side, and in Terby, Niesten, Millochau, and SW crater, the dip of the LD appears to steepen near their southern edge. The LD in these craters also have similar densities of superimposed craters greater than 1 km in diameter. Finally, LD on Mars have a clustered distribution [*Malin and Edgett*, 2000], including the Hellas rim region. Our discussion assumes a common age and depositional environment of the LD in this region, and we draw upon observations from all the craters studied to infer the geologic history reflected by the deposits.

[77] Because of the large volume and widespread occurrence of LD in the Hellas region, origin from local erosion and redeposition is less likely than the production of large amounts of fine-grained sediment outside the region. Explosive volcanism is one mechanism for production, transport, and deposition of fine pyroclastic ash as well as global redistribution of fine ejecta from basin-scale impacts. Aeolian redistribution of fine sediment from deflated regolith and crater ejecta is an additional possible origin, as is abrasion during aeolian saltation of sand-sized sediment. The primitive mineralogical state of weathering observed in the modern Martian global dust blanket [*Christensen et al.*, 2001] and the limited extent of exposures of phylosilicates [*Poulet et al.*, 2005] suggest that erosion of a deep, fine-grained regolith produced by chemical weathering is an unlikely origin of the sediment within the Hellas region craters.

[78] The thick LD in the Hellas region are nearly universally limited to the interior of impact craters, perhaps reflecting either the pattern of initial deposition of sediment transported into the region, or the pattern of later reworking or differential preservation of a deposit that was initially more broadly distributed. The presence of thick, fine-grained LD that exceed the rim height of their enclosing crater in some regions (e.g., Craters Henry and Gale) suggests original deposition as a widespread sedimentary blanket that was subsequently eroded but preservation within craters was differential [*Malin and Edgett*, 2000]. Several observations suggest that the upper surface of the LD within craters in the Hellas region, however, approximates their original depth of accumulation. Both the light-toned and the overlying dark-toned layers are asymmetrically distributed in most of the larger basin deposits, including Terby, Niesten, Millochau and SW crater. The dip of the bedding appears to be broadly conformable to the top surface of the deposits that transition from gently sloping layers on the northern side of the deposit to a steeper inclination on the southern side of the layered deposit. Subsequent erosion of the LD in Niesten appears to be slight, so that the present surface configuration (minimally modified by troughs and pits) approximates the original final surface of accumulation. Where the LD can be traced to the enclosing crater wall (in Terby, Niesten and SW crater), the deposits appear to pinch out at the crater wall without appreciable steepening of dip (basal deposits from airfall or deep water sedimentation would likely steepen near the crater wall to become conformable to the containing vessel (the crater)). The numerous craters exposing LD in central pits on the western rim of Hellas (Figure 1) have smooth crater floors (with the exception of the pits) sloping inward from the interior crater walls, suggestive of an original depositional surface. Because of the limited exposures of the light-toned deposits from beneath a general cover of dark-toned deposits in Niesten, Millochau, SW crater and craters A and B, it is possible that the contact between the light and dark-toned sediments is unconformable, with an uncertain amount of erosion of the light-toned deposits before deposition of the dark-toned layers.

[79] Assuming that the present maximum thickness and general distribution of LD within the Hellas basin craters is close to their original extent, the localization of the deposits within the crater might reflect either selective deposition of sediment transported into the region or later remobilization of more broadly distributed sediment and its concentration within the larger crater basins. We explore below a number of possible scenarios for emplacement of the light- and dark-toned sediment.

5.2. Origin of the Layered Deposits

[80] On the basis of the nature of the LD, a number of potential depositional mechanisms can be readily eliminated. The only mass wasting process capable of distributing the extensive LD would be rapid processes such as debris flows and landslides, which would not likely result in regular, parallel bedding and would require a high-

elevation source region and a means to pass over the crater rims. Also, appreciable coarse debris would likely be present in such mass flow deposits. Glacial flow emplacement would require deep ice over the cratered highlands, for which there are no obvious glacially sculpted features, and glacial flow and meltwater would deliver deposits of a wide range of sediment grain size, rather than well-sorted fines. The fine-grained nature and erodibility of the layers dismiss origins such as volcanic lava flows or intrusions.

[81] Given the history of explosive volcanism on the eastern rim of Hellas, the fine-grained nature of the layers could be indicative of ignimbrite deposits (pumice-dominated, gravity-driven pyroclastic flow deposits with subordinate ash). The thick, well-bedded layering, the geographic limitation of layers to the interior of craters, and the considerable distance from potential sources (such as Tyrrhena Patera and Syrtis Major), however, make direct deposition as pyroclastics implausible.

[82] The layers are not likely related to deposition as an aeolian sand sea because they are too regularly bedded for dunes, and they do not appear to be composed of sand-sized grains. If the deposits were predominantly sand, erosion should result in young, light-toned dunes, which are not prominent within the crater. Additionally, there is no apparent cross-bedding observed at MOC NA or HiRISE resolution in LD_1, LD_3 or LD_4 but cannot be definitively ruled out as an origin for the broad, curved, discontinuous layers in LD_2 (Figures 9e and 9f).

[83] *Ansan and Mangold* [2004] and *Ansan et al.* [2005] proposed a deltaic (fluvial) origin for the LD in Terby. The broad disposition of the LD in Terby, Niesten, and SW crater is suggestive of terrestrial deltas because of the planform radiating into the craters from the north crater walls, the gentle, southward slope of the top surface of the deposits, and the transition in Terby, Niesten and SW crater to a steeper southward slope at the southern margin of the deposits (Figure 21), reminiscent of the transition from topset to foreset environments. However, both the nature of the LD and the physiographic context argue against a deltaic origin. Fluvial deposits derived from erosion of crater rims and intercrater plains should include coarse-grained materials that would be resistant to aeolian scour. Lenticular channels associated with alluvial fan deposition are not observed in the layered terrain within Terby. Furthermore, the continuity of the LD over several kilometers is not typical of alluvial fan deposition, which is characterized by frequent avulsions that are associated with deposition over a small portion of the fan surface. The most compelling argument against an alluvial fan origin is the lack of large valleys capable of supplying the requisite sediment. Where deltaic deposits and large alluvial fans have been identified on Mars (e.g., the fan deposit (FD) radiating from NW crater), they are associated with well-defined source valleys or with deeply eroded alcoves on the crater walls [*Malin and Edgett*, 2003; *Moore et al.*, 2003; *Moore and Howard*, 2005a; *Howard et al.*, 2005; *Irwin et al.*, 2005]. Such contributing sources are not present in the Hellas region craters that contain LD. The topography north of the layered benches in Terby indicates that there is no direct source for the western bench, which abuts extremely rugged topography to the north. A southward sloping upland plain lies northeast of the central trough, but a 300 m ridge separates the uplands from Terby. Likewise, in both Niesten and SW crater, their northern rims are unbroken and higher than the plains to the north. Millochau and craters A and B of *Korteniemi et al.* [2005a] also lack inflowing fluvial channels breaching the basin rims.

[84] The fine-grained, cliff- and terrain-conforming nature of the LD is similar to terrestrial loess deposits [e.g., *Pye*, 1987]. The localization of LD within deep craters and their asymmetrical distribution on the anti-Hellas side of the crater interiors within Terby, Niesten, Millochau and SW crater could be consistent with airfall deposition. Craters are natural sediment traps, and the northern crater walls would offer the greatest protection from upslope winds. This location within the craters might be more problematic for deposition or deposit survival from katabatic downslope winds, for flows could accelerate down the northern crater walls (yardang-like sculpting of LD within SW crater suggest erosion by slope winds flowing towards Hellas). The sediment, if deposited by wind, might either have been derived from outside the Hellas region (originating, for example from volcanic eruptions or aeolian erosion) or may have resulted from the reworking of Hellas deposits after the disappearance of any lakes, or during episodic lowstands, if they occurred.

[85] The gentle gradients of the upper, anti-Hellas portions of the LD in Terby, Niesten, Millochau and SW crater suggest a strong gravitational control on layer deposition. Accumulation as dunes or as direct airfall deposition of aeolian dust, volcanic ash, or global redistributed impact ejecta is unlikely to result in planar, nearly level depositional surfaces. In addition, such depositional mechanisms would not be expected to produce the observed break in slope of the surface of accumulation seen in Niesten, Millochau and SW crater. The observed gravitational control on layered deposit morphology and the hydrated mineral signature of the LD in Terby suggests that the layers were either deposited by, or at least modified by, either fluvial or lacustrine processes, but a loess-like origin for the layers cannot be definitively ruled out.

[86] The nature of the layers is consistent with deposition in a lacustrine environment, as suggested for other craters on Mars. Lacustrine involvement might occur in any of several modes. If lakes were present during airfall deposition events, the water acts as a natural sediment trap whereas on dry land, deposition might not occur or might be subject to later wind scour. The lacustrine environment might encourage diagenetic cementation of trapped sediment (as has clearly occurred for LD in the Hellas region), protecting them from subsequent aeolian deflation. If water were deeper (e.g., a deep lake in the Hellas basin), submersed craters would again be sediment traps, encouraging deposition and discouraging erosion because of protection from waves and currents (including density currents). Longshore drift and density flows could also deliver sediment to shallowly submerged craters as such flows commonly deliver fine sediment to ocean basins that serve as sediment traps [*Milliman and Kao*, 2005; *Lamb et al.*, 2005].

[87] Topographic, morphologic and stratigraphic evidence in Hellas suggests that the interior fill was deposited in water [*Moore and Wilhelms*, 2001], and that Hellas may have been the site of a basin-wide sea [*Malin and Edgett*,

2000] or may have contained one or several ice-covered lakes [*Moore and Wilhelms*, 2001] in the Noachian. Two of the putative stands of water or ice in Hellas mapped by *Moore and Wilhelms* [2001], −4.5 km and −3.1 km, correlate to the elevation of the crater floor and part-way up the crater rim of Terby, respectively (Figure 24a). The position of these putative stands is intriguing on the basis of their correlation to the high and low topographic features in Terby. A histogram of the elevation in the greater Hellas region shows small frequency peaks at elevations of −4.5 km and −3.1 km and larger peaks that correlate to elevations of −2.1 km, −0.7 km and +0.6 km (Figure 24b). In addition, *Crown et al.* [2005] suggest that a textural change in landforms at about the −1.8 km level may correspond to a paleoshoreline of Hellas. The −1.8 to −2.1 km contour range corresponds to the highest, western bench in Terby, and the southern floor of Terby corresponds to the −4.5 km putative shoreline (Figure 24a). The −0.7 km and +0.6 km contours (Figure 24b), which correspond to well-developed inward facing scarp boundaries around Hellas (Figure 24c), suggest that Terby and the entire circum-Hellas region may have once been submerged to lake levels up to 3.6 km deep. Almost all of the craters around Hellas with evidence of pits and layers [*Moore and Howard*, 2005b] that are analogous to the Terby deposits are located at or below the scarp boundary that correlates to the +0.6 km contour level (Figure 24c). The southern rim of Terby at its lowest point is essentially level with the −4.5 km level of the flat southern floor (Figure 2c). Therefore, for lacustrine deposition to have occurred within Terby, the Hellas basin would have had to be flooded to at least the −1.8 km level. The sedimentary deposits in the other craters discussed here (Niesten, Millochau, SW crater and craters A and B) occur below the +0.6 km contour (Figure 24c) but have rims higher than their interior deposits, suggesting they could have hosted isolated lakes.

[88] We have noted that the three major benches in Terby are flat-topped and southward sloping, but occur at distinct levels, the western bench primarily at elevations between −1.7 to −2.2 km, the central bench at about −2.7 to −3.2 km, and the eastern bench crest at about −3.5 km

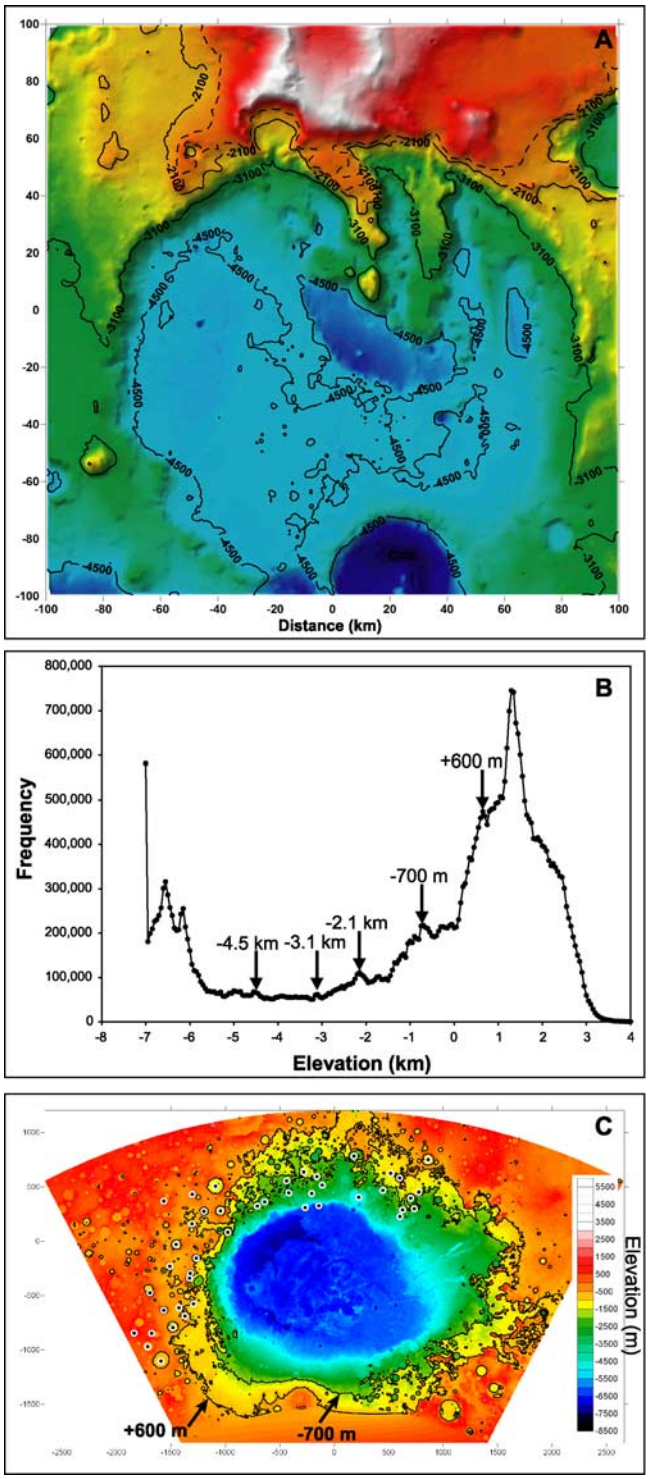

Figure 24. (a) Elevation-cued shaded relief image of Terby showing selected elevation contours. The −4.5-km, −3.1-km, −2.1-km, and −1.8-km (dashed) contours may represent stands of possible water (or ice-covered lakes) based on stratigraphic and morphologic evidence in the circum Hellas region. Two of the putative stands of water or ice in Hellas mapped by *Moore and Wilhelms* [2001], −4.5 km and −3.1 km, correlate to the elevation of the crater floor and the top of the central bench and northeastern and northwestern rims of Terby. Numbers on axes (kilometers) are relative to image center at 74°E and 27.5°S. Top of image is north. (b) Histogram of elevation frequencies around the Hellas basin. The frequency peaks at −4.5 km, −3.1 km, and −2.1 km correspond to the contour lines in Figure 24a. The peaks at −700 m and +600 m correspond to well-developed inward facing scarps (Figure 24c). (c) Shaded relief image of the Hellas basin region (elevation-cued in color version online) highlighting −700 m and +600 m contour lines that correlate to inward-facing scarp boundaries around Hellas. The floors of almost all of the craters with layers and/pits in the circum Hellas region (marked with dots) are located at or below the +600 m contour level [*Moore and Howard*, 2005b]. If water or ice-covered lakes or seas occupied Hellas to either of these elevations at some point during the Noachian, many of the craters in the circum Hellas region, including Terby, would have been under water. Horizontal scale is in kilometers; vertical scale is in meters. Projection is as in Figure 1. Top of image is north.

but sloping southward to the crater floor at −4.5 km (Figure 2, section 2.2.1.). In addition, parts of the southernmost portions of the western and central benches have flat summits at about the same elevation as the eastern bench crest (−3.5 km) (Figure 2). We have suggested a consistent sequence of light-toned LD within the central and western benches (compare Figures 8 and 10 with Figures 9 and 11), but it is also possible that the bench tops are erosional surfaces, with a thin mantling of dark-toned sediment, cut into the light-toned deposits during a sequence of changing (declining?) lake levels within Hellas.

5.3. Origin of the Troughs and Moat in Crater Terby

[89] Of the several basins containing LD, Terby has experienced the most extensive and most varied postdepositional modification of the LD, and thus contains the most definitive evidence of the later geological evolution of the region. The main, north-trending troughs are roughly 10 km wide and the floors exhibit horizontally layered mounds and lobe-like features associated with scarps and ridges (Figures 4 and 6). The troughs could have been formed by a number or combination of different mechanisms including mass wasting, flowing water, erosion by standing water, melting of thick ice deposits, dissolution by groundwater, aeolian deflation, glacial scour, or dissolution by glacial meltwater.

[90] Erosion of the troughs via mass wasting such as debris flows and landslides is unlikely owing to the scale of the troughs, the absence of scarps and associated terminal deposits, and the presence of the enclosed depressions (the exception is the local avalanche deposit along the western bench (Figures 3 and 6)). Dissolution by groundwater would cause erosion at depth, resulting in collapse features at or near the surface (i.e., karst topography), but the troughs and pits lack evidence of collapse-related features such as arcuate scarps, rotational blocks or disturbance of layer sequences along the edges. The scalloped nature of the layered slopes (Figure 8) and the removal of tens of meters of remnant mantling material (Figure 20) indicate at least a moderate amount of aeolian erosion or deflation. The north-south orientation of the troughs may be indicative of upslope or katabatic winds driven by the high relief of the Hellas basin rim. Although aeolian erosion could account for excavation of enclosed depressions, it does not easily explain the broadly curving margin of the moat (MD) or the smoothly curved eastern depression (Figure 2a). Obvious wind-scour-related features occur primarily on the high portions of the main benches and on the northwestern margin of the crater floor (CF) deposit, and they are much smaller in scale than the troughs. These observations do not favor aeolian erosion as the principal formation mechanism for the troughs.

[91] Although we have raised the possibility that the top surfaces of the light-toned LD were sculpted by changing lake levels within Terby, it is unlikely that shoreline processes would create deep embayments perpendicular to the strike of the shoreline. Both erosion and deposition along terrestrial shorelines tends to straighten rather than embay the overall shoreline trend. Dissolution associated with high-standing water could have played a role, but the spatial distribution of the deep troughs is not likely consistent.

[92] Features commonly associated with erosion via flowing water include large-scale dendritic valley systems or fluvial depositional features such as fans or deltas, none of which are apparent on the trough or moat floors (Figure 6). Isolated valleys occur on the steep crater rim but do not form an integrated drainage network (Figure 4a). Localized shallow, intersecting linear depressions occur in the upper troughs near the intersection with the crater walls (Figures 4b and 4c). While they are consistent with fluvial scour in an anastomosing network, their localized occurrence is not indicative of widespread fluvial incision of the troughs. Closed depressions such as the moat and the oblong depressions in eastern Terby and in the center of the western trough are not typical of a landscape primarily modified by fluvial processes.

[93] We suggest that the flow and possible melting of thick ice deposits could have formed the large troughs in Terby. The involvement of ice by glacial scour or dissolution is consistent given the scale and geomorphology of the features and the evidence for the past and present involvement of glaciers on Mars [e.g., *Head and Marchant*, 2003; *Head et al.*, 2003; *Head et al.*, 2005; *Shean et al.*, 2005]. Ice-related features such as lobate debris aprons and modification of the outflow valleys [*Crown et al.*, 2005] as well as ice-rich, glacier-like viscous flow features are common in the circum-Hellas region [*Head et al.*, 2005] during the Hesperian and Amazonian.

[94] The northern rim of Terby would be a natural location for ice to accumulate given the steep, pole-facing slopes, as evidenced by the presence of viscous flow features in the small crater on Terby's northwestern rim (Figure 18). If ice accumulated along the northern wall of Terby, it would flow south toward the center of the basin, setting the stage for glacial erosion and/or dissolution of the troughs and moat (MD). Within Terby, the broad-scale patterns of landforms are consistent with an ice margin associated with a deep ice mass, such as the curved edge of the MD and the eastern depression, the broad-scale streamlined form of the trough margins, and the streamlined remnant layered mounds protruding from the trough floors (TF) (Figures 4 and 6).

[95] The presence of anastomosing shallow valleys in the northern portions of the major TF in Terby (Figures 4b and 4c) may be indicative of subglacial meltwater flow. Erosion by precipitation-driven runoff usually excavates single valleys occupied by meandering or braided streams. Braided streams are typically characterized by shallow, ephemeral channels, not deeply incised anastomosing valleys. On both Earth and Mars, anastomosing valley systems generally originate by erosion of short-lived, high-magnitude floods (e.g., the Martian outflow channels) or as confined flows beneath glacial ice (tunnel valleys [e.g., *Denton and Sugden*, 2005; *Lewis et al.*, 2006]). Because we see no evidence for subsurface or ponded water sources for major floods within the Terby troughs, we suggest a subglacial origin.

[96] A variety of trough-paralleling ridges and depressions on the TF, sometimes with a lobate planform, are also suggestive of sculpture by ice flow (Figure 4a). We also suggest that the lobate indentations of the western and northwestern margin of the CF deposit (Figures 4, 5, and 16) record glacial erosion. These lobate indentations on the

northwestern TF (Figure 3) at the base of Terby's inner rim is a likely place for ice to accumulate. The northwestern TF is sculpted into subparallel ridges and depressions (including short, sinuous, esker-like ridges) that trend downslope towards the lobate indentations into the CF deposits (Figure 16).

[97] Isolated sinuous ridges occur locally on the MD and within the grooved terrain (GT) (Figures 17 and 19). In addition, a number of ridges lacking obvious sinuous planform occur on the TF paralleling the trough trends (Figure 4a). These could be topographically inverted fluvial deposits etched into relief by aeolian deflation [e.g., *Malin and Edgett*, 2003; *Moore et al.*, 2003; *Edgett*, 2005; *Williams and Edgett*, 2005] or possibly eskers [e.g., *Howard*, 1981; *Kargel and Strom*, 1992; *Ghatan and Head*, 2004; *Burr et al.*, 2006]. The subparallel nature of many of the ridges (Figure 17) and the lack of dendritic tributaries favors an origin as eskers.

[98] A major difficulty with the explanation of the troughs forming by glacial erosion is the paucity of obvious landforms and depositional features associated with ice processes, such as cirques, outwash plains and moraines. The gentle, 50- to 100-m rise on the CF at the boundary of the MD might be a low, remnant moraine or outwash plain, but the volume of this feature is much less than the volume eroded from the troughs and moat cavity. If the LD are primarily evaporites, the interaction with ice may have dissolved the underlying terrain. Alternatively, if the LD are mostly loosely cemented silt-sized material (loess) and were disaggregated by ice, the material may have been carried out of the crater by aeolian processes instead of being deposited as moraines or outwash. The depressed lobate indentations on the northwestern TF (Figure 3) might be evidence for easy breakdown of LD material on the margins of the ice sheet (Figure 16). Finally, the depositional glacial features and material removed from the troughs may have been reworked by water in lakes (either a deep lake associated with Hellas, or a shallow lake enclosed by the southern Terby wall and later breached by a channel) and transported into the Hellas basin as discussed in section 5.2.

[99] Although the TF, MD and adjacent CF lack obvious end moraines and outwash, we conclude that morphologic features of these landforms is most consistent with the former presence of deep ice, including the broadly lobate form of the trough margins, anastomosing channels and possible eskers on the TF, and lineations and streamlined features that are suggestive of flow.

5.4. Geologic Evolution of the Terby Region

[100] The following geologic scenario for the evolution of the Terby region is based on crater-count age dating (Figure 23), the detailed geomorphic and stratigraphic observations of Terby's interior deposits from the currently released data, and the regional context of the Hellas impact basin, including other craters with interior layered deposits.

5.4.1. Crater Terby

[101] We first outline the sequence of events that we postulate occurred within the crater (summarized in Table 1), followed by our interpretation of the processes responsible for the deposition and subsequent erosion of the LD (Figure 25).

[102] After the formation of the Hellas impact basin, numerous 80+ km impact basins, including Terby and the others now hosting LD, were created during the period of heavy bombardment. Some crater degradation apparently occurred prior to accumulation of the thick LD, because the rim of Terby (as well as Niesten and SW crater) became rounded prior to layer deposition. The thick sequence of primarily light-toned LD, in at least four major units, then accumulated in the northern half of the crater (Figure 25a) with a slight southward dip (Figures 25a and 25b). We favor a deep lacustrine depositional environment for the LD in Terby, and the depth of the proposed (ice-covered?) lake likely fluctuated so that material was transported through Terby into the greater Hellas basin during periods of high water levels (Figure 25a). The areal density of craters greater than 5 km in diameter superimposed on the LD in Terby and the other craters in this study indicate the LD were deposited during the Noachian (Figure 23). Because of later erosion, the original southern extent of the layers is uncertain; they could have extended well to the southern edge of Terby but likely steepened just beyond their present southern edge (Figure 12), a scenario consistent with the unbroken connection between the layers in the eastern bench and the CF. Another uncertainty is whether the different elevations of the western, central and eastern benches (Figures 2a and 2d) are a consequence of primary depositional levels or of subsequent erosional planation.

[103] The next distinguishable event within Terby is the formation of the flat southern crater floor (CF) at an elevation of about −4.5 km (Figures 24a and 25b). The formation of this surface may have been accompanied by some erosional planation of the southern extent of the LD. This was either followed by, or was concomitant with, the major erosional episode that formed the deep troughs incised into the LD as well as the moat deposit (MD) (Figures 2a and 25b), the northwest TF adjacent to the CF (Figure 16), and the depressions along the western margins of the CF deposit (Figure 5). We propose that high, possibly ice covered lake levels in Hellas persisted through the stage of trough incision (Figure 25b). Unless chemical dissolution of the material in Terby was a dominant process, the existence of an ice-lake boundary in Terby, occurring around −4.5 km, is necessary to account for the material removed from the troughs and the moat. The slight southward slope of the CF at the boundary with the MD might be underlain by material that was excavated and deposited as fan-like structures from glacial melt water activity. Material could have been transported south into the greater Hellas region during high lake levels. One unknown, however, is the number, timing and extent of lake level fluctuations and ice advances in Terby. The density of craters 1–5 km in diameter on the MD and CF deposits suggest that these features were formed by the end of the Hesperian (Figure 23). The crater modifying the southern rim of Terby likely formed during this time, as the ejecta from this impact are embayed by the CF deposits.

[104] Subsequent to the erosional period that formed the major troughs into the LD (Figure 25c), NW crater formed, creating the fluidized ejecta mapped as grooved terrain (GT) (Figures 3 and 19) and possibly triggering the avalanche on the western bench (Figure 25d). Deep depressions were eroded into the LD and at the margin of the GT subsequent

Table 1. Provisional Geologic Timeline for the Northern Hellas Region[a]

Description of Events	Terby, Niesten, and SW Crater Units	Millochau Equivalent[b]	Craters A, B Equivalent[c]	Probable Time Correlation
Continuing aeolian erosion of layered sediments within crater basins. Contemporary viscous flow features in the crater on the northwest rim of Terby. Local aeolian deposits.	VF	Amd, AHt		Hesperian to Amazonian
Modest late-stage fluvial erosion in Terby, Niesten, and SW crater results in sparse, shallow valleys and an alluvial fan debouching from a crater on the northwest rim of Terby.	FD, avalanche deposit			Hesperian
Deposition of a thin, dark, indurated mantle over most of the Hellas region.	MU			Hesperian
Period of extensive erosion of crater fills. Multiple possible episodes of erosional planation in Terby, formation of flat crater floor surfaces in southern part of Terby, Niesten and SW crater. This was followed or accompanied by formation of deep troughs and moats. Dark-toned sediments mantling the rim and interior walls of Terby, Niesten, and SW crater relatively unaffected by erosion. Possible ice and lacustrine erosional involvement in Terby, Niesten, and SW craters. Higher elevation craters northeast of Terby, including Millochau and craters A and B experience considerable fluvial erosion of crater rims and lesser erosion of the layered deposits, resulting in bajada-like mantling of the outer portions of the layered deposits.	CF, MD, TF, GT	HNmr	HNms	Late Noachian to Hesperian
Deposition of dark-toned sediments on top of earlier light-toned sediments. Deposits mostly largely conformable with underlying light-toned sediments. Top surface of dark-toned deposits erosionally resistant, lower layers more erodible than top layers of underlying light-toned sediments. Correlative mantling may have occurred on crater rim and intercrater plains.	dark-toned layered deposit in Niesten and SW crater, MT in Terby	Nmp	Nmc1, Nmc2, Nmr2	Late Noachian
Possible erosional planation of top surface of light-toned deposits. Possible time period of formation of reticulate dikes in light-toned deposits within crater A.				Late Noachian
Deposition of light-toned layered sediments in most major impact basins. Lower portions are more massive and nonresistant, upper portions coarsely layered and resistant. Deposits thickest on anti-Hellas side of crater basins. Original surfaces of deposition exhibited considerable broad-scale relief.	LD	HNme, Hk	Nmh, Nmr1, HNme	Mid to Late Noachian
Interiors of craters filled with several hundred meters of unexposed materials. Probable fluvial involvement.				Mid Noachian
Major impact basins form on rim and ejecta deposits of Hellas.	RT	Millochau Rim	C1A, C1B	Early to Mid Noachian

[a]Oldest events are at the bottom of the table.
[b]*Mest and Crown* [2005].
[c]*Korteniemi et al.* [2005a].

to the emplacement of NW crater, possibly caused by the impact.

[105] The fan deposit (FD) on the north wall of Terby is the next major event, likely forming from episodic releases of meltwater from NW crater (Figure 25e). The fan terminates in incision of shallow, sinuous channels into the fan surface (Figure 19b). The terminal fan incision may be coincident with erosion of sparse, shallow, generally unbranched valleys incised into the northern (Figure 4b) and eastern (Figure 4c) crater rims and TF.

[106] A dark-toned, moderately indurated mantling unit (MU), of meter-scale thickness (Figure 20), was deposited over the LD and probably over the entire Terby landscape (Figure 25e). Subsequent differential erosion, presumably by aeolian deflation, has left some MU exposures in relief above more erosion-prone LD (Figure 20). The age of the MU relative to the NW crater impact and the FD is uncertain.

[107] The final major modification has been the development of the viscous flow features (VF) in NW crater (Figures 3 and 18). The age of this deposit is uncertain, but it is likely related to Hesperian [e.g., *Milkovich et al.*, 2002; *Dickson and Head*, 2006] or perhaps Amazonian-aged [e.g., *Head et al.*, 2003] ice activity.

5.4.2. Comparison With Other Craters in the Hellas Region

[108] A consistent series of depositional and erosional events appears to have characterized the history of crater basins on the Hellas rim and its surrounding ejecta sheet (Table 1). Deposition of light-toned, LD was widespread within larger craters, with preferential deposition on anti-Hellas side of their respective basins. These deposits were mantled, perhaps conformably, by a thinner sequence of dark-toned layered sediment. In Terby, Niesten and SW crater, the upper, northern surface of the dark-toned deposits slope gently towards the basin centers, but display multiple terraced levels. These might have resulted from changing base levels (presumably lake levels) during deposition of the dark-toned deposits or planation of the underlying light-toned deposits prior to deposition of the dark-toned depos-

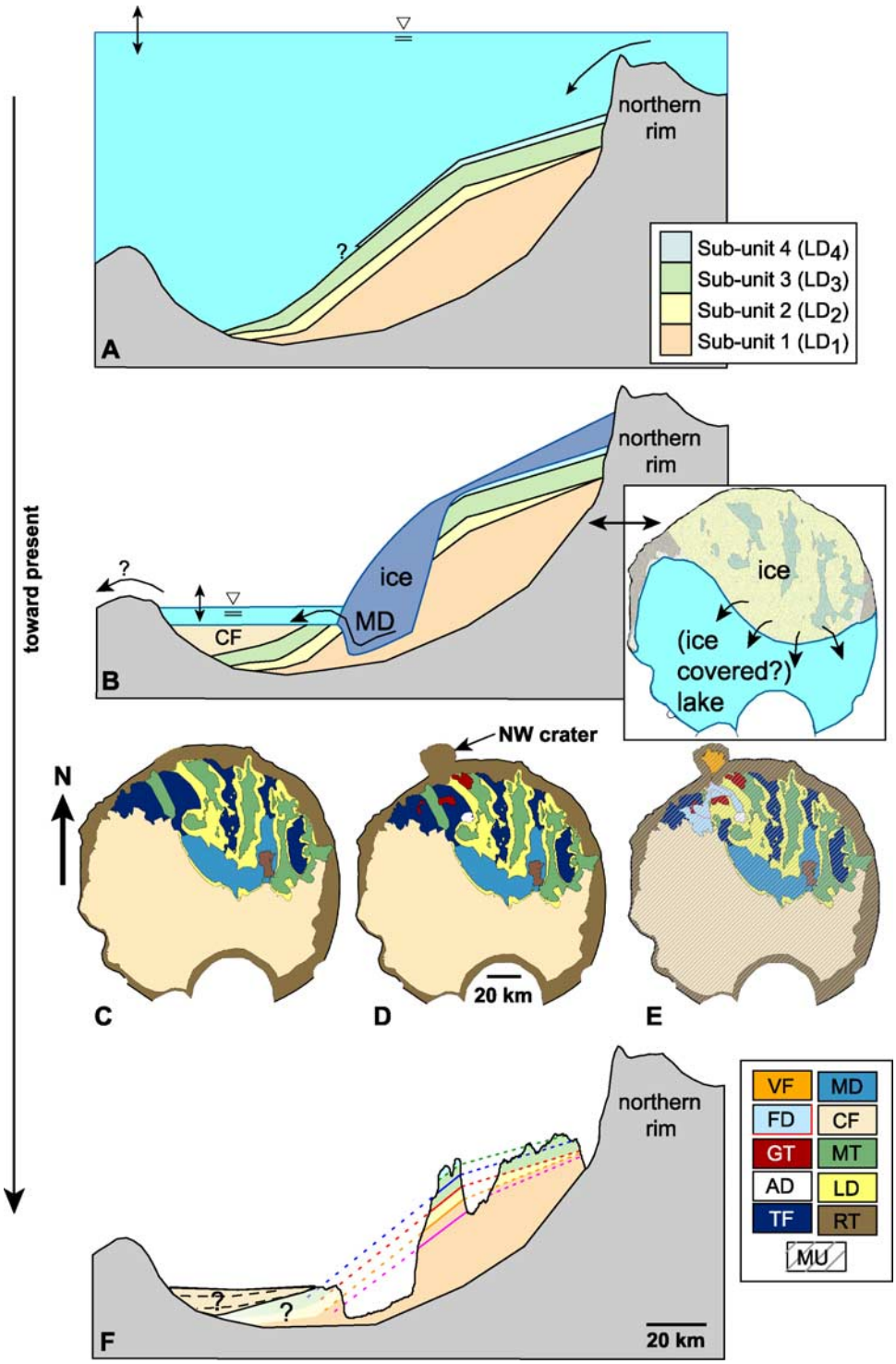

Figure 25

its. The LD have subsequently become eroded, often into deep troughs or depressions. The light-toned layers, when exposed, appear to have been most susceptible to erosion. The erosional history differs somewhat between topographically lower craters on the interior Hellas rim (Terby, Niesten, and SW crater) than in higher craters on the exterior crater rim (Millochau, craters A and B). In the lower craters, erosion produced flat southern crater floors and, in Terby and SW crater, moat-like depressions between the flat crater floor and the eroded layered deposits to the north. Lacustrine and/or ice-related processes may have been involved in this erosion. During the same general time period the rims of the higher craters (Millochau, craters A and B) experienced extensive fluvial erosion and development of a fluvial depositional annulus (the bajada) surrounding exposures of the layered deposits (Figure 22). This fluvial erosion may have eroded and buried the northern portions of the earlier layered sediment deposits in Millochau and crater A. Fluvial rim erosion in the lower craters was absent or less pronounced. This period of fluvial erosion and deposition may have been related to the general mid- to late-Noachian fluvial crater degradation [e.g., *Craddock et al.*, 1997; *Craddock and Howard*, 2002; *Irwin and Howard*, 2002] or to the terminal episode of fluvial activity within the highlands [*Howard et al.*, 2005; *Irwin et al.*, 2005].

[109] Subsequent to this period of extensive erosion, a meter-scale mantling of indurated dark-toned sediment was emplaced over the region, obscuring many of the exposures of the earlier layered sediments. Sparse channels and depression-floor deposits suggest a period of not more than modest precipitation and local lacustrine activity including the formation of the fan deposit in Terby. The relative timing of the mantling and the late fluvial incision is uncertain. The late history of this region has been characterized by aeolian erosion and local development of viscous flow features in some smaller craters.

6. Conclusions

[110] Thick sequences of light-toned layered deposits and their capping unit of intermediate-toned sediment were deposited during the Noachian within Terby and other craters within the Hellas region, including Millochau, Niesten, and the informally named A, B, and SW craters (Figure 1). We infer a Noachian age from crater age determination (Figure 23). The ability of aeolian erosion to scour these indurated deposits and the paucity of a sandy lag that would be expected to form sand dunes suggest they are primarily silt and finer grain size. A number of sources of the sediment were evaluated, and two are most plausible, deposition of silty airfall deposits possibly related to orographic winds associated with the Hellas basin versus accumulation as lacustrine sediments in a deep lake occupying the Hellas basin. The lateral continuity of the layers, their near-horizontality, and the presence of other possible lacustrine features within the Hellas basin in the elevation range of Terby [e.g., *Moore and Wilhelms*, 2001] are most consistent with a lacustrine origin of the layers. Some uncertainty remains about the original extent and lateral continuity of the layers and whether the planar upper surfaces of the benches of layered deposits in Terby (and the other craters with layered deposits) are final surfaces of deposition or are surfaces of subsequent planation.

[111] The fluvial erosion of the rims of craters A, B and Millochau and the formation of a fluvial bajada (Figure 22) may have occurred around the same time as the deep erosion of the layered deposits in Terby to form troughs ~10 km wide, and up to 2 km deep (Figure 2) and lesser erosion in Niesten and SW crater (Figure 21a). We infer the primary agent of layer erosion in Terby was glacial scour or layer dissolution by glacial runoff from ice that accumulated on the steep, pole-facing northern crater rim. Evidence supportive of glacial erosion includes the overall lobate form of the troughs and surrounding depressed moats (Figure 2), lineated terrain on the lower margins of Terby's rim (Figure 16) and in the trough bottoms (Figures 4 and 6), streamlined hills of remnant layered deposit exposures (Figure 6), anastomosing valleys in the northern portions of the trough floors (Figure 4) that may have resulted from subglacial tunnel erosion, sinuous ridges that may be eskers (Figures 16, 17, and 19), and the present-day presence of viscous flow features in NW crater (Figure 18). The flat southern crater floor in Terby may have been formed at about the same time by lacustrine reworking of the layered deposits and possible interaction with the glaciers. Excavation of the troughs in Terby and fluvial modification of Millochau and craters A and B craters was followed by deposition of a thin, indurated mantling unit over the layered deposits (and presumably over the entire region) (Figures 15 and 20) and formation of an alluvial fan on the northern Terby wall (Figures 3 and 19), possibly by meltwater from glacial ice in NW crater. The alluvial fan was subsequently modified by shallow incision of sparse channels, probably during the late-Noachian or Hesperian. Finally, viscous flow features developed (or remained) in

Figure 25. Possible geologic evolution of Terby based on geomorphic and stratigraphic analysis of interior deposits (relative temporal sequence Figures 25a, 25b, 25c, 25d, with 25e and 25f representing present conditions). Alternative scenarios for layer deposition are discussed in the text. (a) Sediment was transported (arrow) into Terby in a lacustrine environment and the layered deposits (LD) were deposited. Lake levels likely fluctuated. (b) Cross section (left) and map view (right) showing the formation of the crater floor (CF) and the ice that carved the trough floors (TF) and moat deposit (MD) into the LD. The vertical extent of the ice is unknown. (c) Period immediately after major ice activity ended. (d) The impact forming NW crater created the fluidized ejecta (GT) and likely triggered the avalanche deposit (AD). The original GT was likely more extensive, but only the present-day exposures of this unit are mapped. (e) The fan deposit (FD) on the north wall of Terby formed from episodic releases of meltwater from NW crater. A dark-toned, indurated mantling unit (MU) was deposited over the entire Terby landscape, and the contemporary viscous flow features (VF) in NW crater developed. (f) Present-day topographic profile of Terby (see Figure 12 for complete explanation). Aeolian processes are presumably ongoing.

NW crater and the layered deposits were eroded by aeolian scour, locally raising the indurated mantling unit into relief (Figure 20).

[112] **Acknowledgments.** The authors sincerely thank Scott Mest and an additional reviewer for their constructive insight. This project was funded by the NASA Mars Data Analysis Program and the Planetary Geology and Geophysics Program. MOC images are courtesy of NASA/JPL/Malin Space Science Systems, THEMIS images are courtesy of NASA/JPL/Arizona State University, and HiRISE images are courtesy of NASA/JPL/University of Arizona.

References

Aittola, M., V. P. Kostama, H. Lahtela, and J. Raitala (2003), Fluvial processes modifications of the impact craters in the greater Hellas region, Mars, *Lunar Planet. Sci.*, *XXXIV*, abstract 1538.

Alfaro, P., M. Moretti, and J. Soria (1997), Soft-sediment deformation structures induced by earthquakes (seismites) in Pliocene lacustrine deposits (Guadix-Baza Basin, central Betic Cordillera), *Eclogae Geol. Helv.*, *90*(3), 531–540.

Allen, J. R. L. (1984), *Sedimentary Structures: Their Character and Physical Basis*, unabridged one-vol. ed., *Dev. Sed.*, vol. 30, Elsevier, Amsterdam.

Alvarez, W., E. Staley, D. O'Connor, and M. A. Chan (1998), Synsedimentary deformation in the Jurassic of southeastern Utah—A case of impact shaking?, *Geology*, *26*, 579–582.

Ansan, V., and N. Mangold (2004), Impact crater paleolakes in Hellas and Thaumasia areas, Mars, paper presented at Second Conference on Early Mars, Lunar and Planet. Inst., Houston, Tex.

Ansan, V., N. Mangold, A. Lucas, A. Gendrin, S. LeMouelic, F. Poulet, J.-P. Bibring, and the OMEGA co-Investigator Team (2005), Analysis of layered deposits in Terby crater (Hellas region, Mars) using multiple datasets MOC, THEMIS, and OMEGA/MEX data, *Lunar Planet. Sci.*, *XXXVI*, abstract 1324.

Ansan, V., N. Mangold, and A. Lucas (2006), Layered deposits in Terby crater (Hellas region, Mars) from multiple datasets (MOLA, THEMIS and MOC): Geologic implications, *Lunar Planet. Sci.*, *XXXVII*, abstract 1877.

Arvidson, R. E., F. P. Seelos, K. S. Deal, W. C. Koeppen, N. O. Snider, J. M. Kieniewicz, B. M. Hynek, M. T. Mellon, and J. B. Garvin (2003), Mantled and exhumed terrains in Terra Meridiani, Mars, *J. Geophys. Res.*, *108*(E12), 8073, doi:10.1029/2002JE001982.

Bibring, J. P., et al. (2006), Global mineralogical and aqueous Mars history derived from OMEGA/Mars Express data, *Science*, *312*, 400–404.

Branney, M. J., and P. Kokelaar (2002), *Pyroclastic Density Currents and the Sedimentation of Ignimbrites*, 143 pp., Geol. Soc., London.

Burr, D. M., R. M. E. Williams, J. Nussbaumer, and J. R. Zimbelman (2006), Multiple, distinct (glacio?) fluvial paleochannels throughout the western Medusae Fossae Formation, Mars, *Lunar Planet Sci.*, *XXXVII*, abstract 1367.

Christensen, P. R. (1986), The spatial distribution of rocks on Mars, *Icarus*, *68*, 217–238.

Christensen, P. R., et al. (2001), Mars Global Surveyor Thermal Emission Spectrometer experiment: Investigation description and surface science results, *J. Geophys. Res.*, *106*, 23,823–23,872.

Christensen, P. R., et al. (2003), Morphology and composition of the surface of Mars: Mars Odyssey THEMIS results, *Science*, *300*, 2056–2061.

Craddock, R. A., and A. D. Howard (2002), The case for precipitation on a warm, wet early Mars, *J. Geophys. Res.*, *107*(E11), 5111, doi:10.1029/2001JE001505.

Craddock, R. A., T. A. Maxwell, and A. D. Howard (1997), Crater morphometry and modification in the Sinus Sabaeus and Margaritifer Sinus regions of Mars, *J. Geophys. Res.*, *102*, 13,321–13,340.

Crown, D. A., L. F. Bleamaster III, and S. C. Mest (2005), Styles and timing of volatile-driven activity in the eastern Hellas region of Mars, *J. Geophys. Res.*, *110*, E12S22, doi:10.1029/2005JE002496.

Dalrymple, R. W. (1979), Wave-induced liquefaction: A modern example from the Bay of Fundy, *Sedimentology*, *26*, 835–844.

Denton, G. H., and D. E. Sugden (2005), Meltwater features that suggest Miocene ice-sheet overriding of the Transantarctic Mountains in Victoria Land, Antarctica, *Geogr. Annal.*, *87*, 67–85.

Dickson, J., and J. W. Head (2006), Evidence for an Hesperian-aged south circumpolar lake margin environment on Mars, *Planet. Space Sci.*, *54*, 251–272, doi:10.1016/J.PSS.2005.12.010.

Edgett, K. S. (2005), The sedimentary rocks of Sinus Meridiani: Five key observations from data acquired by the Mars Global Surveyor and Mars Odyssey Orbiters, *Mars Int. J. Mars Soc. Explor.*, *1*, 5–58, doi:10.1555/mars.2005.0002.

Edgett, K. S., and M. C. Malin (2002), Martian sedimentary rock stratigraphy: Outcrops and interbedded craters of northwest Sinus Meridiani and southwest Arabia Terra, *Geophys. Res. Lett.*, *29*(24), 2179, doi:10.1029/2002GL016515.

Fergason, R. L., P. R. Christensen, and H. H. Kieffer (2006), High-resolution thermal inertia derived from the Thermal Emission Imaging System (THEMIS): Thermal model and applications, *J. Geophys. Res.*, *111*, E12004, doi:10.1029/2006JE002735.

Fisher, R. V., and H.-U. Schmincke (1984), *Pyroclastic Rocks*, 472 pp., Springer, New York.

Forsberg-Taylor, N. K., A. D. Howard, and R. A. Craddock (2004), Crater degradation in the Martian highlands: Morphometric analysis in the Sinus Sabaeus region and simulation modeling suggest fluvial processes, *J. Geophys. Res.*, *109*, E05002, doi:10.1029/2004JE002242.

Garvin, J. B., S. E. H. Sakimoto, and J. J. Frawley (2003), Craters on Mars: Global geometric properties from gridded MOLA topography, paper presented at Sixth International Conference on Mars, Lunar and Planet. Inst., Houston, Tex.

Gendrin, A., et al. (2005), Sulfates in Martian layered terrains: The OMEGA/Mars Express view, *Science*, *307*, 1587–1590.

Ghatan, G. J., and J. W. I. Head (2004), Regional drainage of meltwater beneath a Hesperian-aged south circumpolar ice sheet on Mars, *J. Geophys. Res.*, *109*, E07006, doi:10.1029/2003JE002196.

Grant, J. A. (2000), Valley formation in Margaritifer Sinus, Mars, by precipitation- recharged ground-water sapping, *Geology*, *28*, 223–226.

Hartmann, W. K. (2005), Martian cratering 8: Isochron refinement and the chronology of Mars, *Icarus*, *174*, 294–320.

Head, J. W., III, and D. R. Marchant (2003), Cold-based glaciers on Mars: Western Arsia Mons, *Geology*, *31*, 641–644.

Head, J. W., J. F. Mustard, M. A. Kreslavsky, R. E. Milliken, and D. R. Marchant (2003), Recent ice ages on Mars, *Nature*, *426*, 797–802, doi:10.1038/nature02114.

Head, J. W., et al. (2005), Tropical to mid-latitude snow and ice accumulation, flow and glaciation on Mars, *Nature*, *434*, 346–351.

Heifetz, E., A. Agnon, and S. Marco (2005), Soft sediment deformation by Kelvin Helmholtz Instability: A case from Dead Sea earthquakes, *Earth Planet. Sci. Lett.*, *236*(1–2), 497–504.

Howard, A. D. (1981), Etched plains and braided ridges of the south polar region of Mars: Features produced by basal melting of ground ice? (abstract), in *Reports of the Planetary Geology Program -1981*, *NASA Tech. Memo.*, *84211*, 286–288.

Howard, A. D., J. M. Moore, and R. P. Irwin III (2005), An intense terminal epoch of widespread fluvial activity on Mars: 1. Valley network incision and associated deposits, *J. Geophys. Res.*, *110*, E12S14, doi:10.1029/2005JE002459.

Hynek, B. M., and R. J. Phillips (2001), Evidence for extensive denudation of the Martian highlands, *Geology*, *29*, 407–410.

Hynek, B. M., and R. J. Phillips (2003), New data reveal mature, integrated drainage systems on Mars indicative of past precipitation, *Geology*, *31*, 757–760.

Irwin, R. P., III, and A. D. Howard (2002), Drainage basin evolution in Noachian Terra Cimmeria, Mars, *J. Geophys. Res.*, *107*(E7), 5056, doi:10.1029/2001JE001818.

Irwin, R. P., III, T. A. Maxwell, A. D. Howard, R. A. Craddock, and J. M. Moore (2005), An intense terminal epoch of widespread fluvial activity on early Mars: 2. Increased runoff and paleolake development, *J. Geophys. Res.*, *110*, E12S15, doi:10.1029/2005JE002460.

Iverson, N. R. (1999), Coupling between a glacier and a soft bed: II. Model results, *J. Glaciol.*, *4*(149), 41–53.

Jakosky, B. M., and P. R. Christensen (1986), Global duricrust on Mars: Analysis of remote-sensing data, *J. Geophys. Res.*, *91*, 3547–3559.

Kargel, J. S., and R. G. Strom (1992), Ancient glaciation on Mars, *Geology*, *20*, 3–7.

Kieffer, H. H., T. Z. Martin, A. R. Peterfreund, B. M. Jakosky, E. D. Miner, and F. D. Palluconi (1977), Thermal and albedo mapping of Mars during the Viking primary mission, *J. Geophys. Res.*, *82*, 4249–4291.

Korteniemi, J., V.-P. Kostama, T. Törmänen, M. Aittola, T. Öhman, H. Lahtela, J. Raitala, and G. Neukum (2005a), Complex geology of two large impact craters in Tyrrhena Terra, Mars: Detailed analysis using MEX HRSC camera data, *J. Geophys. Res.*, *110*, E12, E12S18, doi:10.1029/2005JE002427.

Korteniemi, J., H. Lahtela, J. Raitala, G. Neukum, and the HRSC Co-Investigator Team (2005b), Anomalous depressions on the circum-Hellas crater floors as seen in the first year MEX HRSC images, *Lunar Planet. Sci.*, *XXXVI*, abstract 1669.

Lamb, M. P., H. Toniolo, and G. Parker (2005), Trapping of sustained turbidity currents by intraslope minibasins, *Sedimentology*, *53*, 147–160.

Laskar, J., A. C. M. Correia, M. Gastineau, F. Joutel, B. Levrard, and P. Robutel (2004), Long term evolution and chaotic diffusion of the insolation quantities of Mars, *Icarus*, *170*, 343–364.

Leonard, G. J., and K. L. Tanaka (2001), Geologic map of the Hellas Region of Mars, *Geol. Ser. Map I-2694*, scale 1:5,000,000, U. S. Geol. Surv., Boulder, Colo.

Lewis, A. R., D. R. Marchant, D. E. Kowalewski, S. L. Baldwin, and L. E. Webb (2006), The age and origin of the Labyrinth, western Dry Valleys, Antarctica: Evidence for extensive middle Miocene subglacial floods and freshwater discharge to the Southern Ocean, *Geology*, *34*, 513–516.

Malin, M. C., and K. S. Edgett (2000), Sedimentary rocks of early Mars, *Science*, *290*, 1927–1937.

Malin, M. C., and K. S. Edgett (2001), The Mars Global Surveyor Mars Orbiter Camera: Interplanetary cruise through primary mission, *J. Geophys. Res.*, *106*, 23,429–23,570.

Malin, M. C., and K. S. Edgett (2003), Evidence for persistent flow and aqueous sedimentation on early Mars, *Science*, *302*, 1931–1934.

Malin, M. C., et al. (1998), Early views of the Martian surface from the Mars Orbiter Camera of Mars Global Surveyor, *Science*, *279*, 1681–1685.

Mangold, N. (2003), Geomorphic analysis of lobate debris aprons on Mars at Mars Orbiter Camera scale: Evidence for ice sublimation initiated by fractures, *J. Geophys. Res.*, *108*(E4), 8021, doi:10.1029/2002JE001885.

McEwen, A. S., and E. B. Bierhaus (2006), The importance of secondary cratering to age constraints on planetary surfaces, *Annu. Rev. Earth Planet. Sci.*, *34*, 535–567.

McEwen, A. S., et al. (2006), MRO's High Resolution Imaging Science Experiment (HiRISE), *J. Geophys. Res.*, *112*, E05S02, doi:10.1029/2005JE002605.

Mellon, M. T., B. M. Jakosky, H. H. Kieffer, and P. R. Christensen (2000), High-resolution thermal inertia mapping from the Mars Global Surveyor Thermal Emission Spectrometer, *Icarus*, *148*, 437–455.

Mest, S. C., and D. A. Crown (2005), Millochau crater, Mars: Infilling and erosion of an ancient highland impact crater, *Icarus*, *175*, 335–359.

Mest, S. C., and D. A. Crown (2006), Geologic map of the MTM −20272 and −25272 Quadrangles, Tyrrhena Terra Region of Mars, *Sci. Invest. Map 2934*, U. S. Geol. Surv., Boulder, Colo.

Milkovich, S. M., J. W. Head III, and S. Pratt (2002), Meltback of Hesperian-aged ice-rich deposits near the south pole of Mars: Evidence for drainage channels and lakes, *J. Geophys. Res.*, *107*(E6), 5043, doi:10.1029/2001JE001802.

Milliken, R. E., J. F. Mustard, and D. L. Goldsby (2003), Viscous flow features on the surface of Mars: Observations from high-resolution Mars Orbiter Camera (MOC) images, *J. Geophys. Res.*, *108*(E6), 5057, doi:10.1029/2002JE002005.

Milliman, J. D., and S.-J. Kao (2005), Hyperpycnal discharge of fluvial sediment to the ocean: Impact of super-typhoon Herb (1996) on Taiwanese rivers, *J. Geol.*, *113*(5), 50–516.

Moore, J. M., and K. S. Edgett (1993), Hellas Planitia, Mars: Site of net dust erosion and implications for the nature of basin floor deposits, *Geophys. Res. Lett.*, *20*, 1599–1602.

Moore, J. M., and A. D. Howard (2005a), Large alluvial fans on Mars, *J. Geophys. Res.*, *110*, E04005, doi:10.1029/2004JE002352.

Moore, J. M., and A. D. Howard (2005b), Layered deposits and pitted terrain in the circum Hellas region, *Lunar Planet Sci.*, *XXXVI*, abstract 1512.

Moore, J. M., and D. E. Wilhelms (2001), Hellas as a possible site of ancient ice-covered lakes on Mars, *Icarus*, *154*, 258–276.

Moore, J. M., A. D. Howard, W. E. Dietrich, and P. M. Schenk (2003), Martian layered fluvial deposits: Implications for Noachian climate scenarios, *Geophys. Res. Lett.*, *30*(24), 2292, doi:10.1029/2003GL019002.

Mustard, J. F., C. D. Cooper, and M. K. Rifkin (2001), Evidence for recent climate change on Mars from the identification of youthful near-surface ground ice, *Nature*, *412*, 4111–4114.

Neukum, G., R. Jaumann, H. Hoffman, E. Hauber, and J. W. Head (2004), Recent and episodic volcanic and glacial activity on Mars revealed by the High Resolution Stereo Camera, *Nature*, *42*, 971–979.

Owen, G. (1995), Soft-sediment deformation in Upper Proterozoic Torridonian sandstones (Applecross Formation) at Torridon, northwest Scotland, *J. Sediment. Res., Sect. A*, *65*(3), 495–504.

Poulet, F., J.-P. Bibring, J. F. Mustard, A. Gendrin, N. Mangold, Y. Langevin, R. E. Arvidson, B. Gondet, B. Gomez, and Omega Team (2005), Phyllosilicates on Mars and implications for early Martian climate, *Nature*, *438*, 623–627, doi:10.1038/natureе04274.

Pye, K. (1987), *Aeolian Dust and Dust Deposits*, 334 pp., Academic Press, San Diego, Calif.

Quantin, C., P. Allemand, N. Mangold, G. Dromart, and C. Delacourt (2005), Fluvial and lacustrine activity on layered deposits in Melas Chasma, Valles Marineris, Mars, *J. Geophys. Res.*, *110*, E12S19, doi:10.1029/2005JE002440.

Quantin, C., N. Mangold, W. K. Hartmann, and P. Allemand (2007), Possible long-term decline in impact rates: 1. Martian geological data, *Icarus*, *186*, 1–10.

Reading, H. G. (Ed.) (1996), *Sedimentary Environments and Facies*, 3rd ed., 687 pp., Blackwell Sci., Oxford, U.K.

Rossetti, D. D. F., A. M. Góes, W. Truckenbrodt, and J. Anaisse (2000), Tsunami-induced large-scale scour-and-fill structures in Late Albian to Cenomanian deposits of the Grajau Basin, northern Brazil, *Sedimentology*, *47*, 309–323.

Sarkar, S., S. K. Chanfa, and A. Bhattacharya (1982), Soft-sediment deformation fabric in the Precambrian Bhander oolite, central India, *J. Sed. Petrol.*, *52*(1), 95–107.

Shean, D. E., J. W. Head, and D. R. Marchant (2005), Origin and evolution of a cold-based tropical mountain glacier on Mars: The Pavonis Mons fan-shaped deposit, *J. Geophys. Res.*, *110*, E05001, doi:10.1029/2004JE002360.

Silva, P. G., J. C. Cañaveras, S. Del Moral, J. Lario, and E. Sanz (1997), 3D soft-sediment deformation structures: Evidence of Quaternary seismicity in the Madrid Basin, Spain, *Terra Nova*, *9*(5), 208–212.

Smith, D. E., et al. (1999), The global topography of Mars and implications for surface evolution, *Science*, *184*, 1421–1576.

Squyres, S. W., and M. H. Carr (1986), Geomorphic evidence for the distribution of ground ice on Mars, *Science*, *231*, 249–252.

Squyres, S. W., S. M. Clifford, R. O. Kuzmin, J. R. Zimbelman, and F. M. Costard (1992), Ice in the Martian regolith, in *Mars*, edited by H. H. Kieffer, et al., pp. 523–554, Univ. of Ariz. Press, Tucson.

Squyres, S. W., et al. (2004), The Opportunity Rover's Athena science investigation at Meridiani Planum, Mars, *Science*, *306*, 1698–1703.

Tanaka, K. L. (1986), The stratigraphy of Mars, *J. Geophys. Res.*, *91*, E139–E158.

Tanaka, K. L. (1997), Sedimentary history and mass flow structures of Chryse and Acidalia Planitae, Mars, *J. Geophys. Res.*, *102*, 4131–4149.

Van der Wateren, F. M. (1995), Structural geology and sedimentology of push moraines: Processes of soft sediment deformation in a glacial environment and the distribution of glaciotectonic styles, *Meded. Rijks Geol. Dienst.*, *54*, 1–168.

Ward, A. W. (1979), Yardangs on Mars: Evidence of recent wind erosion, *J. Geophys. Res.*, *84*, 8147–8166.

Williams, R. M. E., and K. S. Edgett (2005), Valleys in the Martian Rock Record, *Lunar Planet. Sci.*, *XXXVI*, abstract 1099.

Wilson, S. A., and A. D. Howard (2005), Geomorphic and stratigraphic analysis of layered deposits in Terby Crater, Mars, *Lunar Planet. Sci.*, *XXXVI*, abstract 2060.

J. A. Grant and S. A. Wilson, Center for Earth and Planetary Studies, National Air and Space Museum, Smithsonian Institution, P.O. Box 37012, MRC 315, Washington, DC 20013, USA. (grantj@si.edu; wilsons@si.edu)

A. D. Howard, Department of Environmental Sciences, University of Virginia, P.O. Box 400123, Charlottesville, VA 22904-4123, USA. (ah6p@virginia.edu)

J. M. Moore, Space Sciences Division, NASA Ames Research Center, MS-245-3, Moffett Field, CA 94035, USA. (jeff.moore@nasa.gov)